Article

Lithocholic acid phenocopies anti-ageing effects of calorie restriction

https://doi.org/10.1038/s41586-024-08329-5

Received: 6 November 2023

Accepted: 31 October 2024

Published online: 18 December 2024

Open access

Check for updates

Qi Qu[1,10], Yan Chen[1,10], Yu Wang[1,10], Shating Long[1], Weiche Wang[1], Heng-Ye Yang[1], Mengqi Li[1], Xiao Tian[1], Xiaoyan Wei[1], Yan-Hui Liu[1], Shengrong Xu[1], Cixiong Zhang[1], Mingxia Zhu[1], Sin Man Lam[2], Jianfeng Wu[3], Chuyu Yun[4], Junjie Chen[5], Shengye Xue[1], Baoding Zhang[1], Zhong-Zheng Zheng[1], Hai-Long Piao[6], Changtao Jiang[7], Hao Guo[1,8], Guanghou Shui[9], Xianming Deng[1], Chen-Song Zhang[1]✉ & Sheng-Cai Lin[1]✉

Calorie restriction (CR) is a dietary intervention used to promote health and longevity[1,2]. CR causes various metabolic changes in both the production and the circulation of metabolites[1]; however, it remains unclear which altered metabolites account for the physiological benefits of CR. Here we use metabolomics to analyse metabolites that exhibit changes in abundance during CR and perform subsequent functional validation. We show that lithocholic acid (LCA) is one of the metabolites that alone can recapitulate the effects of CR in mice. These effects include activation of AMP-activated protein kinase (AMPK), enhancement of muscle regeneration and rejuvenation of grip strength and running capacity. LCA also activates AMPK and induces life-extending and health-extending effects in *Caenorhabditis elegans* and *Drosophila melanogaster*. As *C. elegans* and *D. melanogaster* are not able to synthesize LCA, these results indicate that these animals are able to transmit the signalling effects of LCA once administered. Knockout of AMPK abrogates LCA-induced phenotypes in all the three animal models. Together, we identify that administration of the CR-mediated upregulated metabolite LCA alone can confer anti-ageing benefits to metazoans in an AMPK-dependent manner.

The application of CR without causing malnutrition has been recognized as a non-pharmacological dietary intervention for improving health[1]. The benefits of CR on lifespan and healthspan have been tested and observed in a wide range of organisms, including mice, primates, yeast, nematodes and flies, thereby highlighting the general connection of reduced food intake to longevity[2]. During CR, organisms undergo a series of metabolic changes or adaptations that include alterations in the levels of free fatty acids, cholesterol, vitamins, short-chain organic acids and bile acids, among others[3]. Alterations in some serum factors can limit age-associated metabolic changes by controlling the homeostasis of cellular proteins, oxidative damage and inflammation[4,5]. In humans, population studies and randomized clinical trials have shown that CR also produces systemic health benefits, including improvements in age-related frailty and in diseases such as central obesity, insulin resistance, muscle deterioration, dyslipidaemia and cancer without inducing adverse effects on life quality[6]. Consequently, numerous 'anti-ageing diet' modalities such as intermittent fasting[7], fasting-mimicking diets[8] and ketogenic diets[9,10] have been developed. However, hypercaloric ketogenic diets may have adverse effects on lifespan[11].

AMP-activated protein kinase (AMPK), which is highly conserved across eukaryotes[12] and is activated under CR[13], is a crucial mediator of the beneficial effects of CR[14]. AMPK regulates a large number of signalling pathways that impede ageing, such as inhibiting target of rapamycin complex 1 (TORC1)[15] and forkhead box O (FOXO) proteins[16,17] to mimic the reduction in insulin–IGF-1 signalling[18]. AMPK also regulates increases in NAD^+, which activates sirtuins[19], inhibits CREB-regulated transcriptional co-activators[20] and induces TFEB[21]. Moreover, AMPK acts on various anti-ageing-related cellular processes, including autophagy, proteostasis, mitochondrial biogenesis, mitohormesis, germline stemness and viability, inflammation and neurodegeneration (reviewed in ref. 14). AMPK has therefore been a target for identifying caloric restriction mimetics (CRMs). Known CRMs, including metformin[22] and resveratrol[23], can extend lifespan and healthspan in multiple organisms through AMPK activation. However, it is unclear how CR-mediated metabolic adaptations in the body signal to activate AMPK to maintain health and extend lifespan. In particular, whether specific metabolites that are altered through CR are able to or responsible for AMPK modulation is unknown.

In this study, we reasoned that serum metabolites that undergo changes after CR might harbour the ability to induce beneficial effects at cellular and organismal levels. Serum prepared from mice subjected to CR for 4 months (CR serum) was sufficient to activate AMPK in mouse embryonic fibroblasts (MEFs), HEK293T cells, primary hepatocytes and

[1]State Key Laboratory for Cellular Stress Biology, School of Life Sciences, Xiamen University, Fujian, China. [2]LipidALL Technologies, Changzhou, China. [3]Laboratory Animal Research Centre, Xiamen University, Fujian, China. [4]State Key Laboratory of Female Fertility Promotion, Centre for Reproductive Medicine, Department of Obstetrics and Gynaecology, Peking University Third Hospital, Beijing, China. [5]Analysis and Measurement Centre, School of Pharmaceutical Sciences, Xiamen University, Fujian, China. [6]CAS Key Laboratory of Separation Science for Analytical Chemistry, Dalian Institute of Chemical Physics, Chinese Academy of Sciences, Liaoning, China. [7]Department of Physiology and Pathophysiology, Department of Immunology, School of Basic Medical Sciences, School of Basic Medical Sciences, State Key Laboratory of Vascular Homeostasis and Remodelling, Peking University, Beijing, China. [8]Xiang'an Hospital of Xiamen University, School of Medicine, Faculty of Medicine and Life Sciences, Xiamen University, Xiamen, China. [9]Institute of Genetics and Development Biology, Chinese Academy of Sciences, Beijing, China. [10]These authors contributed equally: Qi Qu, Yan Chen, Yu Wang. ✉e-mail: cszhang@xmu.edu.cn; linsc@xmu.edu.cn

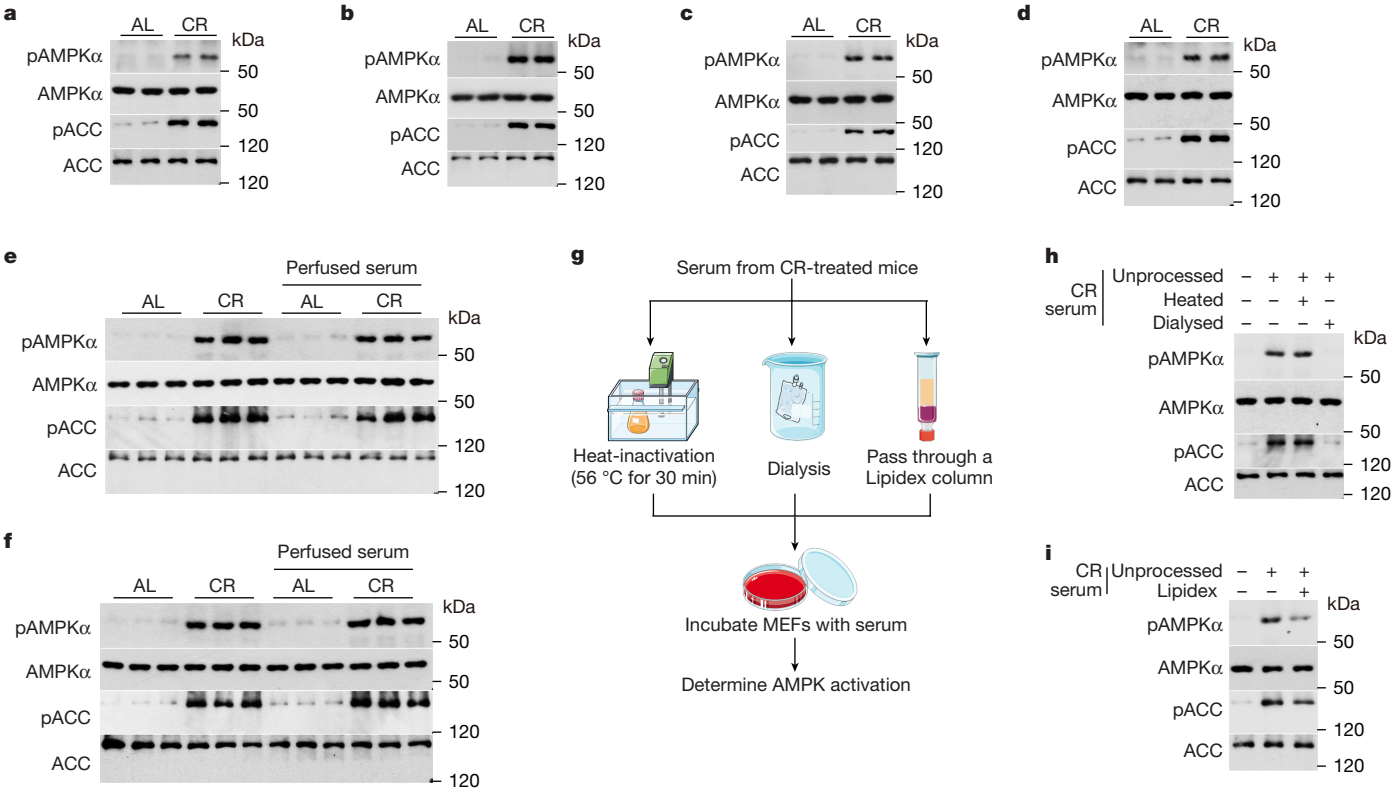

Fig. 1 | Serum from CR-treated mice can activate AMPK in cells and in mice. **a**–**d**, Serum from CR-treated mice can activate AMPK in cells cultured in normal medium. MEFs (**a**), HEK293T cells (**b**), primary hepatocytes (**c**) and primary myocytes (**d**) were cultured in DMEM (**a**,**b**), William's medium E (**c**) or Ham's F-10 medium (**d**). However, FBS (**a**,**b**,**d**) or BSA (**c**) supplemented in the culture medium was replaced with an equal volume of serum from mice subjected to CR for 4 months (collected at 17:00, immediately before the next food supply; this CR serum was used hereafter, unless stated otherwise) or serum from mice on an ad libitum diet, for 4 h (AL serum; control). Cells were then lysed, followed by determination of AMPK activation by immunoblotting (IB) for pAMPKα and pACC levels. **e**,**f**, Serum from CR-treated mice activates AMPK in the muscle and liver of mice perfused with this serum. Ad libitum-fed mice were perfused through the jugular with 100 µl of CR serum or AL serum (as control), followed by determination of AMPK activation in liver (**e**) and muscle tissues (**f**) at 2 h after perfusion by IB for pAMPKα and pACC. **g**–**i**, Heat-stable, polar metabolites with low molecular weights in CR serum mediate AMPK activation. Schematic of experiment (**g**). MEFs were treated with CR serum as in **a**, except that the serum was heat-inactivated, dialysed or passed through a Lipidex column, followed by determination of AMPK activation by IB (**h**,**i**). Experiments were performed three (**c**–**i**) or five (**a**,**b**) times. Artwork in **g** was reproduced from Servier Medical Art under a Creative Commons Attribution 3.0 unported licence.

primary myocytes. AMPK activation was assessed by measuring the phosphorylation levels of AMPKα (pAMPKα) and the substrate acetyl coenzyme A carboxylases (pACC (also known as pACC1/2)) (Fig. 1a–d). This finding was in agreement with previous studies showing that serum from CR-treated animals can mimic the effects of CR in cultured cells[24]. Perfusion of CR serum into mice on an ad libitum diet led to AMPK activation in the liver and muscle (Fig 1e,f), which indicated that CR serum is sufficient to activate AMPK at the organismal level. After heating at 56 °C, CR serum retained the ability to activate AMPK in cultured cells, whereas dialysed CR serum could not (Fig. 1g,h). These results indicate that heat-stable, low-molecular-weight metabolites present in CR serum can confer the ability to activate AMPK.

We next performed a series of metabolomics analyses on serum samples prepared from CR-treated mice and from non-CR-treated mice (control serum). Different mass spectrometry-based approaches (all targeted), including high-performance liquid chromatography–mass spectrometry (HPLC–MS), gas chromatography–MS (GC–MS) and capillary electrophoresis–MS (CE–MS), were applied to resolve small polar metabolites and nonpolar lipids. As summarized in Supplementary Table 1, a total of 1,215 metabolites (778 polar metabolites and 437 lipids) were identified as hits, of which 695 metabolites (341 polar metabolites and 354 lipids) were significantly altered ($P < 0.05$) in CR serum compared with control serum. Long-chain fatty acids, phenylalanine and tyrosine had the largest decreases, whereas short-chain fatty acids, bile acids and acyl-carnitine had the largest increases (Supplementary Table 1). After passing CR serum through a lipophilic Lipidex column, which absorbs nonpolar compounds and lipids[25], the eluted fractions still retained the ability to activate AMPK in MEFs, albeit to a reduced extent (Fig. 1i). This result indicated that nonpolar compounds and lipids are probably not involved in AMPK activation. We therefore focused on the polar metabolites that were altered after CR (212 increased and 129 decreased), and assessed the ability of these individual metabolites to activate AMPK in MEFs. We referred to published studies to ascertain the metabolite concentrations to use for the screening assays. For metabolites with only ad libitum-fed conditions reported, the concentrations used were adjusted by the observed fold changes after CR (Supplementary Table 2). For metabolites with no concentrations reported, we set 10 mM as the highest concentration (Supplementary Table 2) given that even high-abundance serum metabolites fall below this value[26].

Among the 212 metabolites that were increased after CR, 204 were tested for AMPK activation in MEFs (8 were not tested owing to either failure to synthesize the metabolite or prohibition by law). Overall, six metabolites were identified to activate AMPK in the initial screening assays (Supplementary Table 2). For the metabolites that were decreased after CR, we tested 123 (6 were unavailable for testing) for their contribution to AMPK activation as a consequence of counteracting inhibition. None of these metabolites showed an inhibitory effect on

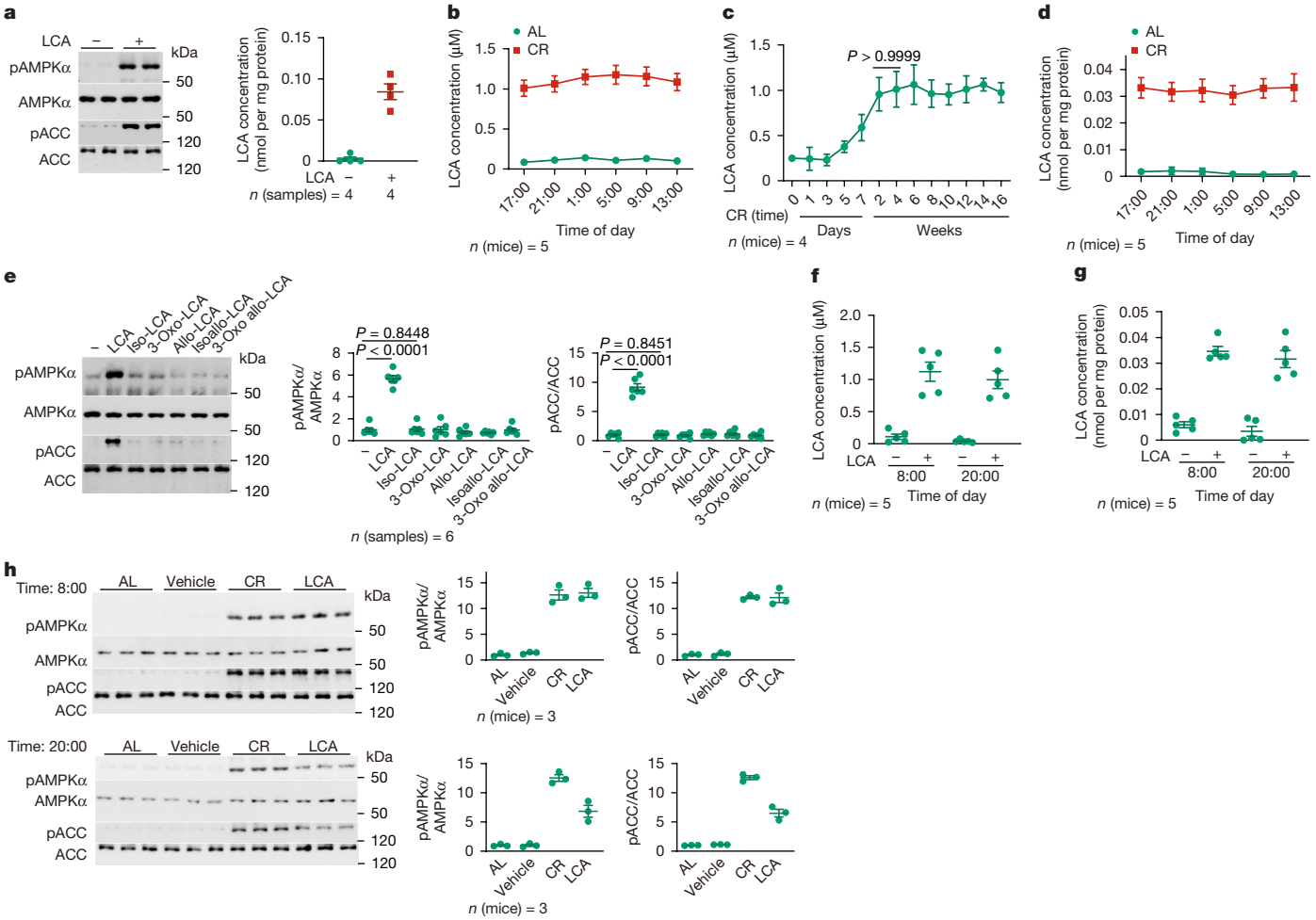

Fig. 2 | LCA is increased after CR and responsible for AMPK activation. **a**, LCA is the AMPK-activating factor in CR serum. MEFs were treated with 1 μM LCA, a concentration roughly equivalent to that in the serum of CR mice, for 4 h, followed by determination of AMPK activity (left) and intracellular concentrations of LCA (right). **b**–**d**, Metabolomics analyses reveals substantial increases of LCA in CR-treated mice. Serum (**b**,**c**) and muscular (**d**) concentrations of LCA in mice subjected to CR for 4 months were determined at different time points of the day (**b**,**d**) or at different time durations of CR (**c**). **e**, Immunoblot (left) and quantification (right) showing that LCA is the sole derivative of bile acids that can activate AMPK. MEFs were treated with 1 μM LCA or 1 μM LCA derivatives for 4 h, followed by determination of AMPK activities. **f**,**g**, Mice treated with LCA through drinking water have similar levels of LCA to that in CR serum. Aged, ad libitum-fed (1.5-year-old) mice were fed (2-hydroxypropyl)-β-cyclodextrin-coated LCA at 1 g l^{-1} in drinking water for 1 month, and concentrations of LCA in serum (**f**) and muscle tissue (**g**) of mice at two different times of the day (8:00, representing the light cycle, and 20:00, representing the dark cycle), were measured. **h**, Immunoblots (left) and quantification (right) showing that LCA administration activates AMPK in mice. Aged mice were subjected to CR as in **b**, or treated with LCA as in **f**, followed by determination of AMPK activities in skeletal muscle at both light and dark cycles. Statistical results are shown as the mean ± s.e.m. Specific numbers of mice or samples used are labelled on each panel. *P* values were calculated using two-way analysis of variance (ANOVA) followed by Tukey's test (**c**) or two-sided Student's *t*-test (**e**). Experiments were performed three (**b**–**e**) or four (**a**,**f**,**g**) times.

AMPK. In detail, at serum concentrations before CR, none attenuated or reversed CR serum-induced AMPK activation in MEFs (Supplementary Table 2). Among the six AMPK-activating metabolites identified in the initial screening assays, LCA was the only metabolite that activated AMPK at 1 μM in the culture medium (a concentration similar to that detected in the serum after CR) when tested in MEFs, HEK293T cells, primary hepatocytes and primary myocytes (Fig. 2a,b and Extended Data Fig. 1a–d). Consistent with AMPK activation, pACC was increased (Fig. 2a and Extended Data Fig. 1a–d) and mTORC1 was inhibited (as determined by the decreased levels of phosphoS6K; Extended Data Fig. 1e). As a consequence of mTORC1 inhibition, we also observed a decrease in phosphoAMPKα2(S345) levels[27] in LCA-treated MEFs (Extended Data Fig. 1f). Another downstream factor of AMPK, TFEB, was translocated into the nucleus when treated with LCA (Extended Data Fig. 1g). In addition, when CR serum was passed through a Lipidex column, LCA was partially absorbed (about 30%; Extended Data Fig. 1h), which explains why filtered CR serum showed a reduced capacity to activate AMPK (Fig. 1i). Notably, although other bile acids, such as cholic acid (CA) and chenodeoxycholic acid (CDCA), were upregulated during CR (Supplementary Table 2), they did not activate AMPK (Extended Data Fig. 1i). The concentration of LCA in serum was around 1.1 μM at 4 months of CR and remained constant in mice before and after feeding (Fig. 2b,c). By contrast, in ad libitum-fed mice, low levels (0.3 μM) of LCA were detected in the serum of postprandial mice, which then gradually decreased to undetectable levels at the fasting (postabsorptive) state (Extended Data Fig. 1j). Treatment of MEFs with LCA at 1 μM, without forming micelles (Extended Data Fig. 1k), led to an accumulation of intracellular LCA at approximately 0.8 μM (around 0.08 nmol mg^{-1} protein mass, equivalent to 0.8 μM after normalization to the average cell volume and cell density). This value was similar to that measured in tissue (that is, around 0.03 nmol mg^{-1} protein mass in muscle or 0.5 μM calculated according to the density of myocytes) of CR-treated mice (Fig. 2a,d). Although serum concentrations of LCA are similar between humans and mice[28,29], the synthesis and interconversion of bile acids

in mice are different from humans, particularly muricholate, which is abundant in mice but barely detectable in humans (reviewed in ref. 30). It has been suggested that muricholate interferes with the synthesis of other bile acids, thereby potentially acting as a positive feedback regulator to increase LCA during CR[31]. We therefore analysed humanized mice that cannot synthesize muricholate owing to lack of expression of the *Cyp2c* gene cluster[32]. *Cyp2c*-null mice had LCA levels of 0.8 μM in the serum after CR (Extended Data Fig. 1l), similar to those in wild-type mice. This result indicates that the CR-induced increase in LCA is unrelated to muricholate. As AMPK can be activated through several modes, we measured AMP-to-ATP and ADP-to-ATP ratios[33] in MEFs, HEK293T cells, primary hepatocytes and primary myocytes treated with LCA. LCA treatment did not change energy levels in these cell types (Extended Data Fig. 1m) and were similar to that seen in the liver and muscle tissue of CR-treated mice (Extended Data Fig. 1n,o). Moreover, unlike taurocholic acid (TCA), LCA did not depend on the cAMP–Epac–MEK pathway to activate AMPK[34], as treatment with the MEK inhibitor PD98059 did not prevent LCA-mediated AMPK activation (Extended Data Fig. 1p). LCA also did not activate AMPK through TGR5 in MEFs (Extended Data Fig. 1q; see validation data for *Tgr5*$^{-/-}$ MEFs in Supplementary Table 3), which is in contrast to its effects in breast cancer cells[35] and osteoclasts[36]. In addition, LCA did not cause bulk Ca^{2+} increases that may lead to CaMKK2-mediated AMPK activation[37–39] (Extended Data Fig. 1r), as assessed by measuring the fluorescence intensities of Fluo-4-AM dye. The LCA derivatives iso-LCA, 3-oxo-LCA, allo-LCA, isoallo-LCA and 3-oxo allo-LCA also did not activate AMPK in MEFs (Fig. 2e). Together, these results indicate that LCA is a specific metabolite in CR serum that activates AMPK at physiological concentrations.

We then determined the effects of LCA on AMPK activation in mice. Through testing different administration routes and titrating various doses in different formulations, we found that (2-hydroxypropyl)-β-cyclodextrin-coated LCA at 1 g l^{-1} in drinking water led to an accumulation of approximately 1.1 μM LCA in the serum of aged (1.5-year-old) mice (Fig. 2f), similar to the LCA concentrations measured in the sera of CR-treated mice (Fig. 2b,c). Administration of LCA dissolved in drinking water also led to an accumulation of muscular LCA levels to approximately 0.04 nmol mg^{-1} protein (approximately 0.5 μM; Fig. 2g), similar to that observed in muscle from CR-treated mice (Fig. 2d). Mice treated with LCA dissolved in drinking water had AMPK activation levels in skeletal muscle that were similar to that seen during CR (Fig. 2h and Extended Data Fig. 2a). Because the basal activity of mTORC1 is much lower in muscle tissue compared to cultured cells, LCA did not further inhibit mTORC1 in muscle (Extended Data Fig. 2b). As a control, we tested CA, CDCA and iso-LCA, and none activated AMPK in mouse muscle (Extended Data Fig. 2c). Furthermore, similar to what was observed in MEFs, LCA treatment led to AMPK activation in the muscles of *Tgr5* knockout (KO) mice (Extended Data Fig. 2d; see validation data in Extended Data Fig. 2e). Consistent with its ability to activate AMPK[40], LCA administration decreased blood glucose levels (Extended Data Fig. 2f), which mirrored the effects of CR on blood glucose in mice[1]. Together, these results show that LCA is sufficient to mediate AMPK activation, similar to CR serum.

We next determined the effects of LCA on ageing-related phenotypes. Administration of LCA to aged male and female mice for 1 month improved various aspects of muscle performance to a similar extent to that observed during CR. In detail, the number of oxidative muscle fibres was increased (Fig. 3a), as determined by measuring the expression levels of MHCI and MHCIIa, markers of oxidative muscle fibres, with MHCI causing greater oxidative capacity compared with MHCIIa. Moreover, the number of glycolytic fibres was decreased (Fig. 3a; determined by measuring the expression levels of MHCIIb) and muscle atrophy was reduced (Fig. 3b; determined by measuring the mRNA levels of *Trim63* and *Fbxo32* (refs. 41,42)). Notably, LCA administration did not cause muscle loss (Extended Data Fig. 3a; determined by measuring muscle weight and lean mass), a result that is in contrast to the decrease in muscle content seen in mice and humans after CR[6,43–45]. LCA treatment also accelerated muscle regeneration after damage (induced using a cardiotoxin) in aged mice. This effect was due to LCA promoting the induction of muscle stem cells (as determined by measuring PAX7 levels[46]) (Extended Data Fig. 3b–d). LCA treatment also increased NAD^+ levels (Fig. 3c) and increased mitochondrial content (assessed through morphology and measuring the mitochondrial-to-nuclear DNA (mtDNA-to-nDNA) ratio and mitochondrial oxidation and phosphorylation (OXPHOS) complex expression; Extended Data Fig. 3e–h) in muscle tissue of aged mice. Mitochondrial respiratory function (as assessed by measuring oxygen consumption rates (OCRs); Extended Data Fig. 3i) was also increased in these mice. In line with previous findings[29,47,48], we observed significant upregulation of plasma GLP-1 levels in LCA-treated mice, both at the basal state and during food uptake, as assessed by oral glucose tolerance tests (Extended Data Fig. 4a). However, we did not observe any increase in UCP1 levels in brown adipose tissue (Extended Data Fig. 4b), as previously seen in obese mice[29,48]. Consistent with the increase in mitochondrial content and GLP-1 levels, energy expenditure was significantly increased in these mice (Extended Data Fig. 4c–e). Running distance, duration and grip strength were also significantly increased in LCA-treated aged mice (Fig. 3d,e). In line with the improvements in muscle function, LCA treatment ameliorated age-associated glucose intolerance and insulin resistance (determined by intraperitoneal glucose tolerance tests (Extended Data Fig. 5a), insulin tolerance tests (Extended Data Fig. 5b) and hyperinsulinaemic–euglycaemic clamp tests (Extended Data Fig. 5c)), without decreasing the rates of glucose production in these mice (Extended Data Fig. 5d–k). Knockout of AMPKα (both AMPKα1 and AMPKα2, encoded by *Prkaa1* and *Prkaa2*, respectively) in mouse muscle (validated in Extended Data Fig. 6a) dampened the effects of LCA in improving muscle function (Fig. 3f–h and Extended Data Fig. 6b–h). Note that although TGR5 can promote muscle hypertrophy in response to LCA[49], LCA treatment was still able to enhance muscle function in *Tgr5* KO mice (Extended Data Fig. 7a–e). As an additional control, iso-LCA, which does not activate AMPK in mouse muscle, did not produce rejuvenating effects in muscle tissue (Extended Data Fig. 7f–j).

We next tested whether LCA can extend lifespan. We used *C. elegans* and *D. melanogaster* as models, as CR can induce lifespan extension[50,51] and AMPK is required for lifespan extension[16,17,52] in these two species. We treated *C. elegans* and *D. melanogaster* with LCA and determined whether AMPK is activated in these animals. LCA was as effectively absorbed into nematodes and flies as into mouse muscle (see Methods for details of culture medium preparation) and activated AMPK (Extended Data Fig. 8a–d). Notably, LCA at these concentrations did not increase AMP levels (Extended Data Fig. 8a–d), which suggested that LCA activates AMPK in nematodes and flies in a similar way to that in mice. Moreover, LCA extended the mean lifespan of hermaphroditic nematodes from 22 to 27 days (Fig. 4a). In flies, lifespan was extended from 47 to 52 days in males and from 52 to 56 days in females (Fig. 4b and Extended Data Fig. 8e), similar to the effects of CR observed in this animal model (Extended Data Fig. 8f). These results were also consistent with a previous report showing that LCA can increase the lifespan of flies[53]. CA, CDCA or iso-LCA, as controls to LCA, did not activate AMPK in nematodes or flies (Extended Data Fig. 8g). In addition, the lifespan-extending effects were not observed with iso-LCA treatment (Extended Data Fig. 8h). LCA also significantly improved healthspan in nematodes and flies. In detail, the following parameters were increased: pharyngeal pumping rates in nematodes (Fig. 4c); oxidative stress resistance in both nematodes and flies (Fig. 4d,e and Extended Data Fig. 9a–c); tolerance to cold, heat and starvation (food-deprivation) in flies (Extended Data Fig. 9d–i); NAD^+ levels (Fig. 4f and Extended Data Fig. 9j); mtDNA-to-nDNA ratios (Extended Data Fig. 9k,l); mitochondrial gene expression (Extended Data Fig. 9m,n) in nematodes and flies; and OCRs in nematodes (Extended Data Fig. 9o). Knockout of AMPK in nematodes (by knocking out *aak-2*, the nematode orthologue of *Prkaa2*)

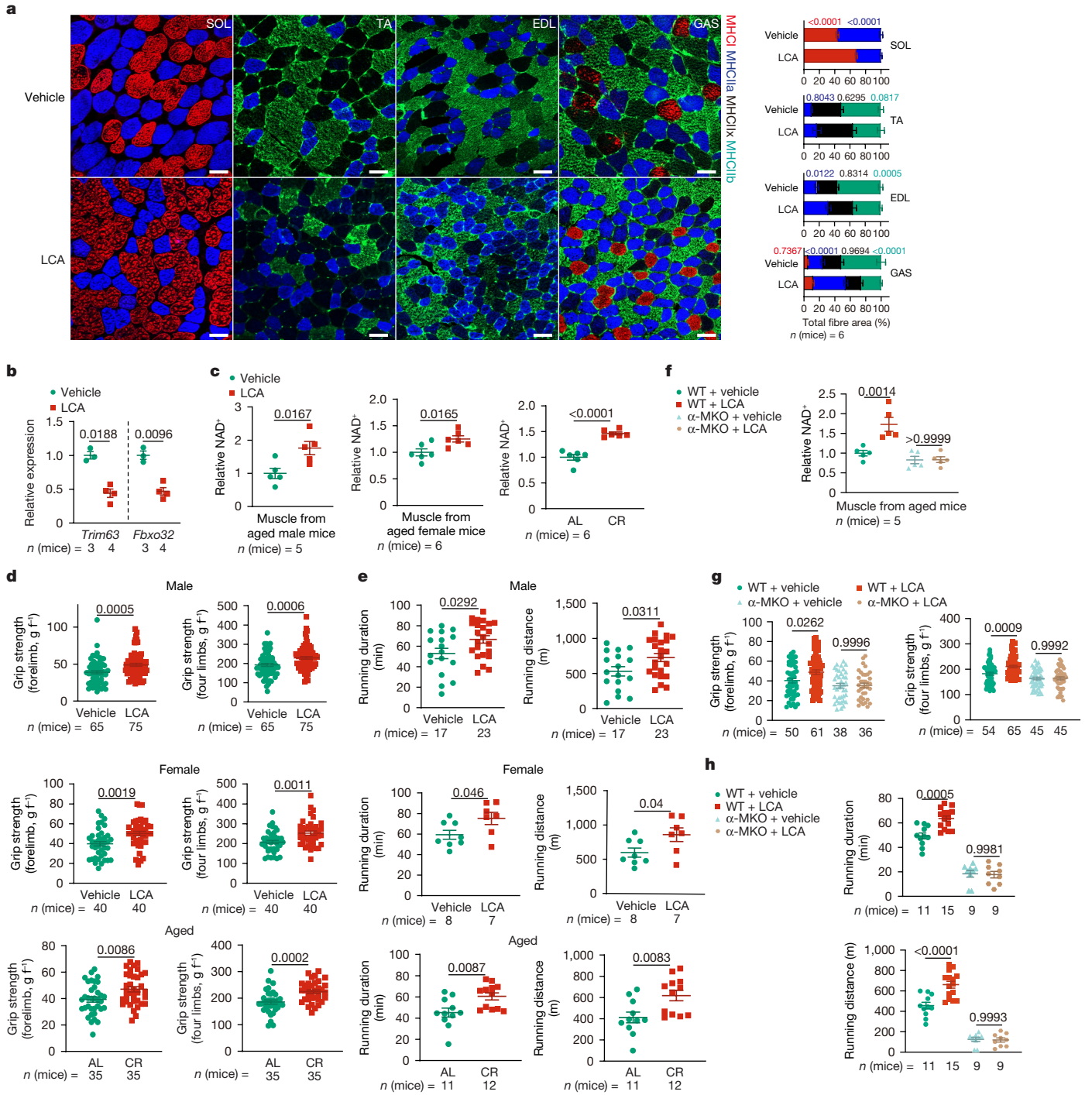

Fig. 3 | LCA exerts rejuvenating effects that depend on AMPK. a,**b**, LCA induces oxidative fibre conversion and prevents muscle atrophy in aged mice. Ad libitum-fed mice were given (2-hydroxypropyl)-β-cyclodextrin-coated LCA at 1 g l^{-1} in drinking water for 1 month, followed by determination of muscle fibre type by immunohistochemistry (**a**) and mRNA levels of the atrophy markers *Trim63* and *Fbxo32* by RT–PCR (**b**). EDL, extensor digitorum longus; GAS, gastrocnemius; SOL, soleus; TA, tibialis anterior. Scale bars, 50 μm. **c**, LCA increases NAD^+ levels in aged mice to a level similar to that induced by CR. Ad libitum-fed male (left) and female (middle) mice were either treated with LCA as in **a** or subjected to CR for 3.5 months (right), followed by determination of muscular NAD^+ levels. **d**,**e**, LCA promotes muscle strength and endurance in aged mice to an extent similar to that induced by CR. Ad libitum-fed mice, both male and female, were treated with LCA as in **a** or subjected to CR for 3.5 months, followed by determination of grip strength (**d**) and running duration (**e**). **f**, AMPK is required for the increase in muscular NAD^+ by LCA. Ad libitum-fed, aged mice with AMPKα specifically knocked out in muscle (α-MKO) and wild-type (WT) littermates were treated as in **a**, followed by determination of muscular NAD^+ levels. **g**,**h**, Muscle-specific AMPK knockout abolishes the effects of LCA on muscle strength and endurance. Mice were treated as in **a**, followed by determination of grip strength (**g**) and running duration (**h**) as in **d** and **e**, respectively. Statistical results are shown as the mean ± s.e.m. Specific numbers of mice used are labelled on each panel. *P* values (shown on the charts) were calculated using two-way ANOVA followed by Tukey's test (**a**,**f**–**h**) or two-sided Student's *t*-test (**b**–**e**). Experiments were performed three times.

and flies (knocking down *AMPKα*) abrogated all the anti-ageing effects of LCA (Fig. 4a–f and Extended Data Fig. 9a,d,e,f,k,m; see validation data in Extended Data Fig. 9p), which indicated that AMPK is necessary for the effects of LCA. Finally, we tested the effect of LCA on mouse lifespan. Mice showed a consistent, albeit nonsignificant, increase in median lifespan (5.1% for male mice and 10.3% for female mice in cohort 1; 9.6%

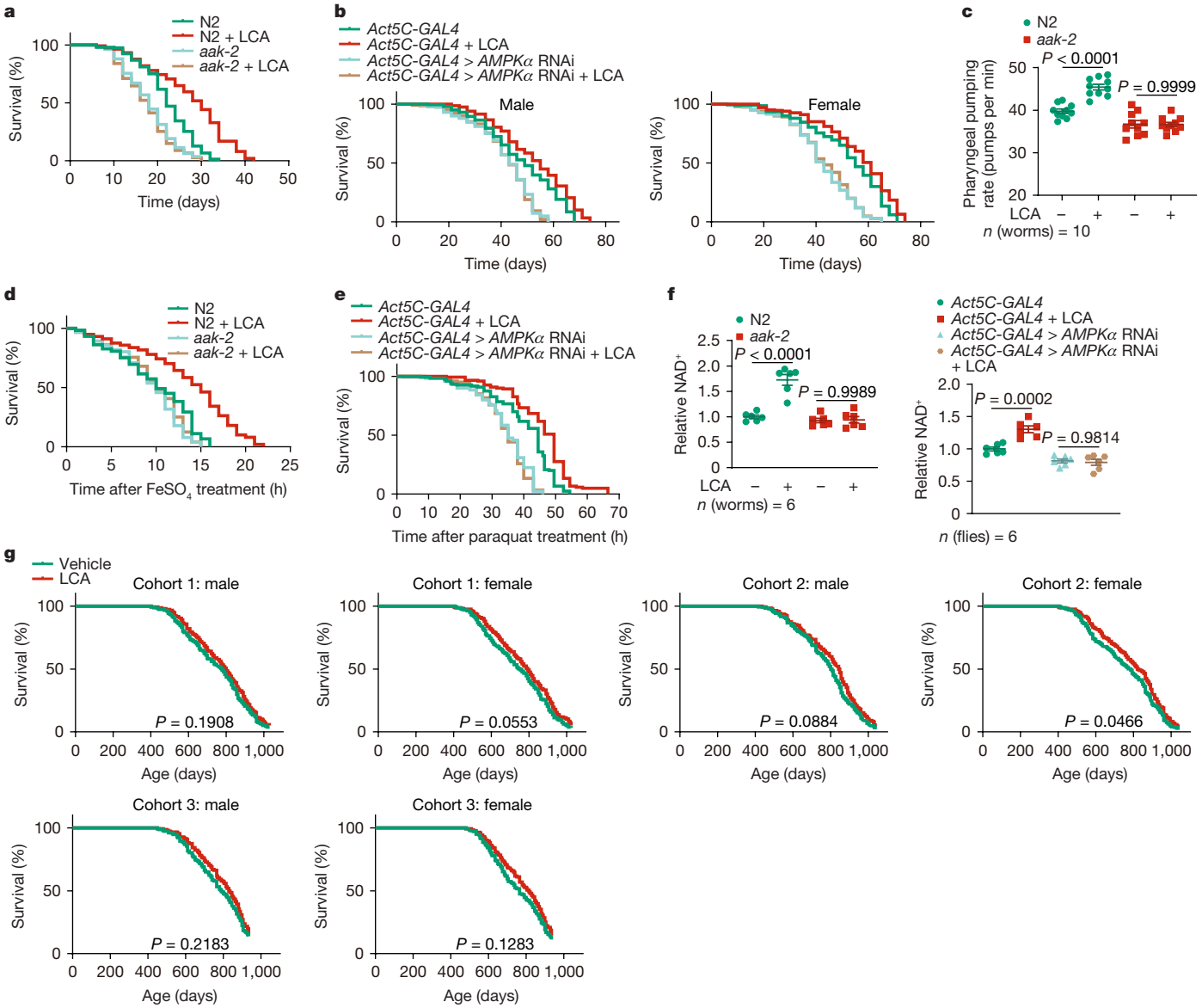

Fig. 4 | LCA extends lifespan and healthspan. a,**b**, LCA extends lifespan in nematodes and flies through AMPK. WT (N2) or *aak-2* knockout nematodes, (**a**) and WT (*Act5C-GAL4*) or *AMPKα* knockdown (*Act5C-GAL4 > AMPKα* RNAi) flies (**b**) were cultured in medium containing LCA at 100 μM, which was capable of activating AMPK as effectively as in mice (Extended Data Fig. 8a–d). Lifespan data are shown as Kaplan–Meier curves (see also statistical analyses data in Supplementary Table 4, and the same hereafter for all lifespan data). **c**, LCA promotes nematode pharyngeal pumping rates in an AMPK-dependent manner. WT or *aak-2* knockout nematodes were treated with LCA for 1 day, followed by determination of pharyngeal pumping rates. **d**,**e**, LCA promotes oxidative stress resistance of nematodes and flies through AMPK. To induce oxidative stress, WT and *aak-2* knockout nematodes (**d**) and WT and *AMPKα* knockdown flies (**e**) were treated with LCA for 2 days (**d**) or 30 days (**e**), followed by transfer to medium containing 15 mM $FeSO_4$ (**d**) or 20 mM paraquat (**e**). Survival curves were derived. **f**, LCA increases NAD^+ levels in nematodes and flies in an AMPK-dependent manner. WT and *aak-2* knockout nematodes (left) and WT and *AMPKα* knockdown flies (right) were treated with LCA as in **d** or **e**, respectively, followed by determination of NAD^+ levels. **g**, Effect of LCA on lifespan in mice. Three cohorts of ad libitum-fed male and female WT mice were fed (2-hydroxypropyl)-β-cyclodextrin-coated LCA at 1 g l^{-1} starting at 52 weeks of age, followed by determination of lifespans. Statistical analysis results are shown as the mean ± s.e.m. Specific numbers of animals used are labelled on each panel. *P* values were calculated using Mantel–Cox tests (**g**, which produced non-significant results) or two-way ANOVA followed by Tukey's test (**c**,**f**). Experiments were performed three times.

for male mice and 8.3% for female mice in cohort 2; and 9.4% for male mice and 12.5% for female mice in cohort 3) when given LCA starting at 1 year of age (Fig. 4g). Therefore, LCA treatment is sufficient to mimic the anti-ageing effects of CR in nematodes, flies and mice.

Discussion

Here we demonstrated that LCA is present in increased concentrations in CR-treated mice, particularly when compared with the post-absorptive state of ad libitum-fed mice. Although there are differences in the composition of bile acids between humans and mice, such as muricholate, which is abundant in mice but hardly detectable in humans (reviewed in ref. 30), the serum concentrations of LCA are similar in both these species[28,29]. In addition, in humanized mice lacking the *Cyp2c* gene cluster, and therefore unable to produce muricholate[32], CR still increased LCA levels in these mice to a similar extent as in wild-type mice (Extended Data Fig. 1l). Notably, LCA was among one of the metabolites that was increased in the serum of healthy humans after 36 h of fasting[54]. As a secondary metabolite of bile acids synthesized in the liver, LCA is produced from the precursors CA and CDCA. These

precursors are secreted from the liver into the intestine, where they are converted to LCA by the gut microbiome, specifically by *Lactobacillus*, *Clostridium* and *Eubacterium* species[55]. These species express bile salt hydrolase and the 7α-dehydroxylase enzymes, which are sequentially responsible for converting CA and CDCA to LCA[55]. Given that these three genera are increased after CR[56,57], it is reasonable to suggest that the LCA increase that occurs during CR may be caused by changes in these gut microbes. Indeed, we observed significantly higher concentrations of LCA in the faeces of CR-treated mice (Extended Data Fig. 10a). This effect was not observed in germ-free mice and in mice in which the gut microbiome was disrupted after treatment with antibiotics (Extended Data Fig. 10b). Furthermore, transplantation of faeces collected from CR-treated mice into germ-free mice and antibiotic-treated mice resulted in a larger increase in LCA than when these mice were transplanted with faeces from ad libitum-fed mice (Extended Data Fig. 10b). In addition, high levels of LCA are found in healthy centenarians who harbour high faecal levels of *Clostridioides*[58]. Consistently, LCA levels in the serum decreased with age in mice (Extended Data Fig. 10c).

We provided multiple lines of evidence to show that LCA acts as a CRM, recapitulating the effects of CR, including AMPK activation and rejuvenating and anti-ageing effects. First, LCA was the only metabolite among the ones we tested that activated AMPK at around 1 μM, a concentration similar to that detected in the serum of CR-treated mice. This concentration is also below (that is, hundreds of micromoles) that which would cause harmful effects such as DNA damage[59,60] or tumour development when combined with other DNA-damaging agents (reviewed in ref. 61). Consistently, 1 μM LCA did not induce the phosphorylation of H2AX[62] or RPA32 (ref. 63), markers of DNA double-strand breaks and DNA single-strand breaks, respectively, in MEFs, primary hepatocytes or primary myocytes treated for up to 48 h (Extended Data Fig. 10d). However, there was a slight increase in phosphorylated H2AX and RPA32 in HEK293T cells when treated with 1 μM LCA for 48 h. This was in contrast to treatment with ultraviolet light, which significantly increased the phosphorylation of H2AX and RPA32 in all cells (Extended Data Fig. 10d). At suprahigh concentrations, other metabolites such as ferulic acid, 4-methyl-2-oxovaleric acid, 1-methyladenosine, methylmalonic acid and mandelic acid activated AMPK (seen in our initial screening assays; Supplementary Table 2). However, the concentrations required for such AMPK activation were too high to be physiologically relevant. In addition, the series of LCA derivatives did not activate AMPK. We noted that a previous study reported that LCA did not activate AMPK in flies[53]. To reconcile this discrepancy, we used the protocol in that study[53] and repeated the experiment to test for AMPK activation by LCA in flies. We still observed AMPK activation by LCA (bottom panels of Extended Data Fig. 8b,c). This discrepancy might be caused by different ways of sample preparation; that is, we routinely froze tissue samples in liquid nitrogen after dissection by freeze-clamping (see the section 'Immunoblotting' in the Methods). Nevertheless, the previous study did observe increased expression of the fly homologue of PGC-1α, a downstream factor of AMPK, in the LCA-treated flies[53], which implies that LCA can activate AMPK in flies. Second, LCA increased the mitochondrial content in muscles of aged mice, which is known to trigger the glycolytic–oxidative fibre type transition[64,65], thereby preserving muscle force and endurance. Moreover, LCA enhanced the ability of muscle cells to regenerate, a hallmark of rejuvenation[66]. This effect is probably due to increases in muscular NAD^+ levels, which is a downstream event of AMPK activation and is a crucial factor for mitochondrial biogenesis[19]. The AMPK-dependent improvement in muscular mitochondrial function also helped ameliorate age-associated insulin resistance that may be caused by increased inflammation and oxidative stress due to impaired mitochondrial function[67]. Along with the observed rejuvenating effects, we observed an increase in median lifespans in male and female mice to a similar extent to that by other AMPK activators such as aldometanib[68]. However, the *P* values for the LCA-mediated extension of mouse lifespan data are larger than 0.05 (Fig. 4g; except for the female mice of cohort 2, $P = 0.0466$) and is therefore considered not significant. However, the requirement of $P < 0.05$ for significance has been challenged (see the section 'Statistical analysis' in the Methods). It is also important to note that the survival curves of mice presented here were obtained using a specific dose administered at a particular age. It is possible that LCA will show greater effects on lifespan extension if administered at different doses and at different ages. Third, we demonstrated that AMPK activation is required for LCA to extend lifespan, as assessed in nematodes and flies, consistent with reports that CR can induce AMPK activation and lifespan extension in nematodes[16,17] and flies[52]. Given that nematodes and flies are not capable of synthesizing LCA de novo, it is reasonable to speculate that these two animal models possess similar LCA-sensing and downstream machineries that can transmit LCA signalling to activate AMPK and therefore extend lifespan. Indeed, as explored in a companion paper[69], nematodes and flies have conserved LCA receptors that are similar to mammalian ones. We demonstrated that LCA activates AMPK by intersecting the conserved lysosomal AMPK pathway through v-ATPase, a crucial node for AMPK activation after sensing low glucose[70], or by metformin[71]. These findings imply that nematodes and flies might have compounds that are structural mimetics of LCA and can act as ligands with sufficient affinities for LCA receptors. In addition to the beneficial effects of LCA treatment in metazoans, LCA can extend the chronological lifespan in yeast[72–74]. It is noteworthy that the effects of LCA in yeast are not attributed to AMPK activation, as LCA can only extend yeast lifespan under glucose-restriction conditions, when Snf1 (the yeast homologue of AMPK) is already activated[75]. In addition, yeast do not have the lysosomal AMPK pathway. Instead, LCA regulates lifespan in yeast by affecting lipid and carbohydrate catabolism, mitochondrial morphology and apoptotic cell death[72–74].

An adverse effect of CR is muscle loss, which may be due to the prolonged need for amino acid supplementation from muscle mass during CR[6,45]. For example, during CR, AMPK in muscle can enhance muscle protein breakdown to supply the glucose–alanine cycle[76] through mechanisms such as autophagy[77]. Here we showed that administration of LCA to ad libitum-fed mice prevented such an effect of muscle loss owing to normal food intake, although LCA could also lead to AMPK activation in muscle. Supporting this notion, it has been shown that activation of AMPK by the activators aldometanib[68], AICAR[78] or O304 (ref. 79) did not lead to any muscle loss in ad libitum-fed mice. Furthermore, LCA even increased food intake (Extended Data Fig. 10e) and energy intake, as calculated by subtracting the energy content of the food consumed from the energy content in the faeces of LCA-treated mice (Extended Data Fig. 10f). Thus, LCA, a natural metabolite, does not cause the adverse effects of muscle loss observed with CR, thereby providing a better means to improve healthspan compared with the practice of CR. In addition, the benefits manifested by LCA treatment under ad libitum feeding conditions imply that the energy deficit that occurs during CR, which affects metabolic rates and hormone levels, may not be required to attain the benefits of CR.

It is important to note that we chose increases in pAMPKα(T172) and pACC levels as criteria for screening AMPK activators in CR serum. There may be other as yet unidentified metabolites that activate AMPK without changing these two factors. For example, the compound A-769662 activates AMPK but does not increase pAMPKα(T172) levels[80], and etoposide activates AMPK without affecting pACC levels[81]. In summary, we identified LCA as a CR-induced metabolite that can phenocopy the effects of CR in an AMPK-dependent manner.

Online content

Any methods, additional references, Nature Portfolio reporting summaries, source data, extended data, supplementary information,

acknowledgements, peer review information; details of author contributions and competing interests; and statements of data and code availability are available at https://doi.org/10.1038/s41586-024-08329-5.

1. Speakman, J. R. & Mitchell, S. E. Caloric restriction. *Mol. Aspects Med.* **32**, 159–221 (2011).
2. Fontana, L., Partridge, L. & Longo, V. D. Extending healthy life span-from yeast to humans. *Science* **328**, 321–326 (2010).
3. Selman, C. et al. Coordinated multitissue transcriptional and plasma metabonomic profiles following acute caloric restriction in mice. *Physiol. Genomics* **27**, 187–200 (2006).
4. Edwards, C. et al. D-β-hydroxybutyrate extends lifespan in *C. elegans*. *Aging* **6**, 621–644 (2014).
5. Youm, Y. H. et al. The ketone metabolite β-hydroxybutyrate blocks NLRP3 inflammasome-mediated inflammatory disease. *Nat. Med.* **21**, 263–269 (2015).
6. Most, J., Tosti, V., Redman, L. M. & Fontana, L. Calorie restriction in humans: an update. *Ageing Res. Rev.* **39**, 36–45 (2017).
7. Goodrick, C. L., Ingram, D. K., Reynolds, M. A., Freeman, J. R. & Cider, N. L. Effects of intermittent feeding upon growth and life span in rats. *Gerontology* **28**, 233–241 (1982).
8. Brandhorst, S. et al. A periodic diet that mimics fasting promotes multi-system regeneration, enhanced cognitive performance, and healthspan. *Cell Metab.* **22**, 86–99 (2015).
9. Roberts, M. N. et al. A ketogenic diet extends longevity and healthspan in adult mice. *Cell Metab.* **26**, 539–546.e5 (2017).
10. Newman, J. C. et al. Ketogenic diet reduces midlife mortality and improves memory in aging mice. *Cell Metab.* **26**, 547–557.e8 (2017).
11. Tomita, I. et al. Ketone bodies: a double-edged sword for mammalian life span. *Aging Cell* **22**, e13833 (2023).
12. Hardie, D. G. AMP-activated/SNF1 protein kinases: conserved guardians of cellular energy. *Nat. Rev. Mol. Cell Biol.* **8**, 774–785 (2007).
13. Shinmura, K., Tamaki, K. & Bolli, R. Short-term caloric restriction improves ischemic tolerance independent of opening of ATP-sensitive K^+ channels in both young and aged hearts. *J. Mol. Cell. Cardiol.* **39**, 285–296 (2005).
14. Burkewitz, K., Zhang, Y. & Mair, W. B. AMPK at the nexus of energetics and aging. *Cell Metab.* **20**, 10–25 (2014).
15. Inoki, K., Zhu, T. & Guan, K. L. TSC2 mediates cellular energy response to control cell growth and survival. *Cell* **115**, 577–590 (2003).
16. Apfeld, J., O'Connor, G., McDonagh, T., Distefano, P. S. & Curtis, R. The AMP-activated protein kinase AAK-2 links energy levels and insulin-like signals to lifespan in *C. elegans*. *Genes Dev.* **18**, 3004–3009 (2004).
17. Greer, E. L. et al. An AMPK–FOXO pathway mediates longevity induced by a novel method of dietary restriction in *C. elegans*. *Curr. Biol.* **17**, 1646–1656 (2007).
18. Kenyon, C., Chang, J., Gensch, E., Rudner, A. & Tabtiang, R. A *C. elegans* mutant that lives twice as long as wild type. *Nature* **366**, 461–464 (1993).
19. Canto, C. et al. AMPK regulates energy expenditure by modulating NAD^+ metabolism and SIRT1 activity. *Nature* **458**, 1056–1060 (2009).
20. Mair, W. et al. Lifespan extension induced by AMPK and calcineurin is mediated by CRTC-1 and CREB. *Nature* **470**, 404–408 (2011).
21. Young, N. P. et al. AMPK governs lineage specification through Tfeb-dependent regulation of lysosomes. *Genes Dev.* **30**, 535–552 (2016).
22. Onken, B. & Driscoll, M. Metformin induces a dietary restriction-like state and the oxidative stress response to extend *C. elegans* healthspan via AMPK, LKB1, and SKN-1. *PLoS ONE* **5**, e8758 (2010).
23. Howitz, K. T. et al. Small molecule activators of sirtuins extend *Saccharomyces cerevisiae* lifespan. *Nature* **425**, 191–196 (2003).
24. de Cabo, R. et al. An in vitro model of caloric restriction. *Exp. Gerontol.* **38**, 631–639 (2003).
25. Mallia, A. K., Smith, P. K. & Hermanson, G. T. *Immobilized Affinity Ligand Techniques* (Elsevier Science, 1992).
26. Psychogios, N. et al. The human serum metabolome. *PLoS ONE* **6**, e16957 (2011).
27. Ling, N. X. Y. et al. mTORC1 directly inhibits AMPK to promote cell proliferation under nutrient stress. *Nat. Metab.* **2**, 41–49 (2020).
28. Zhao, A. et al. Comprehensive characterization of bile acids in human biological samples and effect of 4-week strawberry intake on bile acid composition in human plasma. *Metabolites* **11**, 99 (2021).
29. Li, M. et al. Gut microbiota–bile acid crosstalk contributes to the rebound weight gain after calorie restriction in mice. *Nat. Commun.* **13**, 2060 (2022).
30. Russell, D. W. The enzymes, regulation, and genetics of bile acid synthesis. *Annu. Rev. Biochem.* **72**, 137–174 (2003).
31. Hu, X., Bonde, Y., Eggertsen, G. & Rudling, M. Muricholic bile acids are potent regulators of bile acid synthesis via a positive feedback mechanism. *J. Intern. Med.* **275**, 27–38 (2014).
32. Scheer, N. et al. Generation and characterization of novel cytochrome P450 *Cyp2c* gene cluster knockout and CYP2C9 humanized mouse lines. *Mol. Pharmacol.* **82**, 1022–1029 (2012).
33. Carling, D., Zammit, V. A. & Hardie, D. G. A common bicyclic protein kinase cascade inactivates the regulatory enzymes of fatty acid and cholesterol biosynthesis. *FEBS Lett.* **223**, 217–222 (1987).
34. Fu, D., Wakabayashi, Y., Lippincott-Schwartz, J. & Arias, I. M. Bile acid stimulates hepatocyte polarization through a cAMP–Epac–MEK–LKB1–AMPK pathway. *Proc. Natl Acad. Sci. USA* **108**, 1403–1408 (2011).
35. Miko, E. et al. Lithocholic acid, a bacterial metabolite reduces breast cancer cell proliferation and aggressiveness. *Biochim. Biophys. Acta Bioenerg.* **1859**, 958–974 (2018).
36. Li, Z. et al. Dual targeting of bile acid receptor-1 (TGR5) and farnesoid X receptor (FXR) prevents estrogen-dependent bone loss in mice. *J. Bone Miner. Res.* **34**, 765–776 (2019).
37. Hawley, S. A. et al. Calmodulin-dependent protein kinase kinase-β is an alternative upstream kinase for AMP-activated protein kinase. *Cell Metab.* **2**, 9–19 (2005).
38. Woods, A. et al. $Ca2^+$/calmodulin-dependent protein kinase kinase-β acts upstream of AMP-activated protein kinase in mammalian cells. *Cell Metab.* **2**, 21–33 (2005).
39. Hurley, R. L. et al. The Ca^{2+}/calmoldulin-dependent protein kinase kinases are AMP-activated protein kinase kinases. *J. Biol. Chem.* **280**, 29060–29066 (2005).
40. Cokorinos, E. C. et al. Activation of skeletal muscle AMPK promotes glucose disposal and glucose lowering in non-human primates and mice. *Cell Metab.* **25**, 1147–1159.e10 (2017).
41. Bodine, S. C. et al. Identification of ubiquitin ligases required for skeletal muscle atrophy. *Science* **294**, 1704–1708 (2001).
42. Sandri, M. et al. Foxo transcription factors induce the atrophy-related ubiquitin ligase atrogin-1 and cause skeletal muscle atrophy. *Cell* **117**, 399–412 (2004).
43. Mitchell, S. E. et al. The effects of graded levels of calorie restriction: I. impact of short term calorie and protein restriction on body composition in the C57BL/6 mouse. *Oncotarget* **6**, 15902–15930 (2015).
44. Ham, D. J. et al. Distinct and additive effects of calorie restriction and rapamycin in aging skeletal muscle. *Nat. Commun.* **13**, 2025 (2022).
45. Dirks, A. J. & Leeuwenburgh, C. Caloric restriction in humans: potential pitfalls and health concerns. *Mech. Ageing Dev.* **127**, 1–7 (2006).
46. Seale, P. et al. Pax7 is required for the specification of myogenic satellite cells. *Cell* **102**, 777–786 (2000).
47. Thomas, C. et al. TGR5-mediated bile acid sensing controls glucose homeostasis. *Cell Metab.* **10**, 167–177 (2009).
48. Wei, M. et al. A dysregulated bile acid–gut microbiota axis contributes to obesity susceptibility. *eBioMedicine* **55**, 102766 (2020).
49. Tamai, Y. et al. Association of lithocholic acid with skeletal muscle hypertrophy through TGR5–IGF-1 and skeletal muscle mass in cultured mouse myotubes, chronic liver disease rats and humans. *eLife* **11**, e80638 (2022).
50. Klass, M. R. Aging in the nematode *Caenorhabditis elegans*: major biological and environmental factors influencing life span. *Mech. Ageing Dev.* **6**, 413–429 (1977).
51. Chippindale, A. K., Leroi, A. M., Kim, S. B. & Rose, M. R. Phenotypic plasticity and selection in *Drosophila* life-history evolution. 1. Nutrition and the cost of reproduction. *J. Evol. Biol.* **6**, 171–193 (1993).
52. Johnson, E. C. et al. Altered metabolism and persistent starvation behaviors caused by reduced AMPK function in *Drosophila*. *PLoS ONE* **5**, e12799 (2010).
53. Staats, S. et al. Lithocholic acid improves the survival of *Drosophila melanogaster*. *Mol. Nutr. Food Res.* **62**, e1800424 (2018).
54. Fiamoncini, J. et al. Dynamics and determinants of human plasma bile acid profiles during dietary challenges. *Front. Nutr.* **9**, 932937 (2022).
55. Cai, J., Rimal, B., Jiang, C., Chiang, J. Y. L. & Patterson, A. D. Bile acid metabolism and signaling, the microbiota, and metabolic disease. *Pharmacol. Ther.* **237**, 108238 (2022).
56. Fraumene, C. et al. Caloric restriction promotes rapid expansion and long-lasting increase of *Lactobacillus* in the rat fecal microbiota. *Gut Microbes* **9**, 104–114 (2018).
57. Damms-Machado, A. et al. Effects of surgical and dietary weight loss therapy for obesity on gut microbiota composition and nutrient absorption. *BioMed Res. Int.* **2015**, 806248 (2015).
58. Sato, Y. et al. Novel bile acid biosynthetic pathways are enriched in the microbiome of centenarians. *Nature* **599**, 458–464 (2021).
59. Goldberg, A. A. et al. Lithocholic bile acid selectively kills neuroblastoma cells, while sparing normal neuronal cells. *Oncotarget* **2**, 761–782 (2011).
60. Luu, T. H. et al. Lithocholic bile acid inhibits lipogenesis and induces apoptosis in breast cancer cells. *Cell Oncol.* **41**, 13–24 (2018).
61. Rezen, T. et al. The role of bile acids in carcinogenesis. *Cell. Mol. Life Sci.* **79**, 243 (2022).
62. Rogakou, E. P., Pilch, D. R., Orr, A. H., Ivanova, V. S. & Bonner, W. M. DNA double-stranded breaks induce histone H2AX phosphorylation on serine 139. *J. Biol. Chem.* **273**, 5858–5868 (1998).
63. Nuss, J. E. et al. DNA damage induced hyperphosphorylation of replication protein A. 1. Identification of novel sites of phosphorylation in response to DNA damage. *Biochemistry* **44**, 8428–8437 (2005).
64. Boreham, C. A. et al. Effects of ageing and chronic dietary restriction on the morphology of fast and slow muscles of the rat. *J. Anat.* **157**, 111–125 (1988).
65. Lin, J. et al. Transcriptional co-activator PGC-1α drives the formation of slow-twitch muscle fibres. *Nature* **418**, 797–801 (2002).
66. Lopez-Otin, C., Blasco, M. A., Partridge, L., Serrano, M. & Kroemer, G. Hallmarks of aging: an expanding universe. *Cell* **186**, 243–278 (2023).
67. Petersen, K. F. et al. Mitochondrial dysfunction in the elderly: possible role in insulin resistance. *Science* **300**, 1140–1142 (2003).
68. Zhang, C. S. et al. The aldolase inhibitor aldometanib mimics glucose starvation to activate lysosomal AMPK. *Nat. Metab.* **4**, 1369–1401 (2022).
69. Qu, Q. et al. Lithocholic acid binds TULP3 to activate sirtuins and AMPK to retard ageing. *Nature* https://doi.org/10.1038/s41586-024-08348-2 (2024).
70. Li, M. et al. Transient receptor potential V channels are essential for glucose sensing by aldolase and AMPK. *Cell Metab.* **30**, 508–524.e12 (2019).
71. Zhang, C. S. et al. Metformin activates AMPK through the lysosomal pathway. *Cell Metab.* **24**, 521–522 (2016).
72. Goldberg, A. A. et al. Chemical genetic screen identifies lithocholic acid as an anti-aging compound that extends yeast chronological life span in a TOR-independent manner, by modulating housekeeping longevity assurance processes. *Aging* **2**, 393–414 (2010).
73. Burstein, M. T. et al. Lithocholic acid extends longevity of chronologically aging yeast only if added at certain critical periods of their lifespan. *Cell Cycle* **11**, 3443–3462 (2012).
74. Arlia-Ciommo, A. et al. Mechanisms through which lithocholic acid delays yeast chronological aging under caloric restriction conditions. *Oncotarget* **9**, 34945–34971 (2018).
75. Woods, A. et al. Yeast SNF1 is functionally related to mammalian AMP-activated protein kinase and regulates acetyl-CoA carboxylase in vivo. *J. Biol. Chem.* **269**, 19509–19515 (1994).
76. Felig, P., Pozefsky, T., Marliss, E. & Cahill, G. F. Jr Alanine: key role in gluconeogenesis. *Science* **167**, 1003–1004 (1970).

77. Bujak, A. L. et al. AMPK activation of muscle autophagy prevents fasting-induced hypoglycemia and myopathy during aging. *Cell Metab.* **21**, 883–890 (2015).
78. Narkar, V. A. et al. AMPK and PPARδ agonists are exercise mimetics. *Cell* **134**, 405–415 (2008).
79. Lopez-Perez, A. et al. Pan-AMPK activator O304 prevents gene expression changes and remobilisation of histone marks in islets of diet-induced obese mice. *Sci. Rep.* **11**, 24410 (2021).
80. Goransson, O. et al. Mechanism of action of A-769662, a valuable tool for activation of AMP-activated protein kinase. *J. Biol. Chem.* **282**, 32549–32560 (2007).
81. Vara-Ciruelos, D. et al. Genotoxic damage activates the AMPK-α1 isoform in the nucleus via Ca^{2+}/CaMKK2 signaling to enhance tumor cell survival. *Mol. Cancer Res.* **16**, 345–357 (2018).

Methods

Data reporting

The chosen sample sizes were similar to those used in the field: $n = 4–12$ samples were used to evaluate the levels of metabolites in serum[82,83], cells[68,84], tissues[68,84–86], nematodes[87–89] and flies[90–92]; $n = 4–10$ samples to determine OCRs in tissues[68,93] and nematodes[94–96]; $n = 3–4$ samples to determine mRNA levels of a specific gene[97,98]; $n = 2–6$ samples to determine the expression levels and phosphorylation levels of a specific protein[97]; $n = 200$ worms to determine lifespan[99–101]; $n = 60$ worms to determine healthspan[102–104], except $n = 10$ worms for pharyngeal pumping rates[68,105]; $n = 200$ flies, male or female, to determine lifespan[106–108]; $n = 60$ flies, male or female, to determine healthspan[109–111]; $n = 4–8$ mice for energy expenditure (EE) and respiratory quotients[68]; $n = 10$ mice for hyperinsulinaemic–euglycaemic clamping[68,112]; $n = 5–6$ mice for glucose tolerance tests and insulin tolerance tests[68]; $n = 6$ mice for body composition[68]; $n = 6$ mice for muscle fibre type[44,113,114]; $n = 3$ mice for muscle regeneration[104,115,116]; $n = 53–62$ mitochondria from 3 mice for muscular mitochondrial content[117,118]; $n = 9–23$ mice for running duration[68,70]; and $n = 36–75$ mice for grasp strength[68]. No statistical methods were used to predetermine the sample sizes. All experimental findings were repeated as stated in the figure legends, and all additional replication attempts were successful. For animal experiments, mice, nematodes and flies were housed under the same conditions or places. For cell experiments, cells of each genotype were cultured in the same CO_2 incubator and were parallel seeded. Each experiment was designed and performed along with proper controls, and samples for comparison were collected and analysed under the same conditions. Randomization was applied wherever possible. For example, during MS analyses, samples were processed and subjected to MS in random orders. For animal experiments, sex-matched (for mice and flies) and age-matched littermate animals for each genotype were randomly assigned to LCA or vehicle treatments. In cell experiments, cells of each genotype were seeded in parallel and randomly assigned to different treatments. Otherwise, randomization was not performed. For example, when performing IB, samples needed to be loaded in a specific order to generate the final figures. Blinding was applied wherever possible. For example, samples, cages or agar plates or vials during sample collection and processing were labelled as code names that were later revealed by the individual who picked and treated animals or cells but did not participate in sample collection and processing until assessing the outcome. Similarly, during microscopy data collection and statistical analyses, the fields of view were chosen on a random basis and were often performed by different operators, which prevented potentially biased selection for desired phenotypes. Otherwise, blinding was not performed, such as the measurement of OCRs, as different reagents were added for particular reactions.

Mouse strains

WT C57BL/6J mice (000664) were obtained from the Jackson Laboratory. *AXIN*$^{F/F}$ and *LAMTOR1*$^{F/F}$ mice were generated and validated as previously described[97]. *AMPKA1*$^{F/F}$ (014141) and *AMPKA2*$^{F/F}$ mice (014142) were obtained from the Jackson Laboratory, provided by S. Morrison. AMPKα-MKO mice were generated by crossing *AMPKA1/2*$^{F/F}$ mice with *Mck-Cre* mice, as previously described and validated[68]. *Cyp2c* cluster KO mice (NM-KO-18019) were purchased from Shanghai Model Organisms Center, and *Tgr5* KO mice (S-KO-06069) were from Cyagen. Germ-free C57BL/6J mice were provided by the Laboratory Animal Research Centre of Xiamen University.

The antibiotic-treated mice were generated by exposing C57BL/6J mice to a combination of antibiotics, including 0.5 g l^{-1} vancomycin, 1 g l^{-1} metronidazole, 1 g l^{-1} ampicillin and 1 g l^{-1} neomycin supplemented in their drinking water (ad libitum) for 5 days. The depletion of gut microbiota was confirmed by testing for the presence of bacterial 16S rDNA in the faeces using PCR. About 100 mg of faeces was freshly collected, followed by extraction of bacterial DNA using a TIANamp Stool DNA kit following the manufacturer's instructions. 16S rDNA was amplified using Quick-Load Taq 2× master mix on a thermocycler (T100, Bio-Rad) using the universal bacterial 16S rRNA primers 27F and 1492R[119] (5′-AGAGTTTGATCCTGGCTCAG-3′ and 5′-TACGGCTACCTTGTTACGACTT-3′) with the following programs: pre-denaturing at 95 °C for 30 s; denaturing at 95 °C for 10 s, annealing at 55 °C for 30 s, then extending at 72 °C for 90 s in each cycle; and final extending at 72 °C for 10 min; cycle number: 29. Mice that tested negative for bacterial 16S rRNA were selected for further experiments.

For analysing AMPK activation, WT mice and AMPKα-MKO mice aged 4 weeks were given LCA for 1 week, and WT mice aged 4 months were subjected to CR for 4 months. For determining rejuvenating effects of LCA or iso-LCA, WT, AMPKα-MKO and *Tgr5*$^{-/-}$ mice aged 17 months were treated with LCA or iso-LCA for 1 month. For determining rejuvenating effects of CR, WT mice aged 17 months were subjected to CR for 3.5 months. For analysing the pharmacokinetics of LCA, WT mice aged 17 months (aged mice) were treated with LCA for 1 month. For determining the changes in LCA concentrations in serum and tissue, WT and *Cyp2c*-null mice aged 4 months old were subjected to CR for 4 months, germ-free mice aged 4 months were gavaged with faeces for 1 week and were ad libitum-fed for another 3 weeks, and antibiotic-treated mice aged 4 months were subjected for CR for 3.5 months (except in Fig. 2c, in which mice were subjected to CR for the indicated time durations starting from 4 months old). For determination of the serum metabolome in CR mice, WT mice aged 4 months were subjected to CR for 4 months. For isolating primary hepatocytes and myocytes, WT mice aged 1 month were used.

In this study, the following experiments and measurements were performed using the same group of mice: (1) body weight and body composition, grip strength, EE and running duration; (2) muscle regeneration; (3) mitochondrial content; (4) muscle fibre types; (5) hyperinsulinaemic–euglycaemic clamp tests; (6) intraperitoneal glucose tolerance tests (GTTs) and insulin content; (7) intraperitoneal insulin tolerance tests (ITTs); (8) oral GTTs and GLP-1 measurement; (9) muscular OCRs; (10) muscle weight and muscular mitochondrial mRNA levels; (11) IB; (12) NAD^+ levels and mtDNA-to-nDNA ratios; (13) AMP-to-ATP and ADP-to-ATP ratios; and (14) LCA content.

CR, fasting and cardiotoxin treatment of mice

Protocols for all mouse experiments were approved by the Institutional Animal Care and the Animal Committee of Xiamen University (XMULAC20180028 and XMULAC20220050). Mice were housed with free access to water and a standard diet (65% carbohydrate, 11% fat, 24% protein) under specific pathogen-free (SPF) conditions, except for germ-free mice, which were house in a sterile isolator. The light was on from 8:00 to 20:00, with the temperature kept at 21–24 °C and humidity at 40–70%. Male mice were used in this study, except in the experiments shown in Fig. 3c–e and Extended Data Figs. 3a,c,e,f and 4c–e, in which female mice were also used. Littermate controls were used throughout the study.

Mice were individually caged for 1 week before each treatment. For fasting, the diet was withdrawn from the cage at 17:00, and mice were euthanized at specific time points by cervical dislocation. For CR, each mouse was fed 2.5 g of standard diet (approximately 70% of ad libitum food intake for a mouse at 4 months old and older) at 17:00 each day. To perform CR in germ-free conditions, mice were housed in a sterile isolator. Cardiotoxin treatment was performed as previously described[104]. In brief, mice were anaesthetized with 3% isoflurane in the air using a vaporizer (R540, RWD Life Science). After removal of fur, 50 μl of 20 μM cardiotoxin was intramuscularly injected into the tibialis anterior muscle. Muscles were analysed on day 7 after cardiotoxin injection.

Evaluation of mouse lifespan

Mouse lifespan was determined according to previous reports[68,120]. In brief, mice were examined every 3–5 days for signs of illness, and

the severely moribund ones were killed and recorded. A mouse was considered severely moribund if it showed more than one of the following clinical signs: (1) inability to eat or to drink; (2) severe lethargy, as indicated by lack of response such as reluctance to move when gently prodded with a blunt-tip tweezer; (3) severe balance instability or gait disturbance; (4) rapid weight loss (>3 g) over a period of 1 week; or (5) a severely ulcerated or bleeding tumour. Mice found dead were also noted at each daily inspection.

In Fig. 4g and Supplementary Table 4, cohort 1 started with a total of 679 mice (born around November 2021): 338 males (168 in the vehicle group; 170 in LCA-treatment group) and 341 females (169 in the vehicle group; 172 in the LCA-treatment group). As the experiment progressed, 37 mice were removed (censored) from the study: 25 males (11 vehicle; 14 LCA) and 12 females (8 vehicle; 4 LCA). The reasons for removal included fighting (18 males: 8 vehicle; 10 LCA), paralysis (loss of walking ability; 6 males: 3 vehicle; 3 LCA; and 10 female: 7 vehicle; 3 LCA), and symptoms of gnawing or bruxing (the presence of long, spiral incisors preventing the mouse from eating; 1 male from LCA; and 2 female: 1 vehicle and 1 LCA). Such censored mice were not included in the calculation of lifespan. At the conclusion of the experiment, 14 male mice (6 vehicle; 8 LCA) and 14 female mice (5 vehicle; 9 LCA) were still alive. Cohort 2 started with 687 mice (born around November 2021): 331 males (168 in the vehicle group; 163 in the LCA-treatment group) and 356 females (176 in the vehicle group; 180 in the LCA-treatment group). As the experiment progressed, 56 mice were removed (censored) from the study: 43 males (24 vehicle; 19 LCA) and 13 females (5 vehicle; 8 LCA). The reasons for removal included fighting (35 males: 20 vehicle; 15 LCA) and paralysis (8 males: 4 vehicle; 4 LCA; and 13 females: 5 vehicle; 8 LCA). Such censored mice were not included in the calculation of lifespan. At the conclusion of the experiment, 13 male mice (5 vehicle; 8 LCA) and 13 female mice (5 vehicle; 8 LCA) were still alive. Cohort 3 was started with 622 mice (born around January 2022): 328 males (164 in the vehicle group; 164 in the LCA-treated group) and 294 females (147 in the vehicle group; 147 in the LCA-treated group). As the experiment progressed, 33 mice were removed (censored) from the study: 24 males (12 vehicle; 12 LCA) and 9 females (6 vehicle; 3 LCA). The reasons for removal included fighting (17 males: 10 vehicle; 7 LCA), paralysis (5 males: 2 vehicle; 3 LCA; and 8 females: 5 vehicle; 3 LCA), and symptoms of gnawing or bruxing (2 males from LCA, and 1 female mouse from vehicle). Such censored mice were not included in the calculation of lifespan. At the conclusion of the experiment, 44 male mice (21 vehicle; 23 LCA) and 37 female mice (16 vehicle; 21 LCA) were still alive.

Mouse faecal microbiota transplantation

The faecal transplantation experiment was performed as previously described[121,122]. In brief, freshly collected faeces from SPF mice were homogenized in sterilized, deoxygenated PBS (prepared by incubating sterilized PBS in an anaerobic incubator supplemented with (v/v) 80% N_2, 10% H_2 and 10% CO_2, for 72 h) at a ratio of 100 mg faeces per ml of PBS, followed by centrifuging for 5 min at 200*g*. The supernatant was given to antibiotic-treated or germ-free mice by gavage every 2 days during the first week and then every 3 days during weeks 2 and 3, with each mouse receiving 200 µl. Note that the recipient mice received faeces from CR-treated mice, and ad libitum-fed mice were housed separately in different cages or sterile insulators. At the end of week 8, the mice were euthanized for analysis of LCA content.

Formulation and LCA treatment

For cell-based experiments, LCA powder was dissolved in DMSO to a stock concentration of 500 mM, aliquoted and stored at −20 °C. The solution was placed at room temperature for 10 min (until no precipitate was visible) before adding to the culture medium. Note that any freeze–thaw cycle was prohibited to avoid the re-crystallization of LCA (which otherwise formed sheet-like, insoluble crystals) in the stock solution.

For mouse experiments, LCA was coated with (2-hydroxypropyl)-β-cyclodextrin before given to animals. To coat LCA, LCA powder was dissolved in 100 ml methanol to a concentration of 0.01 g ml^{-1}, followed by mixing with 308 ml (2-hydroxypropyl)-β-cyclodextrin solution (by dissolving (2-hydroxypropyl)-β-cyclodextrin in 30% (v/v, in water) methanol to 0.04 g ml^{-1}, followed by 30 min of sonication). The control vehicle was similarly prepared but with no LCA added to the (2-hydroxypropyl)-β-cyclodextrin solution. After evaporating at 50 °C, 90 r.p.m. in a rotary evaporator (Rotavator R-300, Vacuum Pump V-300, BUCHI), the coated powder was stored at 4 °C for no more than 2 weeks and was freshly dissolved in drinking water to 1 g l^{-1} before given to mice.

For nematode experiments, LCA at desired concentrations was freshly dissolved in DMSO and was added to warm (cooled to approximately 60 °C after autoclaving) nematode growth medium[123] (NGM; containing 0.3% (w/v) NaCl, 0.25% (w/v) bacteriological peptone, 1 mM $CaCl_2$, 1 mM $MgSO_4$, 25 mM KH_2PO_4-K_2HPO_4, pH 6.0, 0.02% (w/v) streptomycin and 5 µg ml^{-1} cholesterol). The medium was used to make NGM plates by adding 1.7% (w/v) agar. The plates were stored at 20 °C for no more than 3 days.

For fly experiments, LCA was coated and dissolved in water as for the mouse experiments, and was added to Bloomington *Drosophila* Stock Center (BDSC) standard cornmeal medium[124] (for regular culture), to 2% cornmeal–sugar–yeast (CSY) agar diet (for CR experiments; see ref. 106) or to 3% CSY agar diet (the control diet for CR experiments). The BDSC standard cornmeal medium was prepared as previously described[124] but with minor modification. In brief, 60.5 g dry yeast, 35 g soy flour, 255.5 g cornmeal, 20 g agar and 270 ml corn syrup were mixed with 3,500 ml water in a stockpot. The mixture was thoroughly stirred using a long-handled soup spoon and then boiled, during which lumps that formed were pressed out using the back of the spoon. After cooling to approximately 60 °C, 16.8 ml propionic acid was added to the medium followed by stirring with the spoon. The 2% or 3% CSY agar diets were prepared as for the BDSC standard cornmeal medium, except that 175 g cornmeal, 367.5 g sucrose, 70 (for 2% CSY agar diet) or 105 g (for 3% CSY agar diet) dry yeast, 24.5 g of agar, 16.8 ml propionic acid and 3,500 ml water were used. The medium was then dispensed into culture vials (6 ml each). The vials of medium were covered with a single-layer gauze, followed by blowing with the breeze from a fan at room temperature overnight. Next, 100 µl LCA solution (coated with (2-hydroxypropyl)-β-cyclodextrin) at the desired concentration was then layered (added dropwise) onto the surface of the medium of each vial, followed by blowing with the breeze from the fan for another 8 h at room temperature. The vials of medium were kept at 4 °C (for no more than 3 days) before experiment.

Determination of mouse running capacity and grip strength

The maximal running capacity was determined as previously described[70,125], but with minor modifications. In brief, mice were trained on a Rodent Treadmill NG (UGO Basile, 47300) for 3 days during the normal light–dark cycle, and tests were performed during the dark period. Before the experiment, mice were fasted for 2 h. The treadmill was set at a 5° incline, and the speed of the treadmill was set to increase in a ramp mode (commencing at a speed of 5 m min^{-1} followed by an increase to a final speed of 25 m min^{-1} within 120 min). Mice were considered exhausted and removed from the treadmill following the accumulation of 5 or more shocks (0.1 mA) per min for 2 consecutive minutes. The distances travelled and the endurance were recorded as the running capacity. Note that mice subjected to the test for running capacity were euthanized and no longer used for other experiments.

Grip strength was determined using a grip strength meter (Ugo Basile, 47200) following a previously described protocol[104]. In brief, the mouse was held by its tail and lowered (landed) until the forelimb or all four limbs grasped the T-bar connected to a digital force gauge. The mouse was further lowered to such an extent that the body was

horizontal to the apparatus, and was then slowly, steadily drawn away from the T-bar until the forelimb or all four limbs were removed from the bar, which gave rise to the peak force in grams. Each mouse was tested 5 times, with 5-min intervals between measurements. Note that the grip strength of the forelimb and four limbs were measured on different days to prevent interference from muscle tiredness caused by earlier measurements.

Serology, GTT and ITT

GTTs and ITTs were performed as previously described[68]. Before GTTs and ITTs, mice were individually caged for 1 week before the experiment. For GTTs, mice were fasted for 16 h (17:00 to 9:00) then administered with glucose at 2 g kg^{-1} (intraperitoneally injected or orally gavaged). For ITTs, mice were fasted for 6 h (8:00 to 14:00), then 0.5 U kg^{-1} insulin was intraperitoneally injected. Blood glucose was then measured at indicated time points through tail vein bleeding using a OneTouch UltraVue automatic glucometer (LifeScan). Note that GTTs and ITTs were performed using different batches of mice to avoid interference from any stress caused by earlier blood collection.

For measuring insulin levels, approximately 100 µl blood was collected (from the submandibular vein plexus) and was placed at room temperature for 20 min, followed by centrifugation at 3,000*g* for 10 min at 4 °C. Next, 25 µl of the resultant serum was used to determine insulin levels using a Mouse Ultrasensitive Insulin ELISA kit according to the manufacturer's instructions. The five-parameter logistic fitted standard curve for calculating the concentrations of insulin was generated from the website of Arigo Biolaboratories (https://www.arigobio.cn/ELISA-calculator/).

For measuring GLP-1 levels, blood samples were collected as for the measurement of insulin, except that the blood collected (approximately 60 µl per sample) was immediately mixed with 2 µl of 50 mM diprotin A for each sample on ice in a K_2EDTA spray-coated tube (366420, BD P800 blood collection system). The blood samples were then centrifuged at 3,000*g* for 10 min at 4 °C, and 10 µl each was used to determine GLP-1 levels using a GLP-1 Multispecies ELISA kit according to the manufacturer's instructions. The standard curve was generated as for the measurement of insulin.

For measuring free fatty acids, glycerol, β-hydroxybutyrate and glucagon, 1.3 µl, 10 µl, 1 µl and 5 µl of freshly prepared serum from 8-h fasted mice was analysed using a LabAssay NEFA kit, a Free Glycerol Assay kit, a Ketone Body Assay kit or a Mouse Glucagon ELISA Kit, respectively, all following the manufacturer's instructions.

Hyperinsulinaemic–euglycaemic clamp

Hyperinsulinaemic–euglycaemic clamp testing was performed as previously described[112,126,127], but with minor modifications. In brief, mice were anaesthetized with 3% isoflurane in the air using a vaporizer (R540, RWD Life Science). Fur was removed from the incision site and the skin was disinfected with 70% (v/v, in water) ethanol. A small incision located approximately 5 mm superior to the sternum and 5 mm to the right of the vertical midline was made, and the fat and connective tissues beneath the pectoral muscle and surrounding the right jugular vein were gently cleaned by blunt dissection. The cephalad end of the exposed vein was then tightly tied (forming an anterior ligature) by passing a 7-0 silk suture beneath the vein. After loosely tying the caudal end of the vein through another thread of suture (posterior ligature), the vein was inserted using a 19-G needle between the two threads a few millimetres below the anterior ligature. After removing the needle, a catheter (C10PUS-MFV1610, Instech) was inserted into the vein through the needle hole, with the bevel of its tip facing towards the opening, followed by pushing forwards towards the caudal end for approximately 1 cm (until the restraining bead reaching the superior vena cava). The catheter was flushed with 100 µl heparin (200 U ml^{-1}, dissolved in saline) and then anchored by tightening the posterior ligature thread. The catheter was then tunnelled (pulled with eye dressing forceps) beneath the skin from the right jugular incision to the interscapular incision (approximately 5-mm long) on the back. After exteriorizing through the interscapular incision, the catheter was connected to a mouse vascular access button (VABM1BSM-25, Instech) sealed with a protective aluminium cap (VABM1C, Instech) and secured using 6-0 silk suture. After closing the two incisions using the 6-0 silk suture, the catheterized mouse was allowed to recover for 4 days. Mice that lost <4% of their pre-cannulation weight after recovery were used for clamp experiments.

One day before the experiments, a magnetic VAB tether kit (KVABM1T/25, Instech; with its 25-G luer stub (LS25/6, Instech) replaced by a PinPor-to-Tubing connector (PNP3MC/25, Instech), which was connected to a PU tube (VAHBPU-T25, Instech), followed by a 4-way X connector (SCX25, Instech), and three separate luer stubs (LS25, Instech): one for infusing unlabelled glucose, one for [U-^{13}C]glucose and the third for insulin, each connected with a PU tube) was anchored onto a counter-balanced lever arm (SMCLA, Instech) and was flushed with each perfusate by a PHD Ultra programmable syringe pump (HA3000P, Instech) in the following order: unlabelled glucose (20% (m/v) in saline), 100 mU ml^{-1} insulin and then 0.45 µg $µl^{-1}$ [U-^{13}C]glucose. The mouse VAB connector on the magnetic VAB tether kit was then connected to the mouse vascular access button on the back of the catheterized mouse after removing the protective aluminium cap. The mice were then fasted for 16 h (starting from 17:00 to 9:00 the following day), and the experiment was performed with a 2-phase protocol consisting of a 90-min equilibration period (t = −90 min to 0 min) and a 120-min experimental period (t = 0 min to 120 min). Next, 0.45 µg $µl^{-1}$ [U-^{13}C]glucose was given at t = −90 min and was infused at a rate of 30 µg kg^{-1} min^{-1} during the remaining time of the experiment. Clamping was begun at t = 0 min with a prime-continuous infusion of insulin (300 mU kg^{-1} min^{-1} for 1 min), followed by 25 mU kg^{-1} min^{-1} continuous infusion during the remaining time of the experiment. Unlabelled glucose (20% (m/v) in saline) was then infused at 50 mg^{-1} kg^{-1} min^{-1} for 10 min (from t = 0 min to t = 10 min), and the rate was adjusted according to the blood glucose level (maintained at 6–7 mM, during which blood glucose was measured every 10 min from t = 0 to 90 min, and every 5 min from t = 90 to 120 min) thereafter. At t = 0, 90, 100, 110 and 120 min (all at the clamped state), 60 µl blood was taken from the tail vein, and the serum ratios of [U-^{13}C]glucose to unlabelled glucose were determined using an ExionLC AD UPLC system (SCIEX) interfaced with a QTRAP 5500 MS (SCIEX), as described in the section 'Determination of the serum metabolome', except that 10 µl serum was used. The resting hepatic glucose output rate (HGP) was calculated by dividing the resting-state infusion rate of [U-^{13}C]glucose with the ratio of [U-^{13}C]glucose to unlabelled glucose, whereas the clamped HGP was calculated by dividing the value of differences between the average, clamp-state infusion rate of the unlabelled glucose and the [U-^{13}C]glucose with the ratio of [U-^{13}C]glucose to unlabelled glucose. The glucose disposal rate during clamping was the sum of the infusion rate of [U-^{13}C]glucose, the infusion rate of unlabelled glucose and the value of clamped HGP.

Determination of body composition

Lean and fat body mass were measured using quantitative magnetic resonance as previously described[68], except that male mice were measured using an EchoMRI-100H Analyzer (Echo Medical Systems), whereas female mice were measured using a Live Mouse Body Composition NMR Analyzer (QMR06-090H, Niumag) that also measures free water, one more parameter than the EchoMRI-100H Analyzer. In brief, the system was calibrated to the oil standard before measurement. Mice were individually weighed, inserted into a restrainer tube and immobilized by gently inserting a plunger. The mouse was then positioned so that it curled up like a doughnut, with its head against the end of the tube. The body composition of each mouse was measured with three repeated runs, and the average values were taken for further analysis.

Determination of EE

Mouse EE was determined using a metabolic cage system (Promethion Line, CAB-16-1-EU; Sable Systems International) as previously described[68,128]. In brief, the system was maintained in a condition identical to that for housing mice. Each metabolic cage in the 16-cage system consisted of a cage with standard bedding, a food hopper and a water bottle connected to load cells for continuous monitoring. To minimize the stress of the new environment, mice were acclimated (by individual housing in the gas-calibrated chamber) for 1 week before data collection. Mice treated with LCA or vehicle control were randomly assigned and housed to prevent systematic errors in measurement. Body weights and fat proportion of mice were determined before and after acclimation, as well as the daily food and water intake. Mice that did not acclimate to the metabolic cage (for example, resisted eating and drinking) were removed from the study. Data acquisition (5-min intervals in each cage) and instrument control were performed using MetaScreen software (v.2.3.15.12, Sable Systems), and raw data were processed using Macro Interpreter (v.2.32, Sable Systems). Ambulatory activity and position were monitored using *xyz* beam arrays with a beam spacing of 0.25 cm (beam breaks), and the distance walked by the mouse within the cage was calculated accordingly. Respiratory gases were measured using a GA-3 gas analyser (Sable Systems) equipped with a pull-mode, negative-pressure system. Air flow was measured and controlled using a FR-8 (Sable Systems), with a set flow rate of 2,000 ml min^{-1}. Oxygen consumption (VO_2) and carbon dioxide production (VCO_2) are reported in ml min^{-1} values. Water vapour was measured continuously, and its dilution effect on O_2 and CO_2 was compensated mathematically in the analysis stream. EE was calculated using kcal $h^{-1} = 60 \times (0.003941 \times VO_2 + 0.001106 \times VCO_2)$ (Weir Equation). Differences in average EE values were analysed by analysis of covariance (ANCOVA) using body weight as the covariate. The respiratory quotient was calculated as VCO_2/VO_2.

Histology

For haematoxylin and eosin (H&E) staining, muscle tissue was quickly excised, followed by freezing in isopentane (pre-chilled in liquid nitrogen) for 2 min (until they appeared chalky white). The tissue samples were then rapidly transferred to embedding moulds containing OCT compound and were frozen in liquid nitrogen for another 10 min. The embedded tissue samples were then sectioned into 6-μm slices at −20 °C using a CM1950 cryostat (Leica), followed by fixing in 4% paraformaldehyde for 10 min and washing with running water for 2 min at room temperature. The sections were stained in Mayer's haematoxylin solution for 5 min, followed by washing in running water for 10 min and then stained in eosin Y solution for another 1 min. The stained sections were dehydrated twice in 95% ethanol, 5 min each, twice in anhydrous ethanol, 1 min each, and 2 changes of xylene, 1 min each. The stained sections were mounted with Canada balsam and visualized on an AxioScan 7 scanner (Zeiss). Images were processed and analysed using Zen 3.4 software (Zeiss) and were formatted in Photoshop 2023 software (Adobe).

For immunohistochemistry staining of PAX7, tibialis anterior muscle tissue was excised, embedded and sectioned as for H&E staining. The sections were fixed with 4% paraformaldehyde for 10 min, followed by washing with PBS for 5 min at room temperature. After incubating with PBST (PBS supplemented with 5% Triton X-100) for 10 min, the sections were blocked with BSA solution (PBS containing 5% BSA) for 30 min at room temperature, followed by incubating with a PAX7 antibody (6 μg ml^{-1}, diluted in BSA solution) for 12 h at 4 °C. The sections were then washed with PBS 3 times, 5 min each at room temperature, followed by incubating with Alexa Fluor 488-conjugated, goat anti-mouse IgG1 secondary antibody (1:200 diluted in BSA Solution) for 1 h at room temperature in a dark, humidified chamber. The sections were washed with PBS 3 times, 5 min each at room temperature, followed by incubating with 4% paraformaldehyde for 2 min and then washed with PBS twice, 5 min each at room temperature. The sections were then incubated with the laminin antibody (1:100 diluted in BSA Solution) for 3 h at room temperature in a dark humidified chamber, followed by washing with PBS buffer 3 times, 5 min each at room temperature. The sections were then incubated with Alexa Fluor 594-conjugated, goat anti-rabbit IgG secondary antibody (1:200 diluted in BSA solution) for 1 h at room temperature in a dark humidified chamber, followed by washing with PBS for 3 times, 5 min each at room temperature. Tissue sections were mounted with 90% glycerol and visualized on a LSM980 microscope (Zeiss). Images were processed and analysed using Zen 3.4 software (Zeiss) and formatted in Photoshop 2023 software (Adobe).

Muscle fibre types were determined as previously described[44,129], but with minor modifications. In brief, muscle tissue was excised, embedded and sectioned as for H&E staining. The sections were fixed in 4% paraformaldehyde for 10 min and were then washed with PBS for 5 min at room temperature. After incubating with PBST (PBS supplemented with 5% (v/v) Triton X-100) for 10 min, the sections were blocked with BSA solution (PBS containing 5% (m/v) BSA) for 30 min at room temperature. Muscle fibres were stained with antibody against MHCIIb (6 μg ml^{-1}, diluted in BSA solution) overnight at 4 °C, followed by washing with PBS 3 times, 5 min each, at room temperature. The sections were then incubated with Alexa Fluor 488-conjugated, goat anti-mouse IgM antibody (1:200 diluted in BSA Solution) for 1 h at room temperature in a dark humidified chamber, followed by washing with PBS for 3 times, 5 min each, incubated with 4% paraformaldehyde for 2 min, and then washed with PBS twice, 5 min each, all at room temperature. The sections were then incubated with antibody against MHCI (6 μg ml^{-1}, diluted in BSA Solution) for 3 h at room temperature in a dark humidified chamber, followed by washing with PBS buffer 3 times, 5 min each at room temperature, and then incubated with Alexa Fluor 594-conjugated, goat anti-mouse IgG2b antibody (1:200 diluted in BSA solution) for another 1 h at room temperature in a dark humidified chamber, followed by washing with PBS buffer for 3 times, 5 min each at room temperature. After fixing with 4% paraformaldehyde for 2 min and washing with PBS twice, 5 min each at room temperature, the sections were incubated with antibody against MHCIIa (6 μg ml^{-1}, diluted in BSA solution) for 3 h at room temperature in a dark humidified chamber, followed by washing with PBS buffer for 3 times, 5 min each at room temperature, and then incubated in Alexa Fluor 647-conjugated goat anti-mouse IgG1 antibody (1:200 diluted in BSA Solution) for another 1 h at room temperature in a dark humidified chamber, followed by washing with PBS buffer for 3 times, 5 min each at room temperature. Tissue sections were mounted with 90% glycerol and visualized on an LSM980 microscope (Zeiss). Images were processed and analysed using Zen 3.4 software (Zeiss) and formatted in Photoshop 2023 software (Adobe).

Measurements of food and faecal energy content

The energy content in food and faeces was determined using bomb calorimetry as previously described[130]. In brief, mice were individually housed for 1 week before measurement. The daily food intake (from 17:00 to 17:00 the next day) was continuously measured for 1 week, and the average food consumed by each mouse per day was recorded. Faeces excreted in a day were also collected from 17:00 to 17:00 the next day, pulverized in a ceramic mortar and then lyophilized in a vacuum concentrator (CentriVap Benchtop Centrifugal Vacuum Concentrator, 7310037; Labconco, equipped with a CentriVap −84 °C Cold Trap, 7460037; Labconco, and an EDWARDS nXDS15i pump) at 4 °C for 12 h before measurements using a bomb calorimeter.

Before measurement, an automatic bomb calorimeter (SJLRY-502T, Xinsanjie Instrument and Meter) was standardized by combusting 1 g benzoic acid as a reference (10590.8 J g^{-1}). Next, 1 g of food or faeces was placed on the crucible attached to the bomb head, followed by attaching the fuse wire to the bomb head and adjusting to ensure it touched the top of the food or faeces without touching any other part of the crucible. The loaded bomb head was inserted into the bomb cylinder

containing 10 ml distilled water and was screwed on tightly. The bomb was then connected to the oxygen-filling unit and filled with oxygen at a pressure of 2.8–3 MPa for at least 15 s, followed by insertion into the calorimeter bucket. The following steps, including filling the bucket with water, ignition and subsequent combustion, were automatically conducted by the calorimeter. The energy contents were then automatically calculated according to the benzoic acid reference at the end of the combustion.

C. elegans strains

Nematodes (hermaphrodites) were maintained on NGM plates spread with *Escherichia coli* OP50 as standard food. All worms were cultured at 20 °C. WT (N2 Bristol) and *aak-2* (ok524) strains were obtained from the *Caenorhabditis* Genetics Center. All mutant strains were outcrossed 6 times to N2 before the experiments. Unless stated otherwise, worms were maintained on NGM plates spread with *E. coli* OP50 as standard food. The administration of LCA was initiated at the L4 stage.

Evaluation of nematode lifespan and healthspan

To determine the lifespan of nematodes, the worms were first synchronized. Worms were washed off from agar plates with 15 ml M9 buffer (22.1 mM KH_2PO_4, 46.9 mM Na_2HPO_4, 85.5 mM NaCl and 1 mM $MgSO_4$) supplemented with 0.05% (v/v) Triton X-100 per plate, followed by centrifugation at 1,000*g* for 2 min. The worm sediment was suspended with 6 ml M9 buffer containing 50% synchronizing bleaching solution (by mixing 25 ml of NaClO solution (5% active chlorine), 8.3 ml of 25% (w/v) NaOH and 66.7 ml M9 buffer, for a total of 100 ml), followed by vigorous shaking for 2 min and centrifugation for 2 min at 1,000 *g*. The sediment was washed with 12 ml M9 buffer twice, then suspended with 6 ml M9 buffer followed by rotating at 20 °C, 30 r.p.m. for 12 h. Synchronized worms were cultured to the L4 stage before transfer to desired agar plates for determination of lifespan. Worms were transferred to new plates every 2 days. Live and dead worms were counted during the transfer step. Worms that displayed no movement after gentle touching with a platinum picker were judged dead. Kaplan–Meier curves were generated using Prism 9 (GraphPad Software), and statistical analysis was performed using SPSS 27.0 (IBM).

Pharyngeal pumping rates, assessed as the number of contraction–relaxation cycles of the terminal bulb on the nematode pharynx within 1 min, were determined as previously described[131], but with minor modifications. In brief, the synchronized nematodes were cultured to the L4 stage and LCA was administered. The 1-day-old nematodes were then picked and placed on a new NGM plate containing *E. coli*. After 10 min of incubation at room temperature, the contraction–relaxation cycles of the terminal bulb of each worm were recorded on a stereomicroscope (M165 FC, Leica) through a ×63 objective for a consecutive 4 min using Capture software (v.2021.1.13, Capture Visualisation), and the average contraction–relaxation cycles per min were calculated using Aimersoft Video Editor software (v.3.6.2.0, Aimersoft).

The resistance of nematodes to oxidative stress was determined as previously described[102]. In brief, synchronized worms were cultured to the L4 stage, after which LCA was administered. After 2 days of LCA treatment, 20 worms were transferred to a NGM plate containing 15 mM $FeSO_4$. Worms were then cultured at 20 °C, during which the number of live and dead worms were counted every 1 h.

D. melanogaster strains

All flies were cultured at 25 °C and 60% humidity with a 12-h light and dark cycle. Adult flies were cultured in BDSC standard cornmeal medium for regular culture or in 2% (for CR) or 3% (the control, ad libitum-fed group for CR) CSY agar. Larvae and the crossed fly strains were reared on a semi-defined, rich medium, which was prepared as previously described[132], but with minor modifications. In brief, 10 g agar, 80 g dry yeast, 20 g yeast extract, 20 g peptone, 30 g sucrose, 60 g glucose, 0.5 g $MgSO_4{\cdot}6H_2O$ and 0.5 g $CaCl_2{\cdot}6H_2O$ were dissolved in 1,000 ml of di-distilled water and then boiled, followed by cooling to 60 °C. Next, 6 ml propionic acid was added to the medium, and the medium was dispensed into culture vials (6 ml each). The vials of medium were covered with gauze and blown with the breeze of a fan as for the BDSC and CSY diets, and were kept at 4 °C (for no more than 3 days) before experiments.

The WT fly strain (w^{1118}; 3605) and the *GAL4*-expressing strain ($y^1\,w^*$; *P{Act5C-GAL4-w}E1/CyO*; 25374) were obtained from the BDSC. The *GAL4*-induced, *AMPKα* RNAi-carrying strain (w^{1118}; *P{GD736}v1827*; 1827) was obtained from the Vienna *Drosophila* Resource Center. The w^{1118}; *Sp/CyO* strain was obtained from the Core Facility of *Drosophila* Resource and Technology, Chinese Academy of Sciences. To obtain flies with *AMPKα* knocked down on the w^{1118} background, a *GAL4*-expressing strain on the w^{1118} background (w^{1118}; *P{Act5C-GAL4-w}E1/CyO*) was first generated by crossing $y^1\,w^*$; *P{Act5C-GAL4-w}E1/CyO* males with w^{1118}; *Sp/CyO* females, followed by crossing the F_1 males with straight wings (w^{1118}; *P{Act5C-GAL4-w}E1/Sp*) with w^{1118}; *Sp/CyO* females. The *GAL4*-expressing flies (w^{1118} background) were then crossed with the *AMPKα* RNAi-carrying flies, and the F_1 offspring with straight wings were the *AMPKα* knockdown flies (w^{1118}; *P{Act5C-GAL4-w}E1/P{GD736}v1827*; +/+). The F_1 offspring of WT flies crossed with the *GAL4*-expressing flies (w^{1118} background), that is, the w^{1118}; *P{Act5C-GAL4-w}E1*/+; +/+ flies, were used as the control files.

In this study, the following ages of flies were used: (1) for analysing AMPK activation and the pharmacokinetics of LCA, third instar larvae or newly eclosed adults were used; (2) for determining lifespan, adults at day 2 after eclosion were used (for LCA or CR treatment); (3) for determining healthspan, mtDNA-to-nDNA ratios, NAD^+ levels and mitochondrial genes expression, adults at day 30 after eclosion (treated with LCA for 28 days starting from 2 days after eclosion) were used.

Evaluation of lifespan and healthspan of flies

Fly lifespan was determined as previously described[133], but with minor modifications. Before the experiment, flies were synchronized. Approximately 200 pairs of flies, housed 10 pairs per tube, were cultured in semi-defined, rich medium and allowed to lay eggs for a day. After discarding the parent flies, the embryos were cultured for another 10 days, and the flies that eclosed at day 12 were anaesthetized and collected with CO_2 (those that emerged before day 12 were discarded), followed by transfer to BDSC standard cornmeal medium and cultured for another 2 days. The male and female adults were then sorted by briefly anaesthetizing with CO_2 on an anaesthetic pad using a home-made feather brush (by attaching the apical region of a vane from the secondary coverts of an adult goose to a plastic balloon stick), and 200 adults of each group and gender were randomly assigned to the BDSC standard cornmeal medium or the CSY medium, with or without LCA, with 20 flies per tube. The flies were transferred to new tubes of medium every 2 days without anaesthesia until the last survivor was dead. During each tube transfer, the sum of dead flies in the old tubes and the dead flies carried to the new tubes were recorded as the numbers of deaths, and the escaped or accidentally killed flies (that is, died within 3 days of same-sex culturing or squeezed by the tube plugs) were censored from the experiments. Kaplan–Meier curves were generated using Prism 9 (GraphPad Software), and statistical analysis was performed using SPSS 27.0 (IBM).

The resistance of flies to oxidative stress was determined as previously described[134]. In brief, synchronized adults were treated with LCA for 30 days, followed by transfer to vials (20 flies each), each containing a filter paper soaked with 20 mM paraquat or 5% (m/v) H_2O_2 dissolved or diluted in 5% (w/v, in water) glucose solution. To determine the resistance of flies to cold and heat stress, synchronized adults were treated with LCA for 30 days, followed by transfer to cold (4 °C) or heat (37 °C) stress conditions. To determine the resistance of flies to starvation (food deprivation), flies treated with LCA for 30 days were transferred to vials with culture medium replaced by the same volume of 1.5% agarose

to remove the food supply. Dead files were recorded every 2 h until the last survivor was dead.

Quantification of mRNA levels of mitochondrial genes in mice, nematodes and flies

Mice treated with LCA were killed by cervical dislocation, immediately followed by dissecting the gastrocnemius muscle. The muscle tissue was roughly sliced into cubes (edge lengths of approximately 2 mm) and then soaked in RNAprotect tissue reagent (1 ml per 100 mg of tissue) for 24 h at room temperature. The tissue was then incubated in 1 ml TRIzol, followed by 3 rounds of freeze–thaw cycles, and was then homogenized. The homogenate was centrifuged at 12,000*g* for 15 min at 4 °C, and 900 µl of clear supernatant (not the lipid layer on the top) was transferred to a RNase-free tube. Chloroform (200 µl) was then added to the supernatant, followed by vigorous vortexing for 15 s. After centrifugation at 12,000*g* for 15 min at 4 °C, 450 µl of the upper aqueous layer was transferred to a RNase-free tube. RNA was then precipitated by adding 450 µl isopropanol, followed by centrifugation at 12,000*g* for 30 min at 4 °C. The pellet was washed twice with 75% ethanol and once with 100% ethanol, and was dissolved with 20 µl DEPC-treated water. The concentration of RNA was determined using a NanoDrop 2000 spectrophotometer (Thermo). Next, 1 µg RNA was diluted with DEPC-treated water to a final volume of 10 µl, heated at 65 °C for 5 min and chilled on ice immediately. Random Primer mix, Enzyme mix and 5× RT buffer (all from the ReverTra Ace qPCR RT Master Mix) were then added to the RNA solution, followed by incubation at 37 °C for 15 min and then at 98 °C for 5 min on a thermocycler. The reverse-transcribed cDNA was quantified using Maxima SYBR Green/ROX qPCR master mix on a LightCycler 480 II system (Roche) with the following programs: pre-denaturing at 95 °C for 10 min; denaturing at 95 °C for 10 s, then annealing and extending at 65 °C for 30 s in each cycle (determined according to the amplification curves, melting curves and bands on agarose gel of serial pilot reactions (in which a serial annealing temperature was set according to the estimated annealing temperature of each primer pair and same hereafter)) for a total of 45 cycles. Primer pairs for mouse *Nd1*, *Nd2*, *Nd3*, *Nd4*, *Nd4l*, *Nd5*, *Nd6*, *Ndufab1*, *Cytb*, *Uqcrc1*, *Uqcrc2*, *Atp5f1b*, *Cox6a1*, *Atp6*, *Atp8*, *Cox1* and *Cox3* were generated as previously described[135], and others were generated using the Primer-BLAST website (https://www.ncbi.nlm.nih.gov/tools/primer-blast/index.cgi). Primer sequences are as follows: mouse *Gapdh*, 5′-GACTTCAACAGCAACTCCCAC-3′ and 5′-TCCACCACCCTGTTGCTGTA-3′; mouse *Nd1*, 5′-TGCACCTACCCTATCACTCA-3′ and 5′-C GGCTCATCCTGATCATAGAATGG-3′; mouse *Nd2*, 5′-ATACTAGCAATTACTTCTATTTTCATAGGG-3′ and 5′-GAGGGATGGGTTGTAAGGAAG-3′; mouse *Nd3*, 5′-AAGCAAATCCATATGAATGCGG-3′ and 5′-GCTCATGGTAGTGGAAGTAGAAG-3′; mouse *Nd4*, 5′-CCTCAGACCCCCTATCCACA-3′ and 5′-GTTTGGTTCCCTCATCGGGT-3′; mouse *Nd4l*, 5′-CCAACTCCATAAGCTCCATACC-3′ and 5′-GATTTTGGACGTAATCTGTTCCG-3′; mouse *Nd5*, 5′-ACGAAAATGACCCAGACCTC-3′ and 5′-GAGATGACAAATCCTGCAAAGATG-3′; mouse *Nd6*, 5′-TGTTGGAGTTATGTTGGAAGGAG-3′ and 5′-CAAAGATCACCCAGCTACTACC-3′; mouse *Tfam*, 5′-GGTCGCATCCCCTCGTCTAT-3′ and 5′-TTGGGTAGCTGTTCTGTGGAA-3′; mouse *Cs*, 5′-CTCTACTCACTGCAGCAACCC-3′ and 5′-TTCATGCCTCTCATGCCACC-3′; mouse *Ndufs8*, 5′-TGGCGGCAACGTACAAGTAT-3′ and 5′-GTAGTTGATGGTGGCAGGCT-3′; mouse *Ndufab1*, 5′-GGACCGAGTTCTGTATGTCTTG-3′ and 5′-AAACCCAAATTCGTCTTCCATG-3′; mouse *Ndufb10*, 5′-TGCCAGATTCTTGGGACAAGG-3′ and 5′-GTCGTAGGCCTTCGTCAAGT-3′; mouse *Ndufv3*, 5′-GTGTGCTCAAAGAGCCCGAG-3′ and 5′-TCAGTGCCGAGGTGACTCT-3′; mouse *Ndufa8*, 5′-GCGGAGCCTTTCACAGAGTA-3′ and 5′-TCAATCACAGGGTTGGGCTC-3′; mouse *Ndufs3*, 5′-CTGACTTGACGGCAGTGGAT-3′ and 5′-CATACCAATTGGCCGCGATG-3′; mouse *Ndufa9*, 5′-TCTGTCAGTGGAGTTGTGGC-3′ and 5′-CCCATCAGACGAAGGTGCAT-3′; mouse *Ndufa10*, 5′-CAGCGCGTGGGACGAAT-3′ and 5′-ACTCTATGTCGAGGGGCCTT-3′; mouse *Sdha*, 5′-AGGGTTTAATACTGCATGCCTTA-3′ and 5′-TCATGTAATGGATGGCATCCT-3′; mouse *Sdhb*, 5′-AGTGCGGACCTATGGTGTTG-3′ and 5′-AGACTTTGCTGAGGTCCGTG-3′; mouse *Sdhc*, 5′-TGAGACATGTCAGCCGTCAC-3′ and 5′-GGGAGACAGAGGACGGTTTG-3′; mouse *Sdhd*, 5′-TGGTACCCAGCACATTCACC-3′ and 5′-GGGTGTCCCCATGAACGTAG-3′; mouse *Cytb*, 5′-CCCACCCCATATTAAACCCG-3′ and 5′-GAGGTATGAAGGAAAGGTATTAGGG-3′; mouse *Uqcrc1*, 5′-ATCAAGGCACTGTCCAAGG-3′ and 5′-TCATTTTCCTGCATCTCCCG-3′; mouse *Uqcrc2*, 5′-TTCCAGTGCAGATGTCCAAG-3′ and 5′-CTGTTGAAGGACGGTAGAAGG-3′; mouse *Atp5f1b*, 5′-CCGTGAGGGCAATGATTTATAC-3′ and 5′-GTCAAACCAGTCAGAGCTACC-3′ mouse *Cox6a1*, 5′-GTTCGTTGCCTACCCTCAC-3′ and 5′-TCTCTTTACTCATCTTCATAGCCG-3′; mouse *Atp6*, 5′-TCCCAATCGTTGTAGCCATC-3′ and 5′-TGTTGGAAAGAATGGAGTCGG-3′; mouse *Atp8*, 5′-GCCACAACTAGATACATCAACATG-3′ and 5′-TGGTTGTTAGTGATTTTGGTGAAG-3′; mouse *Atp5f1a*, 5′-CATTGGTGATGGTATTGCGC-3′ and 5′-TCCCAAACACGACAACTCC-3′; mouse *Cox1*, 5′-CCCAGATATAGCATTCCCACG-3′ and 5′-ACTGTTCATCCTGTTCCTGC-3′; mouse *Cox2*, 5′-TCTACAAGACGCCACATCCC-3′ and 5′-ACGGGGTTGTTGATTTCGTCT-3′; mouse *Cox3*, 5′-CGTGAAGGAACCTACCAAGG-3′ and 5′-CGCTCAGAAGAATCCTGCAA-3′; mouse *Cox5b*, 5′-AGCTTCAGGCACCAAGGAAG-3′ and 5′-TGGGGCACCAGCTTGTAATG-3′. The mRNA level was then calculated using the comparative ΔΔct method with LightCycler software (v.96 1.1, Roche; same hereafter for all qPCR experiments).

Nematodes at the L4 stage treated with LCA for 1 day were used for the analysis of mitochondrial gene expression. Around 1,000 worms were collected into 15 ml M9 buffer containing 0.05% Triton X-100 (v/v), followed by centrifugation for 2 min at 1,000*g*. The sediment was then washed with 1 ml M9 buffer twice and then lysed with 1 ml TRIzol. Worms were then frozen in liquid nitrogen, thawed at room temperature and then the freeze–thaw cycle was repeated for another 2 times. The worm lysates were then placed at room temperature for 5 min, mixed with 0.2 ml of chloroform, followed by vigorous shaking for 15 s. After centrifugation at 12,000*g* for 15 min at 4 °C, 450 µl of the upper aqueous layer was transferred to a RNase-free tube. RNA was then precipitated by adding 450 µl isopropanol, followed by centrifugation at 12,000*g* for 30 min at 4 °C. The pellet was washed twice with 75% ethanol and once with 100% ethanol, and was dissolved with 20 µl of DEPC-treated water. The concentration of RNA was determined using a NanoDrop 2000 spectrophotometer (Thermo). Next, 1 µg RNA was diluted with DEPC-treated water to a final volume of 10 µl, heated at 65 °C for 5 min and chilled on ice immediately. Random Primer mix, Enzyme mix and 5× RT buffer (all from the ReverTra Ace qPCR RT Master Mix) were then added to the RNA solution, followed by incubation at 37 °C for 15 min and then at 98 °C for 5 min on a thermocycler. The reverse-transcribed cDNA was quantified using Maxima SYBR Green/ROX qPCR master mix on a LightCycler 480 II system (Roche) with the following programs: pre-denaturing at 95 °C for 10 min; denaturing at 95 °C for 10 s, then annealing and extending at 65 °C for 30 s in each cycle, for a total of 45 cycles. Primer pairs used for qPCR are as previously described[136,137], except that *C. elegans ctb-1* was designed using the Primer-BLAST website. Primer sequence are as follows: *C. elegans ama-1*, 5′-GACATTTGGCACTGCTTTGT-3′ and 5′-ACGATTGATTCCATGTCTCG-3′; *C. elegans nuo-6*, 5′-CTGCCAGGACATGAATACAATCTGAG-3′ and 5′-GCTATGAGGATCGTATTCACGACG-3′; *C. elegans nuaf-1*, 5′-GAGACATAACGAGGCTCGTGTTG-3′ and 5′-GAAGCCTTCTTTCCAATCACTATCG-3′; *C. elegans sdha-1*, 5′-TTACCAGCGTGCTTTCGGAG-3′ and 5′-AGGGTGTGGAGAAGAGAATGACC-3′; *C. elegans sdhb-1*, 5′-GCTGAACGTGATCGTCTTGATG-3′ and 5′-GTAGGATGGGCATGACGTGG-3′; *C. elegans cyc-2.1*, 5′-CGGA GTTATCGGACGTACATCAG-3′ and 5′-GTCTCGCGGGTCCAGACG-3′; *C. elegans isp-1*, 5′-GCAGAAAGATGAATGGTCCGTTG-3′ and 5′-ATCCGTGACAAGGGCAGTAATAAC-3′; *C. elegans cco-1*, 5′-GCTGGAGATGATCGTTACGAG-3′ and 5′-GCATCCAATGATTCTGAAGTCG-3′; *C. elegans cco-2*, 5′-GTGATACCGTCTACGCCTACATTG-3′ and 5′-GCTCTGGCACGAAGAATTCTG-3′; *C. elegans atp-3*, 5′-GTCCTCGACCCAACTCTCAAG-3′ and 5′-GTCCAAGGAAG

TTTCCAGTCTC-3′; *C. elegans nduo-1*, 5′-AGCGTCATTTATTGGGAA GAAGAC-3′ and 5′-AAGCTTGTGCTAATCCCATAAATGT-3′; *C. elegans nduo-2*, 5′-TCTT TGTAGAGGAGGTCTATTACA-3′ and 5′-ATGTTAAAAAC CACATTAGCCCA-3′; *C. elegans nduo-4*, 5′-GCACACGGTTATACATC TACACTTATG-3′ and 5′-GATGTATGATAAAATTCACCAATAAGG-3′; *C. elegans nduo-5*, 5′-AGATGAGATTTATTGGGTATTTCTAG-3′ and 5′-CAC CTAGACGATTAGTTAATGCTG-3′; *C. elegans ctc-1*, 5′-GCAGCAGGGT TAAGATCTATCTTAG-3′ and 5′-CTGTTACAAATACAGTTCAAACAAAT-3′; *C. elegans ctc-2*, 5′-GTAGTTTATTGTTGGGAGTTTTAGTG-3′ and 5′-CACAATAATTCACCAAACTGATACTC-3′; *C. elegans atp-6*, 5′-TGCT GCTGTAGCGTGATTAAG-3′ and 5′-ACTGTTAAAGCAAGTGGAC GAG-3′; *C. elegans ctb-1*, 5′-TGGTGTTACAGGGGCAACAT-3′ and 5′-TGGCCTCATTATAGGGTCAGC-3′.

Drosophila adults treated with LCA for 30 days were used to determine the expression of mitochondrial genes. For each sample, 20 adults were used. The adults were anaesthetized, transferred to a 1.5-ml Eppendorf tube, followed by quickly freezing in liquid nitrogen and then homogenized using a pellet pestle (Z359963-1EA, Sigma). The homogenate was then lysed in 1 ml TRIzol for 5 min at room temperature, followed by centrifugation at 12,000*g* for 15 min at 4 °C. Next, 900 µl supernatant (without the lipid layer) was transferred to a RNase-free tube and mixed with 200 µl of chloroform. After vigorous vortexing for 15 s, the mixture was centrifuged at 12,000*g* for 15 min at 4 °C, and 450 µl of the upper aqueous layer was transferred to a RNase-free tube. RNA was then precipitated by adding 450 µl isopropanol, followed by centrifugation at 12,000*g* for 30 min at 4 °C. The pellet was washed twice with 75% (v/v, in water) ethanol, and was dissolved with 20 µl of DEPC-treated water. The concentration of RNA was determined using a NanoDrop 2000 spectrophotometer (Thermo). Next, 1 µg RNA was diluted with DEPC-treated water to a final volume of 10 µl, heated at 65 °C for 5 min and chilled on ice immediately. Random Primer mix, Enzyme mix and 5× RT buffer (all from the ReverTra Ace qPCR RT Master Mix) were then added to the RNA solution, followed by incubation at 37 °C for 15 min and then at 98 °C for 5 min on a thermocycler. The reverse-transcribed cDNA was quantified using Maxima SYBR Green/ROX qPCR master mix on a LightCycler 480 II system (Roche) with the following programs: pre-denaturing at 95 °C for 5 min; denaturing at 95 °C for 10 s, then annealing at 60 °C for 20 s, and then extending at 72 °C for 20 s in each cycle, for a total of 40 cycles. Primer pairs used for qPCR are as previously described[138], and are listed as follows: *D. melanogaster CG9172*, 5′-CGTGGCTGCGATAGGATAAT-3′3′ and 5′-ACCACATCTGGAGCGTCTTC-3′; *D. melanogaster CG9762*, 5′-AGTC ACCGCATTGGTTCTCT-3′3′ and 5′-GAGATGGGGTGCTTCTCGTA-3′; *D. melanogaster CG17856*, 5′-ACCTTTCCATGACCAAGACG-3′ and 5′-CTCC ATTCCTCACGCTCTTC-3′; *D. melanogaster CG18809*, 5′-AAGTGAA GACGCCCAATGAGA-3′ and 5′-GCCAGGTACAACGACCAGAAG-3′; *D. melanogaster CG5389*, 5′-ATGGCTACAGCATGTGCAAG-3′ and 5′-GACAGGGAGGCATGAAGGTA-3′; *D. melanogaster Act5C*, 5′-GCAG CAACTTCTTCGTCACA-3′ and 5′-CATCAGCCAGCAGTCGTCTA-3′.

Analysis of mtDNA copy numbers in mice, nematodes and flies

Mouse mtDNA copy numbers were determined as previously described[68]. In brief, mouse tissue DNA was extracted using a Biospin tissue genomic DNA extraction kit (BioFlux) following the manufacturer's instruction, but with minor modifications. In brief, mice treated with LCA were killed by cervical dislocation, quickly followed by dissecting the gastrocnemius muscle. The muscle tissue was then ground in liquid nitrogen on a ceramic mortar. Next, 50 mg ground tissue was transferred to a 1.5-ml Eppendorf tube, followed by addition of 600 µl of FL buffer and 10 µl of PK solution containing 2 µl of 100 mg ml^{-1} RNase A. The mixture was then incubated at 56 °C for 15 min, followed by centrifugation at 12,000*g* for 3 min. Then 500 µl supernatant was transferred to a 2-ml Eppendorf tube, followed by mixing with 700 µl binding buffer and 300 µl absolute ethanol. The mixture was then loaded onto a Spin column and was centrifuged at 10,000*g* for 1 min. The flow through was discarded, and 500 µl PW buffer was added to the Spin column, followed by centrifugation at 10,000*g* for 30 s. Next, 600 µl washing buffer was added to the spin column followed by centrifugation at 10,000*g* for 30 s, and this process was repeated once. The Spin column was then centrifuged for 1 min at 10,000*g* to completely remove the washing buffer, and the DNA on the column was eluted with 100 µl of Elution buffer (added to the Spin column, followed by incubation at room temperature for 5 min and then centrifuged at 12,000*g* for 1 min). Total DNA was quantified using Maxima SYBR Green/ROX qPCR master mix on a LightCycler 480 II system (Roche) with the following programs: 70 ng DNA was pre-denatured at 95 °C for 10 min, and then subjected to PCR for a total of 45 cycles: denaturing at 95 °C for 10 s, annealing and extending at 65 °C for 30 s in each cycle. Primer pairs used for qPCR are as previously described[139] (mouse *Hk2*, 5′-GCCAGCCTCTCCTGATTTTAGTGT-3′ and 5′-GGGAACACAAAAGAC CTCTTCTGG-3′; mouse *Nd1*, 5′-CTAGCAGAAACAAACCGGGC-3′ and 5′-CCGGCTGCGTATTCTACGTT-3′).

Nematode mtDNA copy numbers were determined from worm lysates as previously described[68]. In brief, 30 synchronized early L4 worms were collected and were lysed with 10 µl of worm lysis buffer (50 mM HEPES, pH7.4, 1 mM EGTA, 1 mM $MgCl_2$, 100 mM KCl, 10% (v/v) glycerol, 0.05% (v/v) NP-40, 0.5 mM DTT and protease inhibitor cocktail). The worm lysate was frozen at −80 °C overnight, followed by incubating at 65 °C for 1 h and 95 °C for 15 min. Nematode DNA was then quantified using Maxima SYBR Green/ROX qPCR master mix on a LightCycler 480 II system (Roche) with the following programs: pre-denaturing at 95 °C for 10 min and then for a total of 45 cycles of denaturing at 95 °C for 10 s, and annealing and extending at 65 °C for 30 s in each cycle. Primer pairs used for qPCR are designed as previously described[103] (*C. elegans nd-1*, 5′-AGCGTCATTTATTGGGAAGAAGAC-3′ and 5′-AAGCTTGTGCTAATCCCATAAATGT-3′; *C. elegans act-3*, 5′-TGC GACATTGATATCCGTAAGG-3′ and 5′-GGTGGTTCCTCCGGAAAGAA-3′).

Drosophila DNA copy numbers were determined as previously described[140], but with minor modifications. In brief, 20 anaesthetized adults were homogenized in 100 µl Fly Lysis buffer (75 mM NaCl, 25 mM EDTA and 25 mM HEPES, pH7.5) containing proteinase K (100 µg ml^{-1}). The homogenate was then frozen at −80 °C for 12 h, followed by incubating at 65 °C for 1 h and 95 °C for another 15 min. Fly DNA was then quantified using Maxima SYBR Green/ROX qPCR master mix on a LightCycler 480 II system (Roche) with the following programs: pre-denaturing at 95 °C for 5 min and then for a total of 40 cycles of denaturing at 95 °C for 10 s, and annealing 60 °C for 20 s and extending at 72 °C for 20 s in each cycle. Primer pairs used for qPCR are as previously described[140] (*D. melanogaster* 16S rRNA, 5′-TCGTCCAACCATTCATTCCA-3′ and 5′-TGGCCGCAGTATTTTGACTG-3′; *D. melanogaster RpL32*, 5′-AGGCCCAAGATCGTGAAGAA-3′ and 5′-TGTGCACCAGGAACTTCTTGAA-3′).

Determining muscle atrophy markers in mice

Muscle atrophy markers were determined as previously described[141], but with minor modifications. In brief, mice treated with LCA were killed by cervical dislocation, followed by quickly dissecting the gastrocnemius muscle. Muscle tissue was sliced into cubes (edge lengths of approximately 2 mm) and then soaked in RNAprotect Tissue reagent (1 ml per 100 mg of tissue) for 24 h at room temperature. The tissue was then incubated in 1 ml TRIzol, followed by 3 rounds of freeze–thaw cycles and was then homogenized. The homogenate was centrifuged at 12,000*g* for 15 min at 4 °C, and 900 µl of the clear supernatant (without the lipid layer) was transferred to a RNase-free tube. Chloroform (200 µl) was added to the supernatant, followed by a vigorous vortex for 15 s. RNA was then purified and was transcribed to cDNA as described in the section 'Quantification of mRNA levels of mitochondrial genes in mice, nematodes and flies'. The reverse-transcribed cDNA was quantified using Maxima SYBR Green/ROX qPCR master mix on a LightCycler 480 II system (Roche) with the following programs:

pre-denaturing at 95 °C for 10 min; denaturing at 95 °C for 10 s, then annealing and extending at 65 °C for 30 s in each cycle for a total of 45 cycles. Primer sequences are as previously described[141] (mouse *Fbxo32*, 5′-TAGTAAGGCTGTTGGAGCTGATAG-3′ and 5′-CTGCACCAGTGTG CATAAGG-3′; mouse *Trim63*, 5′-CATCTTCCAGGCTGCGAATC-3′; and 5′-ACTGGAGCACTCCTGCTTGT-3′; mouse *Gapdh*, 5′-TTCACCACCATG GAGAAGGC-3′ and 5′-CCCTTTTGGCTCCACCCT-3′).

Primary hepatocytes and myocytes

Mouse primary hepatocytes were isolated using a modified two-step perfusion method with liver perfusion medium and liver digest buffer as previously described[70]. Before isolation of hepatocytes, mice were first anaesthetized, followed by inserting a 0.72 × 19 mm intravenous catheter into the postcava. After cutting off the portal vein, mice were perfused with 50 ml liver perfusion medium at a rate of 5 ml min^{-1}, followed by 50 ml liver digest buffer at a rate of 2.5 ml min^{-1}. The digested liver was then briefly rinsed by PBS and then dismembered by gently tearing apart the Glisson's capsule with two sterilized, needle-pointed tweezers on a 6-cm dish containing 3 ml PBS. The dispersed cells were mixed with 10 ml ice-cold William's medium E plus 10% FBS, and were filtered through a 100-μm cell strainer (352360; Falcon). Cells were then centrifuged at 50*g* at 4 °C for 2 min, then washed twice with 10 ml ice-cold William's medium E plus 10% FBS. Cells were then immediately plated (at 60–70% confluence) in collagen-coated 6-well plates in William's medium E plus 10% FBS, 100 IU penicillin and 100 mg ml^{-1} streptomycin, and were maintained at 37 °C in a humidified incubator containing 5% CO_2. After 4 h of attachment, the medium was replaced with fresh William's medium E with 1% (w/v) BSA for another 12 h before further use.

Mouse primary myocytes were isolated as previously described[142]. In brief, mice were killed by cervical dislocation, and hindlimb muscles from both legs were excised. Tissue samples were minced and digested in a collagenase B–dispase–$CaCl_2$ solution for 1.5 h at 37 °C in a shaking bath. DMEM supplemented with 10% FBS was then added to the digested tissue samples, and the mixtures were gently triturated, followed by loading onto a 70-μm strainer filter (352350; Falcon). Cell suspensions were then centrifuged at 1,000*g* for 5 min, and the pellets were resuspended in a growth medium (Ham's F-10 medium supplemented with 20% FBS and 2.5 ng ml^{-1} bFGF). Cells were then plated on collagen-coated dishes (354456, Corning) at 60–70% confluence.

Determination of the serum metabolome

For measuring the serum metabolome, blood samples from CR-treated and ad libitum-fed mice were collected at 15:00. The samples were incubated at room temperature for 10 min and then centrifuged at 3,000*g* at 4 °C for another 10 min. The supernatants were serum samples, which were prepared on the same day of blood collection. For heat-inactivation, serum was incubated at 56 °C for 30 min in a water bath. For dialysis, serum was loaded into a D-Tube Dialyzer Maxi (with molecular weight cut-offs from 3.5 to 14 kDa; 71508) and dialysed in a beaker containing 2 l PBS at 4 °C for 24 h on a magnetic stirrer. The PBS was refreshed every 4 h.

Polar metabolites were determined by HPLC–MS, GC–MS and CE–MS as previously described[68,84,143], but with minor modifications[144]. For HPLC–MS and CE–MS, 100 μl serum was instantly mixed with 1 ml pre-cooled methanol containing IS1 (50 μM L-methionine sulfone, 50 μM D-campher-10-sulfonic acid, dissolved in water; 1:500 (v/v) added to the methanol and used to standardize the metabolite intensity and to adjust the migration time), then mixed with 1 ml chloroform and 400 μl water (containing 4 μg ml^{-1} [U-^{13}C]-glutamine), followed by 20 s of vortexing. After centrifugation at 15,000*g* for 15 min at 4 °C, the supernatant (aqueous phase) was then divided into 3 portions: (1) 200 μl for HPLC–MS analysis; (2) 200 μl for CE–MS analysis on anion mode; and (3) 200 μl for CE–MS analysis on cation mode. Portion (1) was then lyophilized in a vacuum concentrator (CentriVap Benchtop Centrifugal Vacuum Concentrator (c7310037; Labconco) equipped with a CentriVap −84 °C Cold Trap (7460037; Labconco) and an EDWARDS nXDS15i pump) at 4 °C for 12 h and then dissolved in 50 μl of 50% (v/v, in water) acetonitrile, followed by centrifugation at 15,000*g* for another 30 min at 4 °C. Next, 20 μl of the supernatant was loaded into an injection vial (5182-0714, Agilent Technologies; with an insert (HM-1270, Zhejiang Hamag Technology)) equipped with a snap cap (HM-2076, Zhejiang Hamag Technology), and 2 μl of the supernatant was injected into a HILIC column (ZICpHILIC, 5 μm, 2.1 mm × 100 mm, PN: 1.50462.0001, Millipore) on an ExionLC AD UPLC system (SCIEX), which was interfaced with a QTRAP 5500 MS (SCIEX). The mobile phase consisted of 15 mmol l^{-1} ammonium acetate containing 3 ml l^{-1} ammonium hydroxide (>28%, v/v) in LC–MS grade water (mobile phase A), and LC–MS grade 90% (v/v) acetonitrile in LC–MS grade water (mobile phase B), and was run at a flow rate of 0.2 ml min^{-1}. The HPLC gradient elution program was 95% B held for 2 min, then to 45% B for 13 min, held for 3 min, and then back to 95% B for 4 min. Each sample was analysed on both positive and negative modes on the HPLC–MS instrument. The mass spectrometer was run on a Turbo V ion source with spray voltages of −4,500 V (negative mode) and 5,500 V (positive mode), source temperature at 550 °C, gas no. 1 at 50 psi, gas no. 2 at 55 psi and curtain gas at 40 psi. Metabolites were measured using the multiple reactions monitoring mode (MRM), and declustering potentials and collision energies were optimized using analytical standards. Data were collected using Analyst software (v.1.7.1, SCIEX), and the relative amounts of metabolites were analysed using MultiQuant software (v.3.0.3, SCIEX). Portions (2) and (3) of the supernatant were filtered through a 5-kDa cut-off filter (OD003C34, PALL) by centrifuging at 12,000*g* for 3 h at 4 °C. The filtered aqueous phase was then lyophilized at 4 °C and then re-dissolved in 100 μl water containing IS2 (50 μM 3-aminopyrrolidine dihydrochloride, 50 μM *N*,*N*-diethyl-2-phenylacetamide, 50 μM trimesic acid and 50 μM 2-naphtol-3,6-disulfonic acid disodium salt, dissolved in methanol; used to adjust the migration time; 1:200 for portion (2) or 1:400 for portion (3)). Next, 20 μl of re-dissolved portion (2) and portion (3) solutions was loaded into an injection vial (9301-0978, Agilent Technologies; equipped with a snap cap (5042-6491, Agilent Technologies)). Before CE–MS analysis, the fused-silica capillary (TSP050375, i.d. 50 μm × 80 cm; Polymicro Technologies) was installed in a CE–MS cassette (G1603A; Agilent Technologies) on a 7100 CE system (Agilent Technologies). For anion mode, the capillary was pre-conditioned with 1 M NaOH for 0.5 h, flushed with di-distilled water for 2 h and then washed with anion conditioning buffer (25 mM ammonium acetate and 75 mM diammonium hydrogen phosphate, pH 8.5) for 1 h, followed by balancing with anion running buffer (50 mM ammonium acetate, pH 8.5; freshly prepared) for another 2 h. The capillary was then washed again using anion conditioning buffer for 5 min, followed by injection of the samples at a pressure of 50 mbar for 25 s, and then separation with a constant voltage at −30 kV for another 40 min in the anion running buffer. Sheath liquid (0.1 μM hexakis(1*H*, 1*H*, 3*H*-tetrafluoropropoxy)phosphazine, 10 μM ammonium trifluoroacetate, dissolved in methanol–water (50% v/v); freshly prepared) was flowed at 1 ml min^{-1} through a 1:100 flow splitter (1260 Infinity II; Agilent Technologies; actual flow rate to the MS: 10 μl min^{-1}) throughout each run. The parameters of 6545 MS (Agilent Technologies) were set as follows: ion source, dual AJS ESI; polarity, negative; nozzle voltage, 2,000 V; fragmentor voltage, 110 V; skimmer voltage, 50 V; OCT RFV, 500 V; drying gas (N_2) flow rate, 7 l min^{-1}; drying gas (N_2) temperature, 300 °C; nebulizer gas pressure, 8 psig; sheath gas temperature, 125 °C; sheath gas (N_2) flow rate, 4 l min^{-1}; capillary voltage (applied onto the sprayer), 3,500 V; reference (lock) masses, *m/z* 1,033.988109 for hexakis(1*H*, 1H, 3*H*-tetrafluoropropoxy) phosphazine and *m/z* 112.985587 for trifluoroacetic acid; scanning range, 50–1,100 *m/z*; and scanning rate, 1.5 spectra s^{-1}. For cation mode, the capillary was pre-conditioned with 1 M NaOH for 30 min, followed by flushing with di-distilled water for 2 h and then cation running buffer (1 mol l^{-1} formic acid, freshly prepared) for another 2 h. Samples were

separated as for the anion mode, except that cation running buffer was used, the capillary voltage was set to 3,500 V and the fragmentor voltage was 80 V. Data were collected using MassHunter LC–MS acquisition 10.1.48 (Agilent Technologies) and were processed using Qualitative Analysis B.06.00 (Agilent Technologies).

To analyse polar metabolites by GC–MS[68], 50 µl of each serum sample was instantly mixed with 200 µl methanol containing 40 µg ml^{-1} tridecanoic acid and 10 µg ml^{-1} myristic-d27 acid as internal standards, followed by 20 s of vortexing and 30 min of incubation at −20 °C. The mixture was then centrifuged at 15,000*g* for 15 min at 4 °C, and 200 µl of supernatant (aqueous phase) was lyophilized at 4 °C for 24 h. The lyophilized sample was then vortexed for 1 min after mixing with 50 µl of freshly prepared methoxyamine hydrochloride (20 mg ml^{-1} in pyridine), followed by incubation at 4 °C for 1 h. The mixture was sonicated at 0 °C by bathing in an ice slurry for 10 min, and was then incubated at 37 °C for 1.5 h, followed by mixing with 50 µl MSTFA and incubated at 37 °C for 1 h. Before subjecting to GC–MS, samples were centrifuged at 15,000*g* for 10 min, and 60 µl of each supernatant was loaded into an injection vial (5182-0714, Agilent; with an insert (HM-1270, Zhejiang Hamag Technology)) equipped with a snap cap (HM-0722, Zhejiang Hamag Technology). GC was performed on a HP-5MS column (30 m × 0.25 mm i.d., 0.25 µm film thickness) using a GC/MSD instrument (7890-5977B, Agilent Technologies). The injector temperature was set to 260 °C. The column oven temperature was first held at 70 °C for 2 min, then increased to 180 °C at the rate of 7 °C min^{-1}, then to 250 °C at the rate of 5 °C min^{-1}, then to 310 °C at the rate of 25 °C min^{-1}, at which it was held for 15 min. The MSD transfer temperature was 280 °C. The MS quadrupole and source temperature were maintained at 150 °C and 230 °C, respectively. Data were collected using MassHunter GC–MS Acquisition software (v.B.07.04.2260, Agilent Technologies) and were analysed using GC–MS MassHunter Workstation Qualitative Analysis software (v.10.1.733.0, Agilent Technologies).

Quantitative lipidomics was performed using stable isotope dilution methods[145,146]. In brief, lipids were extracted from 50 µl of serum using previously described method[147], but with modifications. Serum samples were mixed with 750 µl chloroform–methanol–MilliQ water (same hereafter for lipidomics) (3:6:1 v/v/v). After incubating at 1,500 r.p.m. for 1 h at 4 °C on a ThermoMixer C (Eppendorf), 350 µl water and 250 µl chloroform were added to the mixture to induce phase separation. After transferring the organic phase to a clean Eppendorf tube, the remaining lipid in the mixture was extracted again through the addition of another 450 µl chloroform. The organic phase obtained from the two rounds of extraction was pooled and lyophilized using a SpeedVac Vacuum Concentrator (Genevac) under OH mode. Samples were then dissolved in 100 µl of chloroform–methanol (1:1) (v/v) containing an internal standard cocktail (see ref. 147). Lipidomics analyses were conducted at LipidALL Technologies using a Nexera 20-AD HPLC (Shimadzu) coupled with QTRAP 6500 PLUS MS (SCIEX), as previously described[146]. For polar lipids, normal phase (NP) HPLC was performed using a TUP-HB silica column (i.d. 150 × 2.1 mm, 3 µm; Tuplabs), and the gradient elution program was as follows: 2% B (chloroform–methanol–ammonium hydroxide–water, mixed at 55:39:0.5:5.5 (v/v); with mobile phase A: chloroform–methanol–ammonium hydroxide, 89.5:10:0.5 (v/v)) held for 2 min, followed by 3 incremental increases: (1) to 35% B at the 3rd min, (2) to 55% B at the 5th min, and (3) to 85% B at the 6th min; and then maintained at 85% B for 1 min, followed by increasing to 100% B within 0.2 min and maintained for another 3.8 min, and finally decreased to 2% B within 0.5 min. The column was equilibrated at 2% B for 4.5 min between each run. Polar lipids were qualified by three separate injections under ESI mode, with two injections in positive mode at two separate dilutions (for phosphatidylcholine (PC), lysophosphatidylcholine (LPC), sphingomyelin (SM), ceramide (Cer), glucosylceramide (GluCer), lactosylceramide (LacCer) and sphingosine (Sph); to guarantee that all polar lipids detected fall within the linear ranges of intensities), and one injection in negative mode (for phosphatidylethanolamine (PE), phosphatidylglycerol (PG), phosphatidylinositol (PI), phosphatidic acid (PA), phosphatidylserine (PS), bis(monoacylglycero)phosphate (BMP), also known as lysobisphosphatidic acid), cardiolipin (CL), ganglioside (GM3), saccharolipids (SL), free fatty acid (FFA), lysophosphatidylethanolamine (LPE), lysophosphatidylinositol (LPI), lysophosphatidic acid (LPA), lysophosphatidylserines (LPS) and PC with fatty acyl-specific transitions). MS source parameters were set as follows: curtain gas flow (CUR), 20; temperature (TEM), 400 °C; ion source gas 1 (GS1), 20; and ion source gas 2 (GS2), 20. MRM transitions were set up for the quantitative analysis of polar lipids. Each polar lipid species was quantified by referencing to spiked internal standards, including d9-PC32:0(16:0/16:0), d9-PC36:1p(18:0p/18:1), d7-PE33:1(15:0/18:1), d9-PE36:1p(18:0p/18:1), d31-PS(d31-16:0/18:1), d7-PA33:1(15:0/18:1), d7-PG33:1(15:0/18:1), d7-PI33:1(15:0/18:1), C17-SL, Cer d18:1/15:0-d7, C12:0 Cer-1-P, d9-SM d18:1/18:1, C8-GluCer, C8-GalCer, d3-LacCer d18:1/16:0 Gb3 d18:1/17:0, d7-LPC18:1, d7-LPE18:1, C17-LPI, C17-LPA, C17-LPS, C17-LPG, d17:1 Sph, d17:1 S1P (Avanti Polar Lipids), GM3-d18:1/18:0-d3 (Matreya), d31-16:0 (Sigma) and d8-20:4 (Cayman Chemicals). For neutral lipids (TAGs and DAGs), a Kinetex-C18 column (i.d. 4.6 × 100 mm, 2.6 µm; Phenomenex) and an isocratic mobile phase containing chloroform–methanol–0.1 M ammonium acetate 100:100:4 (v/v/v) at a flow rate of 300 µl min^{-1} for 10 min were used. MS source parameters were set as described above, and ESI-positive mode was used. Levels of short-chain, medium-chain and long-chain TAGs were quantified by referencing to spiked internal standards of TAG(14:0)3-d5, TAG(16:0)3-d5 and TAG(18:0)3-d5 (CDN isotopes), whereas DAGs d5-DAG17:0/17:0 and d5-DAG18:1/18:1 (Avanti Polar Lipids) were used. For free Cho and total cholesteryl esters, the method involving atmospheric pressure chemical ionization in positive mode on a 1260 Infinity II HPLC (Agilent Technologies) coupled to a QTRAP 5500 MS (SCIEX), as established previously[148], was used, during which lipids were separated on an Eclipse XDB C18 5-µm column (i.d. 150 × 4.6 mm; Agilent Technologies) using an isocratic mobile phase comprising chloroform–methanol (1:1 v/v) at a flow rate of 700 µl min^{-1}, and the MS source was set as follows: CUR 20; temperature, 500 °C; GS1, 45; and GS2 35. MS data were acquired and analysed using Analyst 1.6.3 software (SCIEX). During the analysis, quality control samples, pooled from analysis samples, were inserted into the sample queue across every ten biological samples.

Measurement of adenylates and NAD$^+$

ATP, ADP, AMP and NAD$^+$ from cells, tissues or flies were analysed by CE–MS as described in the section 'Determination of the serum metabolome', except that cells collected from a 10-cm dish (60–70% confluence), 100 mg of liver or muscle tissue dissected by freeze clamping, or 20 anaesthetized adult flies were used. Before CE–MS analysis, cells were rinsed with 20 ml of 5% (m/v) mannitol solution (dissolved in water) and instantly frozen in liquid nitrogen. Cells were then lysed with 1 ml methanol containing IS1 (1:500 dilution) and were scraped from the dish. For analysis of metabolites in the liver and muscle, mice were anaesthetized after indicated treatments. The tissue was then quickly excised by freeze clamping and then ground in 1 ml methanol with IS1. For analysis of metabolites in flies, anaesthetized flies were ground in 1 ml methanol with IS1 after freezing by liquid nitrogen. The lysate was then mixed with 1 ml chloroform and 400 µl water by 20 s of vortexing. After centrifugation at 15,000*g* for 15 min at 4 °C, 420 µl of the aqueous phase was collected, filtrated, lyophilized, dissolved and subjected to CE–MS analysis in the negative mode as described in the section 'Determination of the serum metabolome'. Data were collected using MassHunter LC–MS acquisition 10.1.48 (Agilent Technologies) and were processed using Qualitative Analysis B.06.00 (Agilent Technologies). Levels of AMP, ADP, ATP and NAD$^+$ were measured using full scan mode with *m/z* values of 346.0558, 426.0221, 505.9885 and 662.1019, respectively. Note that a portion of ADP and ATP could lose one phosphate group during in-source fragmentation, thus leaving the same *m/z* ratios as AMP and ADP, and should be corrected according

to their different retention times in the capillary. Therefore, the total amount of ADP is the sum of the latter peak of the *m/z* 346.0558 spectrogram and the former peak of the *m/z* 426.0221 spectrogram, and the same is applied for ATP. Note that the retention time of each metabolite (and IS1 and IS2) may vary between each run and can be adjusted using isotope-labelled standards (dissolved in individual cell or tissue lysates) run between each sample.

Levels of ATP, ADP, AMP and NAD^+ in nematodes were analysed by HPLC–MS as described in the section 'Determination of the serum metabolome', except that 150 nematodes maintained on NGM plates (with or without 50 mM) for 48 h were used. Nematodes were washed with ice-cold M9 buffer containing Triton X-100. Bacteria were removed by quickly spinning down the slurry at 100*g* for 5 s. Nematodes were then instantly lysed in 1 ml methanol then mixed with 1 ml chloroform and 400 µl water (containing 4 µg ml^{-1} [U-^{13}C]-glutamine), followed by 20 s of vortexing. After centrifugation at 15,000*g* for another 15 min at 4 °C, 800 µl of the aqueous phase was collected, lyophilized in a vacuum concentrator at 4 °C and then dissolved in 30 µl of 50% (v/v, in water) acetonitrile. Metabolites were determined by HPLC–MS in the negative mode as described in the section 'Determination of the serum metabolome'. The following transitions (Q1/Q3) were used for monitoring each compound: 505.9/158.9 and 505.9/408.0 for ATP; 425.9/133.9, 425.9/158.8 and 425.9/328.0 for ADP; 345.9/79.9, 345.9/96.9 and 345.9/133.9 for AMP; 662.0/540.1 for NAD^+; and 149.9/114 for [U-^{13}C]-glutamine. Data were collected using Analyst software (v.1.7.1, SCIEX), and the relative amounts of metabolites were analysed using MultiQuant software (v.3.0.3, SCIEX). Similar to CE–MS analysis, a portion of ADP and ATP could lose one or two phosphate groups during in-source-fragmentation, thus leaving the same *m/z* ratios as AMP and ADP, which was corrected according to their different retention times in the column.

Determination of bile acid concentrations

To measure bile acid concentrations, MEFs (60–70% in 10-cm dish, rinsed with PBS and trypsinized), tissues (50 mg of liver or muscle tissues collected from each mouse after anaesthetizing and blood-draining), nematodes (1,000 nematodes at L4 stage, washed with M9 buffer containing Triton X-100 for 3 times and frozen in liquid nitrogen) and flies (20 anaesthetized adults washed with PBS for 3 times and frozen in liquid nitrogen) were rinsed in PBS for 5 times, each in a fresh Eppendorf tube, or serum (50 µl collected from each mouse) was vigorously mixed (for serum) or homogenized (for others) with 1 ml of 80% methanol (v/v, in water) containing 100 µg l^{-1} CA-d5 and 4 µg ml^{-1} [U-^{13}C]-glutamine as internal standards. After centrifugation at 15,000*g* for 15 min at 4 °C, 30 µl of the supernatant was loaded into an injection vial (5182-0714, Agilent Technologies; with an insert (HM-1270, Zhejiang Hamag Technology)) equipped with a snap cap (HM-2076, Zhejiang Hamag Technology), and 2 µl of supernatant was injected into an ACQUITY HSS T3 column (Waters). Measurement was performed on a QTRAP 6500 Plus MS (SCIEX) connected to an ACQUITY I-class UPLC system (Waters). The mobile phase consisted of 10 mM ammonium formate containing 0.005% formic acid (v/v) in LC–MS grade water (mobile phase A) and LC–MS grade acetonitrile (mobile phase B) run at a flow rate of 0.4 ml min^{-1}. The HPLC gradient was as follows: 30% B for 1 min, then to 100% B at the 10th min, hold for 2 min, and then back to 30% B, hold for another 3 min. The mass spectrometer was run on a Turbo V ion source and running in negative mode at a spray voltage of −5,500 V, with source temperature at 550 °C, gas no. 1 at 50 psi, gas no. 2 at 60 psi, curtain gas at 35 psi, and collision gas at medium. Compounds were measured using the MRM mode, and declustering potentials and collision energies were optimized using analytical standards. The following transitions (Q1/Q3) were used for monitoring each compound: 391.2/345.2 for deoxycholate; 407.2/345.2 for CA; 448.4/74.0 for glycochenodeoxycholate; 464.2/74.0 for glycocholate; 498.3/80.0 for taurodeoxycholate; 391.2/391.2 for ursodeoxycholate; 375.2/375.2 for LCA; 391.2/373.2 for CDCA; 482.2/80.0 for taurolithocholate; 498.2/79.9 for tauroursodeoxycholate; 448.4/74.0 for glycodeoxycholate; 514.3/79.9 for taurocholate; 498.3/80.0 for taurochenodeoxycholate; 407.3/387.3 for α-muricholate; 407.3/371.1 for β-muricholate; 407.3/405.3 for ω-muricholate; 514.3/123.9 for tauro-α-muricholate; 514.3/79.8 for tauro-β-muricholate; 149.9/114 for [U-^{13}C]-glutamine; and 412.3/348.3 for CA-d5. For quantification of LCA, the LCA-d4 dissolved in individual lysates was used to generate corresponding standard curves by plotting the area ratios of labelled LCA (areas of LCA divided by the two ISs) against the added or actual concentrations of labelled LCA. The concentrations of LCA were estimated according to standard curves. The average volume and density were 2,000 $µm^3$ (ref. 85) and 1.1 g ml^{-1} (ref. 149), respectively, for MEFs; 3,500 $µm^3$ and 1.06 g ml^{-1}, respectively, for mouse myocytes[150,151]; and 1×10^6 $µm^3$ and 1.07 g ml^{-1}, respectively, for nematodes[152,153]. Data were collected using Analyst software (v.1.6.3, SCIEX), and the relative amounts of metabolites were analysed using MultiQuant software (v.3.0.2, SCIEX).

Reagents

The following antibodies were purchased from Cell Signaling Technology: rabbit anti-phospho-AMPKα-Thr172 (2535, RRID: AB_331250; 1:1,000 for IB); anti-AMPKα (2532, RRID: AB_330331; 1:1,000 for IB); anti-phospho-ACC-Ser79 (3661, RRID: AB_330337; 1:1,000 for IB); anti-ACC (3662, RRID: AB_2219400; 1:1,000 for IB); anti-GAPDH (5174, RRID: AB_10622025; 1:1,000 for IB); anti-phospho-p70 S6K-S389 (9234, RRID: AB_2269803; 1:1,000 for IB); anti-p70 S6K (2708, RRID: AB_390722; 1:1,000 for IB); anti-TFEB (83010, 1:100 for immunofluorescence (IF)); anti-phospho-RPA32/RPA2-S8 (54762, RRID: AB_2799471; 1:1,000 for IB); anti-RPA32/RPA2 (35869, RRID: AB_2799086; 1:1,000 for IB); and anti-AXIN1 (2074, RRID: AB_2062419; 1:1,000 for IB). Rabbit anti-tubulin (10068-1-AP; RRID: AB_2303998; 1:1,000 for IB) was purchased from Proteintech. The following antibodies were purchased from Abcam: mouse anti-total OXPHOS (ab110413, RRID: AB_2629281; 1:5,000 for IB); rabbit anti-laminin (ab11575, RRID: AB_298179; 1:200 for IF); anti-gamma H2A.X (ab11174, RRID: AB_297813; 1:1000 for IB); and anti-UCP1 (ab10983, RRID: AB_2241462; 1:1,000 for IB). The following antibodies were purchased from Developmental Studies Hybridoma Bank: mouse anti-eMHC (BF-G6, RRID: AB_10571455; 1:100 for IHC); anti-Pax7 (Pax-7, RRID: AB_2299243; 1:100 for IHC); anti-MHCIIa (SC71, RRID: AB_2147165; 1:100 for IHC); anti-MHCIIb (BF-F3, RRID: AB_2266724; 1:100 for IHC); and anti-MHCI (C6B12, RRID: AB_528351; 1:100 for IHC). Mouse anti β-acting (A5316, RRID: AB_476743; 1:1,000 for IB) was purchased from Sigma. The following antibodies were purchased from Thermo: goat anti-Mouse IgM (heavy chain) cross-adsorbed secondary antibody, Alexa Fluor 488 (A-21042, RRID: AB_2535711; 1:200 for IHC); goat anti-mouse IgG2b cross-adsorbed secondary antibody, Alexa Fluor 594 (A-21145, RRID: AB_2535781; 1:200 for IHC); goat anti-mouse IgG1 cross-adsorbed secondary antibody, Alexa Fluor 647 (A-21240, RRID: AB_2535809; 1:200 for IHC); goat anti-mouse IgG1 cross-adsorbed secondary antibody, Alexa Fluor 488 (A-21121, RRID: AB_2535764; 1:200 for IHC); goat anti-rabbit IgG (H+L) cross-adsorbed secondary antibody, Alexa Fluor 594 (A-11012, RRID: AB_2534079; 1:200 for IHC); and goat anti-rabbit IgG (H+L) highly cross-adsorbed secondary antibody, Alexa Fluor 488 (A-11034, RRID: AB_2576217; 1:100 for IF). The horseradish peroxidase (HRP)-conjugated goat anti-mouse IgG (115-035-003, RRID: AB_10015289; 1:5,000 dilution for IB) and goat anti-rabbit IgG (111-035-003, RRID: AB_2313567; 1:5,000 dilution for IB) antibodies were purchased from Jackson ImmunoResearch.

Information on supplier and catalogue numbers of metabolites for screening are listed in Supplementary Table 1. The following reagents were purchased from Sigma (catalogue numbers in parentheses): DMSO (D2650), LCA (L6250), ferulic acid (PHR1791), (2-hydroxypropyl)-β-cyclodextrin (C0926), NaCl (S7653), $CaCl_2$ (C5670), $MgSO_4$ (M2643), H_2O_2 (H1009), KH_2PO_4 (P5655), K_2HPO_4 (P9666), streptomycin (85886), cholesterol (C3045), agar (A1296), propionic acid (P5561), sucrose

(S7903), glucose (G7021), haematoxylin solution (51275), heparin (H3149), 2-methylbutane (isopentane; M32631), paraformaldehyde (158127), eosin Y-solution (318906), methanol (646377), ethanol (459836), chloroform (C7559), PBS (P5493), Triton X-100 (T9284), xylene (534056), D-mannitol (M4125), Canada balsam (C1795), BSA (A2153), glycerol (G5516), Na_2HPO_4 (S7907), sodium hypochlorite solution (NaClO; 239305), NaOH (S8045), iron(II) sulfate heptahydrate ($FeSO_4$; F8633), isopropanol (34863), diethylpyrocarbonate (DEPC)-treated water (693520), paraquat (36541), HEPES (H4034), EDTA (E6758), EGTA (E3889), $MgCl_2$ (M8266), KCl (P9333), IGEPAL CA-630 (NP-40, I8896, for IF only), IGEPAL CA-630 (NP-40; 3021), dithiothreitol (DTT; 43815), hexadimethrine bromide (polybrene; H9268), collagenase B (11088831001), dispase II (4942078001), proteinase K (P6556), agarose (A9539), L-methionine sulfone (M0876), D-campher-10-sulfonic acid (1087520), acetonitrile (34888), ammonium acetate (73594), ammonium hydroxide solution (338818), 3-aminopyrrolidine dihydrochloride (404624), *N*,*N*-diethyl-2-phenylacetamide (384011), trimesic acid (482749), diammonium hydrogen phosphate (1012070500), ammonium trifluoroacetate (56865), formic acid (5.43804), tridecanoic acid (T0502), myristic-d27 acid (68698), methoxyamine hydrochloride (89803), hexane (34859), pyridine (270970), MSTFA (M-132), cholic acid-2,2,3,4,4-d5 (CA-d5; 614106), ammonium formate (70221), lithocholic acid-2,2,4,4-d4 (LCA-d4; 589349), Trizma base (Tris; T1503), sodium pyrophosphate (P8135), β-glycerophosphate (50020), SDS (436143), sodium deoxycholate (S1827), glutaraldehyde solution (G5882), glycine (G8898), $K_3Fe(CN)_6$ (455946), thiocarbonohydrazide (223220), $Pb(NO_3)_2$ (203580), acetone (534064), sodium citrate (71497), PD98059 (P215), FCCP (C2920), sodium azide (NaN_3; S2002), gentamycin (345814), collagenase A (11088793001), oligomycin A (75351), cardiotoxin (217503), Tween-20 (P9416), NaH_2PO_4 (S8282), formaldehyde solution (formalin; F8775), ampicillin (A9518), metronidazole (M3761), neomycin (N6386), benzoic acid (NIST39J), Nile Red (72485), and Ketone Body Assay kit (MAK134). Vancomycin (V32969) was purchased from InvivoChem. CA (HY-N0324), CDCA (HY-76847), TUDCA (HY-19696), TCA (HY-B1788), 1-methyladenosine (HY-113081) and diprotin A (HY-111174) were purchased from MedChemExpress. Rapamycin (S1039), 4-methyl-2-oxovaleric acid (S2987), mandelic acid (S9003) and methylmalonic acid (S3683) were purchased from Selleck. 3-Hydroxynaphthalene-2,7-disulfonic acid disodium salt (2-naphtol-3,6-disulfonic acid disodium salt; H949580) was purchased from Toronto Research Chemicals. Hexakis(1*H*,1*H*,3*H*-perfluoropropoxy)phosphazene (hexakis(1*H*,1*H*,3*H*-tetrafluoropropoxy)phosphazine; sc-263379) was purchased from Santa Cruz Biotechnology. Protease inhibitor cocktail (70221) was purchased from Roche. Seahorse XF base medium (103334) was purchased from Agilent Technologies. RNAprotect Tissue Reagent (76106) was purchased from Qiagen. OsO_4 (18465) and uranyl acetate (19481) were purchased from Tedpella. SPI Low Viscosity "Spurr" Kit (02680-AB) was purchased from Structure Probe. Isolithocholic acid (iso-LCA; 700195) was purchased from Avanti Polar Lipids. 3-Oxo-5β-cholanoic acid (3-oxo-LCA; HY-125801), allolithocholic acid (allo-LCA; HY-143712), isoallolithocholic acid (isoallo-LCA; HY-B0172A) and 3-oxoallo-LCA (customized) were purchased from MCE. Free Glycerol Assay kit (ab65337) and Glycogen Assay kit (ab65620) were purchased from Abcam. Bacteriological peptone (LP0037) and yeast extract (LP0021) were purchased from Oxoid. Insulin (Novolin R) was purchased from Novo Nordisk. Quick-Load Taq 2× Master Mix (M0271), NEBNext Poly(A) mRNA Magnetic Isolation Module (E7490), and NEBNext Ultra RNA Library Prep kit for Illumina (E7530) were purchased from NEB. AMPure XP Beads (63881) was purchased from Beckman Coulter. TruSeq PE Cluster kit v3-cBot-HS kit (PE-401-3001) was purchased from Illumina. Biospin Tissue Genomic DNA Extraction kit (BSC04M1) was purchased from BioFlux. The following reagents were purchased from Thermo: DMEM-high glucose (12800082), Liver Perfusion Medium (17701038), Liver Digest Medium (17703034), William's E Medium (12551032), Ham's F-10 medium (11550043), basic fibroblast growth factor (bFGF; 13256-029), Schneider's *Drosophila* Medium (21720024), DMEM containing HEPES (21063029), DMEM without phenol (31053028), MEM non-essential amino acids solution (11140050), GlutaMAX (35050061), sodium pyruvate (11360070), Maxima SYBR Green/ROX qPCR Master Mix (K0223), Trypan Blue Stain (T10282), FBS (10099141C), Fluo-4-AM (F14217), ProLong Diamond antifade mountant (P36970), ProLong Live Antifade reagent (P36975), penicillin–streptomycin (15140163), Prestained Protein MW Marker (26612), BCA Protein Assay kit (A55865), Maxima SYBR Green/ROX qPCR master mix (K0223), TRIzol (15596018), and GLP-1 Multispecies ELISA Kit (BMS2194). ReverTra Ace qPCR RT master mix with gDNA remover (FSQ-301) was purchased from Toyobo. WesternBright ECL and peroxide solutions (210414-73) were purchased from Advansta. Dry yeast (FLY804020F) and cornmeal (FLY801020) were purchased from LabScientific. Soy flour (62116) was purchased from Genesee. Light corn syrup was purchased from Karo. O.C.T. Compound (4583) was purchased from Sakura. Mouse Ultrasensitive Insulin ELISA kit (80-INSMSU-E10) was purchased from ALPCO. LabAssay Triglyceride Kit (LABTRIG-M1) and LabAssay NEFA kit (LABNEFA-M1) were purchased from Wako. Mouse Glucagon ELISA Kit (81518) was purchased from Crystal Chem. [U-^{13}C]-glucose (CLM-1396-PK) and [U-^{13}C]-glutamine (CLM-1822-H-PK) were purchased from Cambridge Isotope Laboratories.

Cell lines

In this study, no cell line used is on the list of known misidentified cell lines maintained by the International Cell Line Authentication Committee (https://iclac.org/databases/cross-contaminations/). HEK293T cells (CRL-3216) and *Drosophila* Schneider 2 (S2) cells (CRL-1963) were purchased from the American Type Culture Collection. MEFs were established by introducing SV40 T antigen through lentivirus into cultured primary embryonic cells from mouse litters as previously described[97]. HEK293T cells and MEFs were maintained in DMEM supplemented with 10% FBS, 100 IU penicillin and 100 mg ml^{-1} streptomycin at 37 °C in a humidified incubator containing 5% CO_2. S2 cells were cultured in Schneider's *Drosophila* medium supplemented with 10% heat-inactivated FBS, 100 IU penicillin and 100 mg ml^{-1} streptomycin at 37 °C in a humidified incubator containing 5% CO_2. All cell lines were verified to be free of mycoplasma contamination. HEK293T cells and MEFs were authenticated by STR sequencing, and *Drosophila* S2 cells by species identification using DNA-barcode assay, performed by Immocell Biotechnology.

The *Tgr5* gene was deleted from MEFs using the CRISPR–Cas9 system. Oligonucleotides were annealed to their complements containing the cloning tag aaac and inserted into the back-to-back BsmB I restriction sites of the lentiCRISPRv2 vector. The sequence for sgRNA is as follows: 5′-TAGTGGTGGGCGACGCTCAT-3′ and 5′-ATGAGCGTCGCCCACCACTA-3′ (1), 5′-GGCTGCGCAAGTGGCGGTCC-3′ and 5′-GGACCGCCACTTGCGCAGCC-3′ (2). The constructs were then subjected to lentivirus packaging using HEK293T cells that were transfected with 2 μg of DNA in Lipofectamine 2000 transfection reagent per well of a 6-well plate. At 30 h after transfection, medium (DMEM supplemented with 10% FBS and MEM non-essential amino acids; approximately 2 ml) was collected and centrifuged at 5,000*g* for 3 min at room temperature. The supernatant (virus) was mixed with 10 μg ml^{-1} polybrene and was added to MEFs (cultured to 15% confluence), followed by centrifuging at 3,000*g* for 30 min at room temperature (spinfection). Cells were incubated with the virus for 72 h. When cells were approaching confluence, they were single-cell sorted into 96-well dishes. Clones were expanded and evaluated for knockout status by sequencing.

IB analysis

To analyse pAMPKα and pACC levels in HEK293T cells, MEFs, S2 cells, mouse primary hepatocytes and primary myocytes, cells grown to 70–80% confluence in a well of a 6-well dish were lysed with 250 μl

ice-cold Triton lysis buffer (20 mM Tris-HCl, pH 7.5, 150 mM NaCl, 1 mM EDTA, 1 mM EGTA, 1% (v/v) Triton X-100, 2.5 mM sodium pyrophosphate, 1 mM β-glycerophosphate and protease inhibitor cocktail). The lysates were then centrifuged at 20,000*g* for 10 min at 4 °C, and an equal volume of 2× SDS sample buffer was added into the supernatant. Samples were then boiled for 10 min and then directly subjected to IB. To analyse of pAMPKα and pACC levels in muscle and liver tissues, mice were anaesthetized after indicated treatments. For CR-treated and LCA-treated mice, tissue samples were collected at 8:00 unless stated otherwise. Freeze-clamped tissue samples were immediately lysed with ice-cold Triton lysis buffer (10 μl mg^{-1} tissue weight for liver, and 5 μl mg^{-1} tissue weight for muscle), followed by homogenization and centrifugation as described above. The lysates were then mixed with 2× SDS sample buffer, boiled and subjected to IB. To analyse pAMPKα and pACC levels in flies, 20 adults or third instar larvae were lysed with 200 μl ice-cold RIPA buffer (50 mM Tris-HCl, pH 7.5, 150 mM NaCl, 1% NP-40, 0.5% sodium deoxycholate and protease inhibitor cocktail) containing 0.1% SDS, followed by homogenization and centrifugation as described above. The lysates were then mixed with 5× SDS sample buffer, boiled and subjected to IB. To analyse pAMPKα and pACC levels in nematodes, 150 nematodes cultured on NGM plates were collected for each sample. Worms were quickly washed with ice-cold M9 buffer containing Triton X-100 and were lysed with 150 μl ice-cold lysis buffer. The lysates were then mixed with 5× SDS sample buffer, followed by homogenization and centrifugation as described above, and then boiled before being subjected to IB. Precautions in sample preparation were taken for determination of AMPK activation, as previously described[154]. In brief, for cultured cells, the culture medium was rapidly removed and the cells were immediately lysed with ice-cold lysis buffer or frozen in liquid nitrogen. Tissue samples were freeze-clamped on anaesthetized mice, followed by immediate transfer to liquid nitrogen, as any ischaemia would lead to activation of CaMKK2, which strongly activates AMPK, to such an extent that it could overshadow the lysosomal pathway-mediated activation of AMPK. When homogenizing the tissue, it was directly transferred to ice-cold lysis buffer from liquid nitrogen and homogenized immediately without allowing it to thaw to room temperature. In addition, any exposure to a poor medium such as PBS would cause a higher background of AMPK. All samples were subjected to IB on the same day of preparation, and any freeze–thaw cycles were avoided.

For IB, SDS–PAGE gels were prepared in-house as previously described[155]. The thickness of the gels used in this study was 1.0 mm. Samples of less than 10 μl were loaded into wells, and electrophoresis was run at 100 V (by PowerPac HC High-Current Power Supply, Bio-Rad) in a Mini-PROTEAN Tetra electrophoresis cell (Bio-Rad). In this study, all samples were resolved on 8% resolving gels, except those for OXPHOS proteins, which were on 15% gels (prepared as those for 8%, except that a final concentration of 15% acrylamide–Bis was added to the resolving gel solution), and β-actin which was on 10% gels. The resolved proteins were then transferred to a PVDF membrane (0.45 μm, IPVH00010, Merck) as previously described[155]. The PVDF membrane was then blocked with 5% (w/v) BSA (for all antibodies against phosphorylated proteins) or 5% (w/v) non-fat milk (for all antibodies against total proteins) dissolved in TBST for 2 h on an orbital shaker at 60 r.p.m. at room temperature, followed by rinsing with TBST twice, for 5 min each. The PVDF membrane was then incubated with the desired primary antibody overnight at 4 °C on an orbital shaker at 60 r.p.m., followed by rinsing with TBST 3 times, 5 min each at room temperature, and then secondary antibodies for 3 h at room temperature with gentle shaking. The secondary antibody was then removed, and the PVDF membrane was further washed with TBST 3 times, 5 min each at room temperature. The PVDF membrane was incubated in an ECL mixture (by mixing equal volumes of ECL solution and peroxide solution for 5 min), then life with medical X-ray film (Fujifilm). The films were then developed using X-OMAT MX developer (Carestream) and X-OMAT MX Fixer and Replenisher solutions (Carestream) on a medical X-ray processor (Carestream) using developer (model 002, Carestream). The developed films were scanned using a Perfection V850 Pro scanner (Epson) with Epson Scan software (v.3.9.3.4), and were cropped using Photoshop 2023 software (Adobe). Levels of total proteins and phosphorylated proteins were analysed on separate gels, and representative immunoblots are shown. The band intensities on developed films were quantified using ImageJ software (v.1.8.0, National Institutes of Health Freeware) and formatted using Illustrator 2022 (Adobe). Uncropped immunoblots are shown in Supplementary Fig. 1.

Confocal microscopy

For determining the localization of TFEB, MEFs grown to 80% confluence on coverslips in 6-well dishes were fixed for 20 min with 4% (v/v) formaldehyde in PBS at room temperature. The coverslips were rinsed twice with PBS and permeabilized with 0.5% (v/v) NP-40 in PBS for 15 min at room temperature. After rinsing twice with PBS, the sections were blocked with PBS containing 5% BSA for 30 min at room temperature. The coverslips were then incubated with anti-TFEB antibodies (1:100, diluted in PBS) for 8 h at room temperature, followed by rinsing 3 times with 1 ml of PBS. Cells were then incubated with Alexa Fluor 488-conjugated, goat anti-rabbit IgG secondary antibody (1:100, diluted in PBS) for 2 h at room temperature, and at 37 °C for another 30 min in the dark. Cells were washed another 4 times each with 1 ml of PBS and then mounted on slides using ProLong Diamond antifade mountant. Confocal microscopy images were taken using a STELLARIS 8 FALCON (Leica) systems equipped with HyD SMD detectors and a HC PL APO CS2 ×63/1.40 OIL objective (Leica). All parameters were kept unchanged between imaging. Images were taken and analysed using LAS X Software (Leica) and formatted using Photoshop 2023 software (Adobe).

Transmission electron microscopy imaging

Transmission electron microscopy (TEM) imaging was performed based on the in situ embedding and sectioning method as previously described[156], but with minor modifications. In brief, the tibialis anterior muscle was quickly excised and sliced to around 1 × 1 × 5 mm cubes, followed by rapid immersion in 1 ml of 2.5% (v/v) glutaraldehyde solution (freshly prepared by diluting 25% (v/v) glutaraldehyde in 0.1 M phosphate buffer (by mixing 0.2 M Na_2HPO_4 with 0.2 M NaH_2PO_4 (both dissolved in water, and adjusted pH to 7.4) at a ratio of 81:19, and then diluted with equal volume of water) at 4 °C for 12 h. Muscle samples were then washed with 1 ml of 0.1 M phosphate buffer 3 times at 4 °C, 20 min each, followed by staining with 1% (w/v) OsO_4 solution (in 0.1 M phosphate buffer, supplemented with 1.5% $K_3Fe(CN)_6$) at 4 °C for 2 h, and then washed by for 5 times, 10 min each with ice-cold di-distilled water. Muscle samples were stained in ice-cold 2% (w/v, in water) uranyl acetate solution for 12 h at 4 °C in the dark, and were then washed 4 times, 10 min each, with ice-cold water. Dehydration was then performed by sequentially incubating muscles in the following solutions: 30, 50 and 70% (v/v) ethanol (in water), each for 12 min at 4 °C, followed by incubating in 90, 100 and 100% (v/v) ethanol (in water), each for 12 min at room temperature, and then in acetone twice at room temperature. Muscle samples were then quickly submerged in acetone–Spurr resin (3:1; the Spurr resin was prepared by mixing 15 g NSA, 7.3 g DER 736, 7.5 g ERL 4206 with 320 μl DMAE, all supplied in the SPI Low Viscosity 'Spurr' kits, for 1.5 h at room temperature) mixture at room temperature for a 1-h incubation, and then in acetone/resin (1:1) mixture at room temperature for 2 h, followed by acetone–resin (1:3) at room temperature for 2 h, and finally 100% resin at room temperature for 12 h. The resin was then completely drained, and the tissue samples were baked in a hot-wind drying oven at 70 °C. After baking for 24 h, the tissues were then sectioned into 70-nm slices on an EM UC7 ultramicrotome (Leica) after cooling down to room temperature. Sections were then stained with lead citrate solution (by dissolving 1.33 g of $Pb(NO_3)_2$ and 1.76 g

of sodium citrate in 42 ml of di-distilled water, followed by addition of 8 ml of 1 M NaOH) for 5 min at room temperature before imaging using an AMT-XR81DIR camera on an electron microscope (HT-7800, Hitachi) with TEM system control software (v.01.20, Hitachi). The area of mitochondria was quantified using ImageJ software (v.1.8.0, National Institutes of Health Freeware).

Determination of intracellular Ca^{2+} levels

Intracellular Ca^{2+} levels in MEFs treated with LCA were determined as previously described[70]. In brief, cells were loaded with 5 μM (final concentration) Fluo-4-AM for 30 min, then washed twice with PBS and incubated in fresh, desired medium for another 30 min. Before imaging, ProLong Live Antifade reagent was added to the medium. During imaging, live cells were kept at 37 °C, 5% CO_2 in a humidified incubation chamber (Incubator PM S1; Zeiss). Images were taken on an LSM980 microscope (Zeiss). Images were processed and analysed using Zen 3.4 software (Zeiss) and formatted in Photoshop 2023 software (Adobe).

Determination of OCRs

The OCR of nematodes was measured as previously described[157]. In brief, nematodes were washed with M9 buffer 3 times. Next, 15–25 nematodes were suspended in 200 μl M9 buffer and were added into a well on a 96-well Seahorse XF Cell Culture microplate. The measurement was performed in a Seahorse XFe96 analyzer (Agilent Technologies) at 20 °C following the manufacturer's instructions, with a Seahorse XFe96 sensor cartridge (Agilent Technologies) pre-equilibrated in Seahorse XF Calibrant solution in a CO_2-free incubator at 37 °C overnight. Concentrations of respiratory chain inhibitors used during the assay were FCCP at 10 μM and sodium azide at 40 mM. At the end of the assay, the exact number of nematodes in each well was determined using a Cell Imaging Multi-Mode reader (Cytation 1, BioTek) and was used for normalizing/correcting OCR results. Data were collected using Wave 2.6.1 Desktop software (Agilent Technologies) and exported to Prism 9 (GraphPad) for further analysis according to the manufacturer's instructions.

The OCR of intact muscle tissue was measured as previously described[93,158]. In brief, mice were starved for desired durations and were killed through cervical dislocation. The gastrocnemius muscle from two hindlegs were then excised, followed by incubating in 4 ml of dissociation medium (DM; by dissolving 50 μg ml^{-1} gentamycin, 2% (v/v) FBS, 4 mg ml^{-1} collagenase A in DMEM containing HEPES) in a 35-mm culture dish in a humidified chamber at 37 °C, 5% CO_2, for 1.5 h. The digested muscle mass samples were then washed with 4 ml pre-warmed collagenase-A-free DM, incubated in 0.5 ml pre-warmed collagenase-A-free DM and dispersed by passing through a 20 G needle 6 times. Next, 20 μl of muscle homogenate was transferred to a well of a Seahorse XF24 Islet Capture microplate (Agilent Technologies). After placing an islet capture screen by a Seahorse Capture Screen Insert Tool (Agilent Technologies) into the well, 480 μl pre-warmed aCSF medium (120 mM NaCl, 3.5 mM KCl, 1.3 mM $CaCl_2$, 0.4 mM KH_2PO_4, 1 mM $MgCl_2$, 5 mM HEPES, 15 mM glucose, 1× MEM non-essential amino acids, 1 mM sodium pyruvate and 1 mM GlutaMAX; adjusted to pH 7.4 before use) was added, followed by equilibrating in a CO_2-free incubator at 37 °C for 1 h. OCR was then measured at 37 °C in a XFe24 Extracellular Flux analyzer (Agilent Technologies), with a Seahorse XFe24 sensor cartridge (Agilent Technologies) pre-equilibrated in Seahorse XF Calibrant solution (Agilent Technologies) in a CO_2-free incubator at 37 °C overnight. Respiratory chain inhibitors used during the assay were oligomycin at 100 μM, FCCP at 100 μM, 50 μM antimycin A and 1 μM rotenone (all final concentrations). Data were collected using Wave 2.6.3 Desktop software (Agilent Technologies) and exported to Prism 9 (GraphPad) for further analysis according to the manufacturer's instructions.

Determination of the critical micelle concentration of LCA

The critical micelle concentration (CMC) of LCA was determined using a fluorometric assay, with some modifications[159,160]. In brief, 1 μl Nile Red dye (5 mM stock solution dissolved in DMSO) was diluted with 2 ml PBS or DMEM (without phenol and supplemented with sodium pyruvate and GlutaMAX) in a quartz cuvette. The LCA stock solution at a concentration of 100 μM (prepared by diluting 100 mM LCA solution in DMSO with PBS or DMEM in a 1:1,000 ratio) was then gradually added to the Nile Red mixture, with 20 μl added each time to create a series of concentrations ranging from 0 to 12 μM (at concentrations higher than 12 μM, LCA precipitated in the medium). As a control, equal concentrations of Tween-20 were added to the mixture. The fluorescence of Nile Red was excited at 543 nm and recorded with a PMT detector at a voltage of 600 V, covering the emission spectrum of Nile Red (570–700 nm) by a Cary Eclipse spectrophotometer (Varian). The emission intensities recorded at each concentration of LCA were plotted to the concentration of LCA, and the inflection point of a Boltzmann fit of the resulting sigmoidal curve provides the CMC of LCA.

Statistical analysis

Statistical analyses were performed using Prism 9 (GraphPad Software), except for the survival curves, which were analysed using SPSS 27.0 (IBM) by log-rank (Mantel–Cox) test. Each group of data was subjected to Kolmogorov–Smirnov tests, Anderson–Darling tests, D'Agostino–Pearson omnibus tests or Shapiro–Wilk tests for normal distribution when applicable. An unpaired two-sided Student's *t*-test was used to determine the significance between two groups of normally distributed data. Welch's correction was used for groups with unequal variances. An unpaired two-sided Mann–Whitney test was used to determine the significance between data without a normal distribution. For comparison between multiple groups with two fixed factors, an ordinary two-way ANOVA or two-way repeated-measures ANOVA (for blood glucose measured during GTT, ITT and clamping) was used, followed by Tukey's or Sidak's multiple comparisons test as specified in the figure legends. The assumptions of homogeneity of error variances were tested using *F*-test ($P > 0.05$). Geisser–Greenhouse's correction was used where applicable. The adjusted means and s.e.m., or s.d., were recorded when the analysis met the above standards. Differences were considered significant when $P < 0.05$, or $P > 0.05$ with large differences of observed effects (as suggested in refs. 161,162).

Reporting summary

Further information on research design is available in the Nature Portfolio Reporting Summary linked to this article.

Data availability

The data supporting the findings of this study are available within the paper and its Supplementary Information files. The MS proteomics data for the validation of *Tgr5*$^{-/-}$ MEFs have been deposited to the ProteomeXchange Consortium (http://proteomecentral.proteomexchange.org) through the iProX partner repository[163,164] with the dataset identifier IPX0007019000. Materials and reagents are available upon request. Questions regarding the details of experiments are welcome. Full immunoblots are provided as Supplementary Fig. 1. Source data are provided with this paper.

Code availability

The analysis was performed using standard protocols with previously described computational tools. No custom code was used in this study.

82. Nguyen, L. N. et al. Mfsd2a is a transporter for the essential omega-3 fatty acid docosahexaenoic acid. *Nature* **509**, 503–506 (2014).
83. Green, C. L. et al. The effects of graded levels of calorie restriction. XIII. Global metabolomics screen reveals graded changes in circulating amino acids, vitamins, and bile acids in the plasma of C57BL/6 Mice. *J. Gerontol. A Biol. Sci. Med. Sci.* **74**, 16–26 (2019).
84. Zhang, C. S. et al. Fructose-1,6-bisphosphate and aldolase mediate glucose sensing by AMPK. *Nature* **548**, 112–116 (2017).

85. Zong, Y. et al. Hierarchical activation of compartmentalized pools of AMPK depends on severity of nutrient or energy stress. *Cell Res.* **29**, 460–473 (2019).
86. Garcia-Flores, L. A. et al. The effects of graded calorie restriction XVII: multitissue metabolomics reveals synthesis of carnitine and NAD, and tRNA charging as key pathways. *Proc. Natl Acad. Sci. USA* **118**, e2101977118 (2021).
87. Perez, C. L. & Van Gilst, M. R. A ^{13}C isotope labeling strategy reveals the influence of insulin signaling on lipogenesis in *C. elegans*. *Cell Metab.* **8**, 266–274 (2008).
88. Falk, M. J. et al. Stable isotopic profiling of intermediary metabolic flux in developing and adult stage *Caenorhabditis elegans*. *J. Vis. Exp.* https://doi.org/10.3791/2288 (2011).
89. Vergano, S. S. et al. In vivo metabolic flux profiling with stable isotopes discriminates sites and quantifies effects of mitochondrial dysfunction in *C. elegans*. *Mol. Genet. Metab.* **111**, 331–341 (2014).
90. Liu, Y., Wang, W., Shui, G. & Huang, X. CDP-diacylglycerol synthetase coordinates cell growth and fat storage through phosphatidylinositol metabolism and the insulin pathway. *PLoS Genet.* **10**, e1004172 (2014).
91. Cox, J. E., Thummel, C. S. & Tennessen, J. M. Metabolomic studies in *Drosophila*. *Genetics* **206**, 1169–1185 (2017).
92. Ding, L. et al. Seipin regulates lipid homeostasis by ensuring calcium-dependent mitochondrial metabolism. *EMBO J.* **37**, e97572 (2018).
93. Schuh, R. A., Jackson, K. C., Khairallah, R. J., Ward, C. W. & Spangenburg, E. E. Measuring mitochondrial respiration in intact single muscle fibers. *Am. J. Physiol. Regul. Integr. Comp. Physiol.* **302**, R712–R719 (2012).
94. Koopman, M. et al. A screening-based platform for the assessment of cellular respiration in *Caenorhabditis elegans*. *Nat. Protoc.* **11**, 1798–1816 (2016).
95. Sarasija, S. & Norman, K. R. Measurement of oxygen consumption rates in intact *Caenorhabditis elegans*. *J. Vis. Exp.* https://doi.org/10.3791/59277 (2019).
96. Ng, L. F. & Gruber, J. Measurement of respiration rate in live *Caenorhabditis elegans*. *bio-protocol* **9**, e3243 (2019).
97. Zhang, C. S. et al. The lysosomal v-ATPase–Ragulator complex Is a common activator for AMPK and mTORC1, acting as a switch between catabolism and anabolism. *Cell Metab.* **20**, 526–540 (2014).
98. Yu, Y. et al. Organelle proteomic profiling reveals lysosomal heterogeneity in association with longevity. *eLife* **13**, e85214 (2024).
99. Espada, L. et al. Loss of metabolic plasticity underlies metformin toxicity in aged *Caenorhabditis elegans*. *Nat. Metab.* **2**, 1316–1331 (2020).
100. Wu, L. et al. An ancient, unified mechanism for metformin growth inhibition in *C. elegans* and cancer. *Cell* **167**, 1705–1718.e13 (2016).
101. Martin-Montalvo, A. et al. Metformin improves healthspan and lifespan in mice. *Nat. Commun.* **4**, 2192 (2013).
102. De Rosa, M. J. et al. The flight response impairs cytoprotective mechanisms by activating the insulin pathway. *Nature* **573**, 135–138 (2019).
103. Yuan, J. et al. Two conserved epigenetic regulators prevent healthy ageing. *Nature* **579**, 118–122 (2020).
104. Zhang, H. et al. NAD$^+$ repletion improves mitochondrial and stem cell function and enhances life span in mice. *Science* **352**, 1436–1443 (2016).
105. Mallick, A., Ranawade, A., van den Berg, W. & Gupta, B. P. Axin-mediated regulation of lifespan and muscle health in *C. elegans* requires AMPK–FOXO signaling. *iScience* **23**, 101843 (2020).
106. Wood, J. G. et al. Sirtuin activators mimic caloric restriction and delay ageing in metazoans. *Nature* **430**, 686–689 (2004).
107. Libert, S. et al. Regulation of *Drosophila* life span by olfaction and food-derived odors. *Science* **315**, 1133–1137 (2007).
108. Rogina, B. & Helfand, S. L. Sir2 mediates longevity in the fly through a pathway related to calorie restriction. *Proc. Natl Acad. Sci. USA* **101**, 15998–16003 (2004).
109. Broughton, S. J. et al. Longer lifespan, altered metabolism, and stress resistance in *Drosophila* from ablation of cells making insulin-like ligands. *Proc. Natl Acad. Sci. USA* **102**, 3105–3110 (2005).
110. Minois, N. et al. Spermidine promotes stress resistance in *Drosophila melanogaster* through autophagy-dependent and -independent pathways. *Cell Death Dis.* **3**, e401 (2012).
111. Sanchez, J. A. et al. FOXO-mediated repression of Dicer1 regulates metabolism, stress resistance, and longevity in *Drosophila*. *Proc. Natl Acad. Sci. USA* **120**, e2216539120 (2023).
112. Hui, X. et al. Adipocyte SIRT1 controls systemic insulin sensitivity by modulating macrophages in adipose tissue. *EMBO Rep.* **18**, 645–657 (2017).
113. Lin, L. et al. Regulation of skeletal muscle oxidative capacity and muscle mass by SIRT3. *PLoS ONE* **9**, e85636 (2014).
114. Liu, Y. et al. TLR9 and beclin 1 crosstalk regulates muscle AMPK activation in exercise. *Nature* **578**, 605–609 (2020).
115. von Maltzahn, J., Jones, A. E., Parks, R. J. & Rudnicki, M. A. Pax7 is critical for the normal function of satellite cells in adult skeletal muscle. *Proc. Natl Acad. Sci. USA* **110**, 16474–16479 (2013).
116. Sincennes, M. C. et al. Acetylation of PAX7 controls muscle stem cell self-renewal and differentiation potential in mice. *Nat. Commun.* **12**, 3253 (2021).
117. Khan, N. A. et al. Effective treatment of mitochondrial myopathy by nicotinamide riboside, a vitamin B3. *EMBO Mol. Med.* **6**, 721–731 (2014).
118. Owen, A. M. et al. Chronic muscle weakness and mitochondrial dysfunction in the absence of sustained atrophy in a preclinical sepsis model. *eLife* **8**, e49920 (2019).
119. Monciardini, P., Sosio, M., Cavaletti, L., Chiocchini, C. & Donadio, S. New PCR primers for the selective amplification of 16S rDNA from different groups of actinomycetes. *FEMS Microbiol. Ecol.* **42**, 419–429 (2002).
120. Harrison, D. E. et al. Rapamycin fed late in life extends lifespan in genetically heterogeneous mice. *Nature* **460**, 392–395 (2009).
121. Truax, A. D. et al. The inhibitory innate immune sensor NLRP12 maintains a threshold against obesity by regulating gut microbiota homeostasis. *Cell Host Microbe* **24**, 364–378.e6 (2018).
122. Guo, H. et al. Multi-omics analyses of radiation survivors identify radioprotective microbes and metabolites. *Science* **370**, eaay9097 (2020).
123. Brenner, S. The genetics of *Caenorhabditis elegans*. *Genetics* **77**, 71–94 (1974).
124. Lakovaara, S. Malt as a culture medium for *Drosophila* species. *Drosophila Inf. Serv.* **44**, 128 (1969).
125. Park, S. J. et al. DNA-PK promotes the mitochondrial, metabolic, and physical decline that occurs during aging. *Cell Metab.* **26**, 447 (2017).
126. Shiota, M. Measurement of glucose homeostasis in vivo: combination of tracers and clamp techniques. *Methods Mol. Biol.* **933**, 229–253 (2012).
127. Zhang, Y., Xu, L., Liu, X. & Wang, Y. Evaluation of insulin sensitivity by hyperinsulinemic–euglycemic clamps using stable isotope-labeled glucose. *Cell Discov.* **4**, 17 (2018).
128. Liu, P. et al. Blocking FSH induces thermogenic adipose tissue and reduces body fat. *Nature* **546**, 107–112 (2017).
129. Liu, L. et al. Histone methyltransferase MLL4 controls myofiber identity and muscle performance through MEF2 interaction. *J. Clin. Invest.* **130**, 4710–4725 (2020).
130. Brown, J. C. in *Encyclopedia of Food Sciences and Nutrition* 2nd edn (ed. Caballero, B.) 2087–2091 (Academic Press, 2003).
131. Fang, E. F. et al. NAD$^+$ replenishment improves lifespan and healthspan in ataxia telangiectasia models via mitophagy and DNA repair. *Cell Metab.* **24**, 566–581 (2016).
132. Backhaus, B., Sulkowski, E. & Schlote, F. W. A semi-synthetic, general-purpose medium for *Drosophila melanogaster*. *Drosophila Inf. Serv.* **60**, 210–212 (1984).
133. Linford, N. J., Bilgir, C., Ro, J. & Pletcher, S. D. Measurement of lifespan in *Drosophila melanogaster*. *J. Vis. Exp.* https://doi.org/10.3791/50068 (2013).
134. Wu, Q. et al. 2,5-Dimethyl-celecoxib extends *Drosophila* life span via a mechanism that requires insulin and target of rapamycin signaling. *J. Gerontol. A Biol. Sci. Med. Sci.* **72**, 1334–1341 (2017).
135. Gomes, A. P. et al. Declining NAD$^+$ induces a pseudohypoxic state disrupting nuclear–mitochondrial communication during aging. *Cell* **155**, 1624–1638 (2013).
136. Nargund, A. M., Fiorese, C. J., Pellegrino, M. W., Deng, P. & Haynes, C. M. Mitochondrial and nuclear accumulation of the transcription factor ATFS-1 promotes OXPHOS recovery during the UPR^{mt}. *Mol. Cell* **58**, 123–133 (2015).
137. Zhang, Q. et al. The memory of neuronal mitochondrial stress is inherited transgenerationally via elevated mitochondrial DNA levels. *Nat. Cell Biol.* **23**, 870–880 (2021).
138. Copeland, J. M. et al. Extension of *Drosophila* life span by RNAi of the mitochondrial respiratory chain. *Current Biol.* **19**, 1591–1598 (2009).
139. Quiros, P. M., Goyal, A., Jha, P. & Auwerx, J. Analysis of mtDNA/nDNA ratio in mice. *Curr. Protoc. Mouse Biol.* **7**, 47–54 (2017).
140. Rodrigues, A. P. C., Camargo, A. F., Andjelkovic, A., Jacobs, H. T. & Oliveira, M. T. Developmental arrest in *Drosophila melanogaster* caused by mitochondrial DNA replication defects cannot be rescued by the alternative oxidase. *Sci. Rep.* **8**, 10882 (2018).
141. Palla, A. R. et al. Inhibition of prostaglandin-degrading enzyme 15-PGDH rejuvenates aged muscle mass and strength. *Science* **371**, eabc8059 (2021).
142. Rando, T. A. & Blau, H. M. Primary mouse myoblast purification, characterization, and transplantation for cell-mediated gene therapy. *J. Cell Biol.* **125**, 1275–1287 (1994).
143. Zhang, C. S. et al. Identification of serum metabolites enhancing inflammatory responses in COVID-19. *Sci. China Life Sci.* **65**, 1971–1984 (2022).
144. Wu, Y. Q. et al. Low glucose metabolite 3-phosphoglycerate switches PHGDH from serine synthesis to p53 activation to control cell fate. *Cell Res.* **33**, 835–850 (2023).
145. Lam, S. M. et al. A multi-omics investigation of the composition and function of extracellular vesicles along the temporal trajectory of COVID-19. *Nat. Metab.* **3**, 909–922 (2021).
146. Miao, H. et al. Lipidome atlas of the developing heart uncovers dynamic membrane lipid attributes underlying cardiac structural and metabolic maturation. *Research* **2022**, 0006 (2022).
147. Song, J. W. et al. Omics-driven systems interrogation of metabolic dysregulation in COVID-19 pathogenesis. *Cell Metab.* **32**, 188–202.e5 (2020).
148. Shui, G. et al. Derivatization-independent cholesterol analysis in crude lipid extracts by liquid chromatography/mass spectrometry: applications to a rabbit model for atherosclerosis. *J. Chromatogr. A* **1218**, 4357–4365 (2011).
149. Milo, R. What is the total number of protein molecules per cell volume? A call to rethink some published values. *Bioessays* **35**, 1050–1055 (2013).
150. Gabella, G. Quantitative morphological study of smooth muscle cells of the guinea-pig taenia coli. *Cell Tissue Res.* **170**, 161–186 (1976).
151. Méndez, J. & Keys, A. B. Density and composition of mammalian muscle. *Metab. Clin. Exp.* **9**, 184–188 (1960).
152. Uppaluri, S. & Brangwynne, C. P. A size threshold governs *Caenorhabditis elegans* developmental progression. *Proc. Biol. Sci.* **282**, 20151283 (2015).
153. Reina, A., Subramaniam, A. B., Laromaine, A., Samuel, A. D. & Whitesides, G. M. Shifts in the distribution of mass densities is a signature of caloric restriction in *Caenorhabditis elegans*. *PLoS ONE* **8**, e69651 (2013).
154. Zhang, C. S., Li, M., Zong, Y. & Lin, S. C. Determining AMPK activation via the lysosomal v-ATPase–Ragulator–AXIN/LKB1 axis. *Methods Mol. Biol.* **1732**, 393–411 (2018).
155. Ma, T. et al. Low-dose metformin targets the lysosomal AMPK pathway through PEN2. *Nature* **603**, 159–165 (2022).
156. Martell, J. D., Deerinck, T. J., Lam, S. S., Ellisman, M. H. & Ting, A. Y. Electron microscopy using the genetically encoded APEX2 tag in cultured mammalian cells. *Nat. Protoc.* **12**, 1792–1816 (2017).
157. Preez, G. D. et al. Oxygen consumption rate of *Caenorhabditis elegans* as a high-throughput endpoint of toxicity testing using the Seahorse XF^{e}96 Extracellular Flux Analyzer. *Sci. Rep.* **10**, 4239 (2020).
158. Li, M. et al. AMPK targets PDZD8 to trigger carbon source shift from glucose to glutamine. *Cell Res.* **34**, 683–706 (2024).
159. Scholz, N., Behnke, T. & Resch-Genger, U. Determination of the critical micelle concentration of neutral and ionic surfactants with fluorometry, conductometry, and surface tension—a method comparison. *J. Fluoresc.* **28**, 465–476 (2018).
160. Salem, J. K., El-Nahhal, I. M. & Salama, S. F. Determination of the critical micelle concentration by absorbance and fluorescence techniques using fluorescein probe. *Chem. Phys. Lett.* **730**, 445–450 (2019).
161. Amrhein, V., Greenland, S. & McShane, B. Scientists rise up against statistical significance. *Nature* **567**, 305–307 (2019).

162. Wasserstein, R. L., Schirm, A. L. & Lazar, N. A. Moving to a world beyond "*p*<0.05". *Am. Stat.* **73**, 1–19 (2019).
163. Ma, J. et al. iProX: an integrated proteome resource. *Nucleic Acids Res.* **47**, D1211–D1217 (2019).
164. Chen, T. et al. iProX in 2021: connecting proteomics data sharing with big data. *Nucleic Acids Res.* **50**, D1522–D1527 (2022).

Acknowledgements We thank S. Morrison for providing the *AMPKα1*$^{F/F}$ and *AMPKα2*$^{F/F}$ mice; M. Zhang for technical assistance with hyperinsulinaemic–euglycaemic clamp assays; S.-Q. Wu, Y. He and J. Song for mouse in vitro fertilization; K. Mao, W. Lin and W. Lv for technical help with the germ-free mice; Y. Yu and Y. Liu for the nematode strains and experiments; B. Liu and K. Zheng for the fly strains and experiments; Q. Guo for help with analysis of fibre types of muscle tissues; T.-J. Zhao and H. Bia for discussions; X. Guo for importing the fly strains; all the other members of the S.-C.L. laboratory for technical assistance; staff at the *Caenorhabditis* Genetics Center and National BioResource Project for supplying nematode strains; and staff at the BDSC, the Vienna *Drosophila* Resource Center, and the Core Facility of *Drosophila* Resource and Technology, Center for Excellence in Molecular Cell Science, Chinese Academy of Sciences, for providing fly strains and reagents. The artwork in Fig. 1g was modified from elements created by Servier Medical Art (https://smart.servier.com/), licenced under a Creative Commons Attribution 3.0 Unported licence. This work was supported by grants from the National Key R&D Program of China (2020YFA0803402), the National Natural Science Foundation of China (92057204, 82088102, 32070753, 323B2035, 91854208 and 31922034), the Fundamental Research Funds for the Central Universities (20720200069 and 20720190101), the Project '111' sponsored by the State Bureau of Foreign Experts and Ministry of Education of China (BP2018017), the Joint Funds for the Innovation of Science and Technology, Fujian province (2021Y9232, 2021Y9227 and 2023Y9448), the Fujian provincial health technology project (2022ZD01005 and 2022ZQNZD009), the Special Research Funds for Local Science and Technology Development Guided by Central Government (2023L3020), the XMU–Fujian Cancer Hospital cooperation grant for the Research Center of Metabolism, the XMU Open Innovation Fund and Training Programme of Innovation and Entrepreneurship for Undergraduates (KFJJ-202103 and S202210384682), and the Agilent Applications and Core Technology–University Research Grant (4769).

Author contributions Q.Q., C.-S.Z. and S.-C.L. conceived the study and designed the experiments. Q.Q., W.W. and H.-Y.Y. performed mouse CR and LCA treatments. Q.Q. screened the metabolites responsible for AMPK activation, with assistance from S.L., H.-Y.Y. and X.T. Y.C. determined the benefits of LCA on mice and flies, with assistance from Q.Q., M.L., W.W., H.-Y.Y. and J.W. Y.W. performed nematode experiments. X.W. determined the OCRs of mouse muscles. Y.-H.L., S.Xu and Z.-Z.Z. determined the mRNA levels of the mitochondrial OXPHOS complex. MS analyses of polar metabolites in serum, tissues and cells was performed by C.Z. (HPLC–MS), H.-L.P. (CE–MS) and M.Z. (GC–MS). S.M.L. and G.S. performed lipidomics analyses. B.Z. and X.D. designed the formulation of LCA for mouse administration. C.Y. and C.J. determined the energy content of the food and faeces by bomb calorimetry. J.C. measured the CMC values of LCA. S.Xue and H.G. performed CR and gut microbiome transplantation experiments on germ-free mice and antibiotic-treated mice. C.-S.Z. and S.-C.L. wrote the manuscript.

Competing interests The authors declare no competing interests.

Additional information

Supplementary information The online version contains supplementary material available at https://doi.org/10.1038/s41586-024-08329-5.

Correspondence and requests for materials should be addressed to Chen-Song Zhang or Sheng-Cai Lin.

Peer review information *Nature* thanks Sandra Galic, David Sinclair and the other, anonymous, reviewer(s) for their contribution to the peer review of this work. Peer reviewer reports are available.

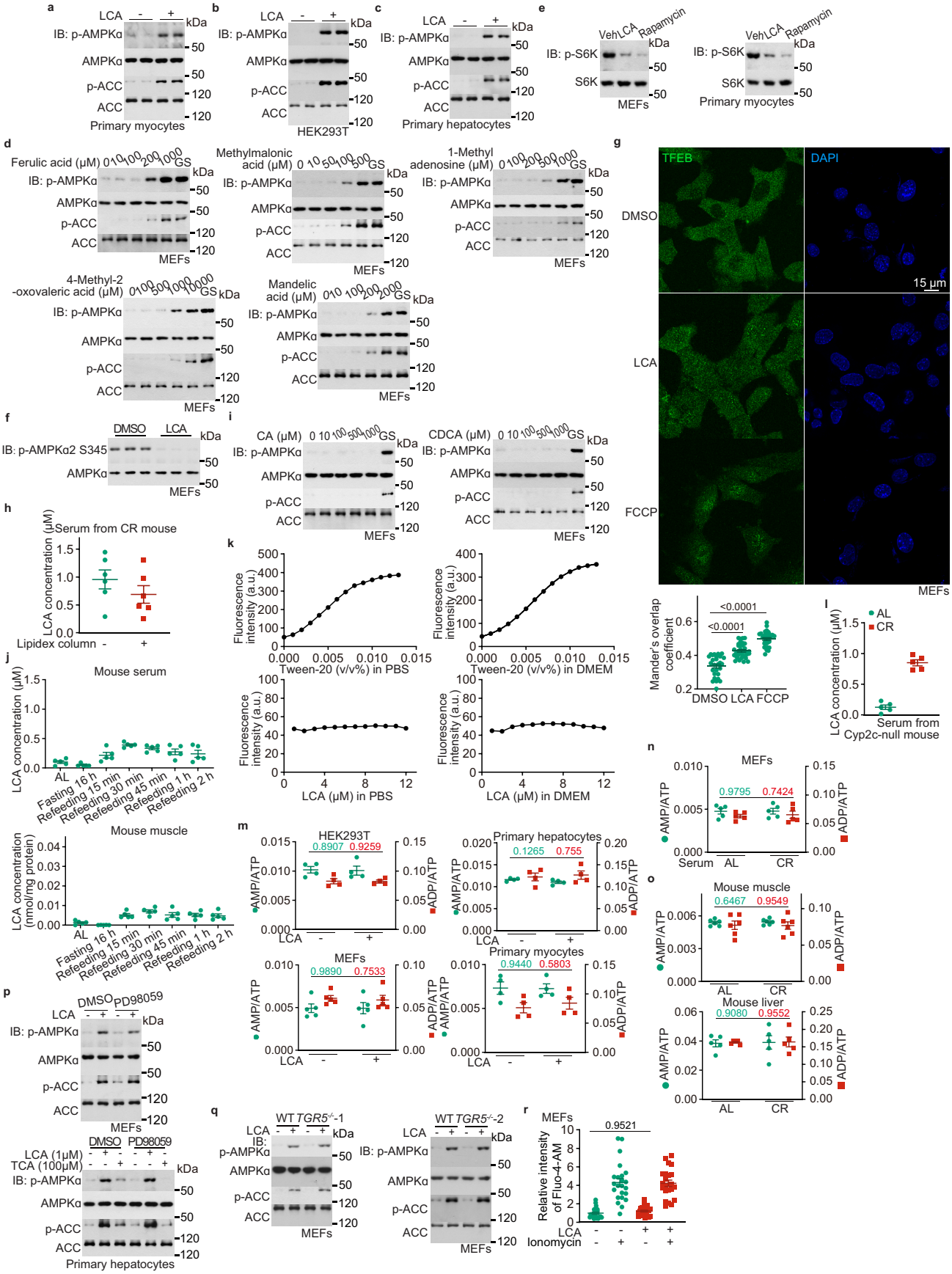

Extended Data Fig. 1 | See next page for caption.

Extended Data Fig. 1 | LCA activates AMPK in cultured cells at a level seen in CR serum. a-**c**, LCA at concentrations similar to that in the CR serum activates AMPK in HEK293T cells, primary hepatocytes, and primary myocytes. Primary myocytes (**a**), HEK293T cells (**b**), and primary hepatocytes (**c**) were treated with 1 μM LCA for 4 h, followed by determination of AMPK activation by immunoblotting. **d**, The compounds ferulic acid, 4-methyl-2-oxovaleric acid, 1-methyladenosine, methylmalonic acid and mandelic acid activate AMPK at concentrations much exceeding those in the CR serum. MEFs were treated with each compound at indicated concentrations for 4 h, or starved for glucose for 2 h as a control, followed by determination for AMPK activity by immunoblotting. **e**, **f**, LCA inhibits mTORC1 in cultured cells. MEFs (left panel of **e**, and **f**) and primary myocytes (right panel of **e**) were treated with 1 μM LCA for 4 h (**e**, **f**), or 100 nM rapamycin for 2 h as a control (**e**), followed by determination for the phosphorylation of S6K-S389 (**e**) and AMPKα2-S345 (**f**) by immunoblotting. **g**, LCA induces nuclear translocation of TFEB. MEFs were treated with 1 μM LCA for 4 h, or 10 μM FCCP as a control, followed by determination for the localization of TFEB by immunofluorescent staining (accessed by the co-localization, i.e., the Mander's overlap coefficients, between TFEB and DAPI). Results are shown as mean ± s.e.m.; $n = 27$ (DMSO), 35 (LCA), or 29 (FCCP) cells, and P value by two-way ANOVA followed by Tukey's test. **h**, The Lipidex column partially absorbs LCA of the serum. Serum collected from 3.5-month CR mice was passed through the Lipidex column, and the concentrations of LCA before and after passing the column were determined by mass spectrometry. Results are shown as mean ± s.e.m.; $n = 6$ replicates. **i**, CA and CDCA do not activate AMPK. MEFs were treated with CA (left) or CDCA (right) at indicated concentrations for 4 h, followed by determination for AMPK activity. **j**, Ad libitum-fed mouse serum and muscles contain low levels of LCA, with levels increased after refeeding. The ad libitum-fed mice were fasted for 16 h and re-fed. LCA concentrations in the serum and muscle at different time points after refeeding were determined. Results are shown as mean ± s.e.m.; $n = 5$ mice for each time point. **k**, LCA does not form micelles at the concentrations sufficient for AMPK activation. LCA, and Tween-20 as a control, were dissolved in PBS (left) or DMEM (right) at indicated concentrations, followed by determination of the critical micelle concentration (CMC) by fluorescent spectroscopy. Representative spectrograms are shown. $n = 3$ replicates for each condition. **l**, Metabolomic analysis reveals elevation of LCA after CR in the serum of Cyp2c-humanized mice. Serum concentrations of LCA in 4-month-calorie-restricted Cyp2c-null were determined. Results are shown as mean ± s.e.m.; $n = 5$ mice for each condition. **m**-**o**, CR or LCA alone activates AMPK in an AMP-independent manner. The AMP:ATP and ADP:ATP ratios from MEFs, primary myocytes, HEK293T cells and primary hepatocytes treated with 1 μM LCA (**m**) or serum from CR mice (**n**) for 4 h, or muscle and liver tissues from CR mice (**o**, collected at 17:00, right before the food supply), were determined. Results are shown as mean ± s.e.m.; $n = 4$ (**m**, primary myocytes, HEK293T cells and primary hepatocytes), 6 (**o**, muscle tissues) or 5 (others) biological replicates, and P value by two-sided Student's t-test. **p**, LCA does not activate AMPK through the cAMP-Epac-MEK pathway. MEFs (upper) or primary hepatocytes (lower) were treated with 1 μM LCA or 100 μM TCA, with or without 100 μM PD98059, for 4 h, followed by determination of the activation of AMPK by immunoblotting. **q**, TGR5 is not required for LCA-induced AMPK activation. MEFs (clone #1 of *TGR5*$^{-/-}$ MEFs on the left panel, and clone #2 of *TGR5*$^{-/-}$ MEFs on the right, validated in the Supplementary Table 3) were treated with 1 μM LCA for 4 h. The AMPK activities in MEFs were then determined by immunoblotting. **r**, LCA does not elevate intracellular calcium levels. The bulk calcium, as assessed by the intensities of the Fluo-4-AM dye, was determined in MEFs treated with 1 μM LCA for 4 h, or with 1 μM ionomycin for 5 min as a positive control. Results are shown as mean ± s.e.m., normalized to the group without LCA or ionomycin treatment; $n = 22$-23 cells, and P value by two-way ANOVA, followed by Tukey. Experiments in this figure were performed three times.

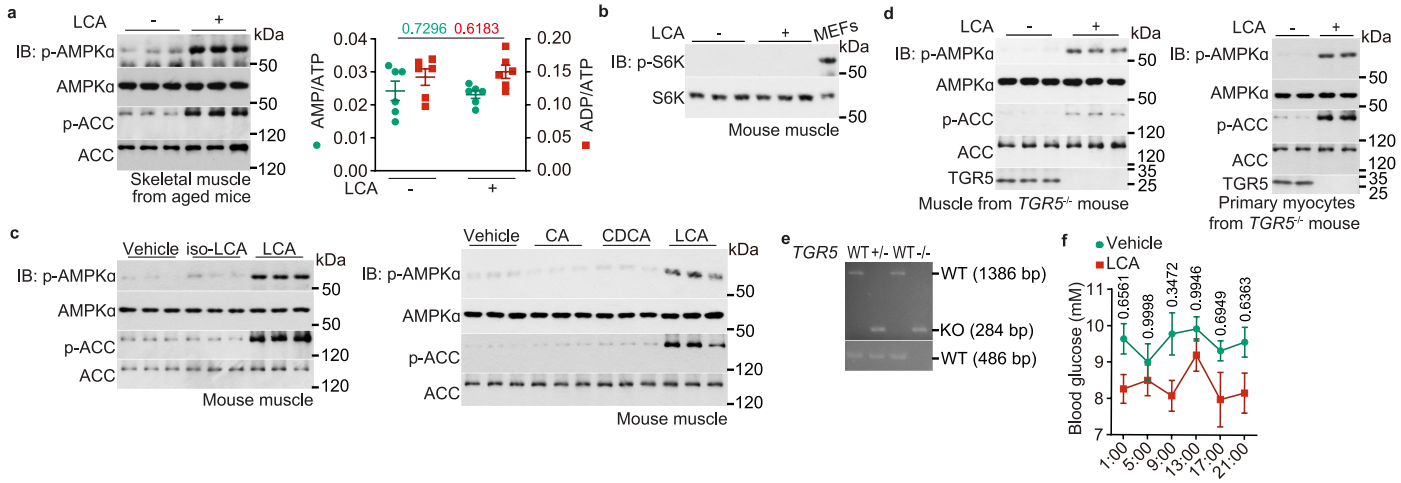

Extended Data Fig. 2 | LCA activates AMPK in mice at a level seen after CR. **a**, Administration of mice with LCA to a similar accumulation to that induced by CR does not elevate AMP in mice. Ad libitum-fed, aged (1.5-year-old) mice were treated with (2-hydroxypropyl)-β-cyclodextrin-coated LCA at 1 g/l in drinking water for 1 month, followed by determination of the AMP:ATP and ADP:ATP ratios in muscle (right panel). Results are shown as mean ± s.e.m.; $n = 6$ mice for each condition, and P value by two-sided Student's t-test. See also activation of AMPK in these tissues (left panel). **b**, LCA does not affect basal mTORC1 in muscle tissues. Ad libitum-fed mice were treated with LCA as in **a**, followed by determination of p-S6K levels in muscle tissues by immunoblotting. See also p-S6K in MEFs as a control. **c**, LCA derivative iso-LCA is unable to activate AMPK in the muscle. Ad libitum-fed mice were treated with (2-hydroxypropyl)-β-cyclodextrin-coated iso-LCA, CA, CDCA, or LCA as a control, all at 1 g/l in drinking water for 1 month, followed by determination of AMPK activities in the muscle by immunoblotting. **d**, **e**, TGR5 is not required for LCA to induce AMPK activation in the muscle. Ad libitum-fed mice with *TRG5* knocked out (validated in **e**) were fed with (2-hydroxypropyl)-β-cyclodextrin-coated LCA at 1 g/l in drinking water for 1 month (**d**). The AMPK activities in the muscle (**d**, left), or primary myocytes (**d**, right) were then determined by immunoblotting. **f**, LCA decreases blood glucose as does CR. Levels of blood glucose at different times of the day in ad libitum-fed mice treated with LCA (as in **a**), for 1 month, were determined. Results are shown as mean ± s.e.m.; $n = 5$ mice for each treatment/time point, and P value by two-way ANOVA, followed by Tukey. Experiments in this figure were performed three times.

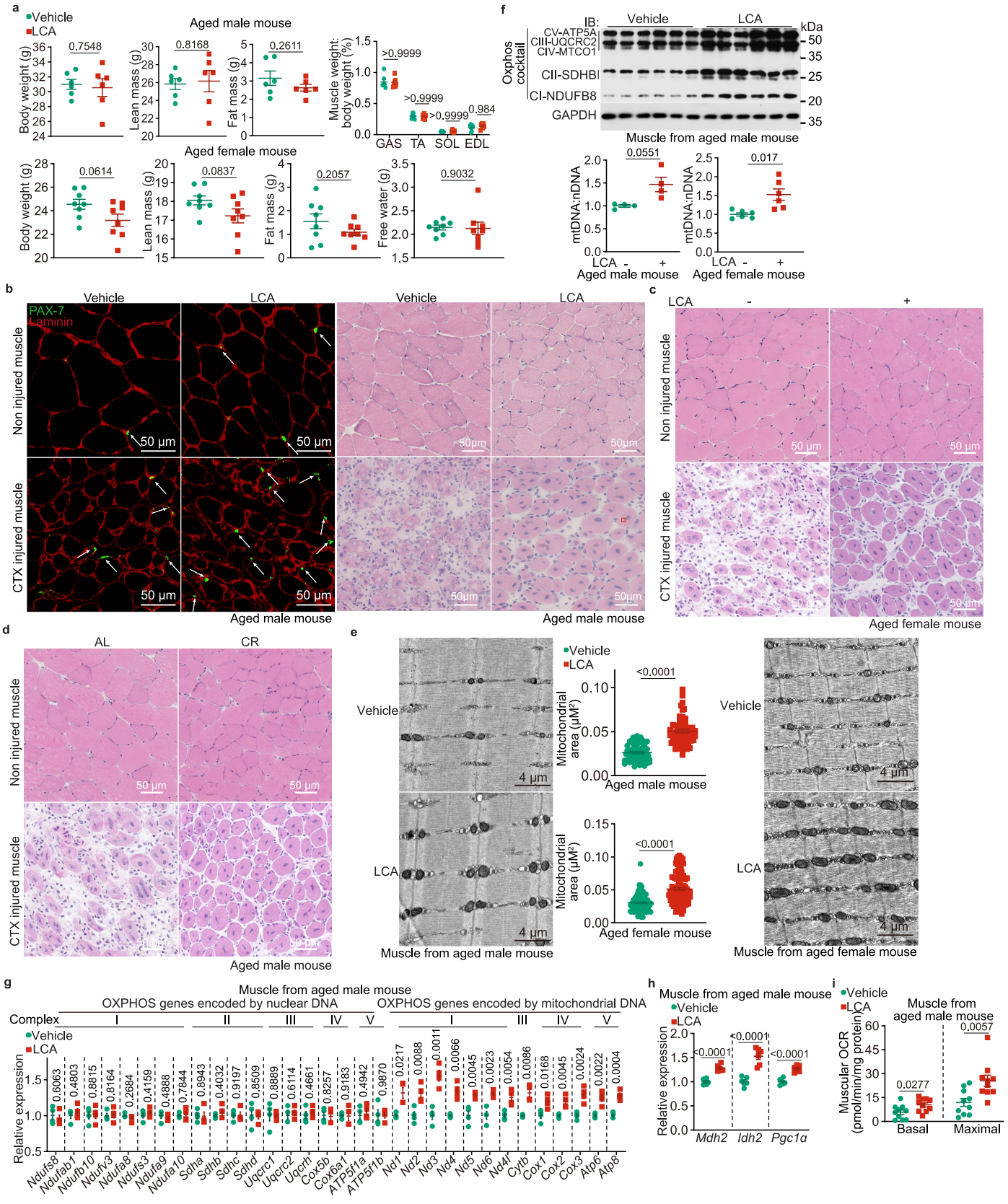

Extended Data Fig. 3 | See next page for caption.

Extended Data Fig. 3 | LCA improves muscle functions in aged mice. a, LCA prevents muscle atrophy in aged mice. Aged ad libitum-fed mice, both male (upper panel) and female (lower panel), were fed with (2-hydroxypropyl)-β-cyclodextrin-coated LCA at 1 g/l in drinking water for 1 month, followed by determination of the body composition (the lean mass, fat mass, body weight, and muscle mass). Results are shown as mean ± s.e.m.; $n = 7$ (muscle mass of male mice), 8 (female mice) or 6 (others) mice, and P value by two-way ANOVA, followed by Tukey (muscle mass of male mice) or by two-sided Student's t-test (others). **b**-**d**, LCA accelerates muscle regeneration in damaged mice similarly to CR. Aged mice, both male (**b**, **d**) and female (**c**), were fed with LCA as in **a** (**b**, **c**), or subjected to CR for 3.5 months (**d**), and were intramuscularly injected with cardiotoxin to induce muscle damage. The morphology (right panel of **b**, and "**c**, **d**; by H&E staining) and the PAX7-positive muscle stem cells (left panel of **b**; by immunohistochemistry, and the muscle stem cells were pointed to by white arrows) were used to determine muscle regeneration at 7 days after cardiotoxin injection. Representative images of male mice are shown in this figure. **e**-**h**, LCA improves mitochondrial contents in aged mouse muscles. Aged ad libitum-fed mice, both male (left panel of **e**, **g**, **h**, and lower left panel of **f**) and female (right panel of **e**, and lower right panel of **f**), were fed with LCA as in **a**, followed by quantification of muscular mitochondrial contents by TEM (**e**; representative images are shown on the left and right panel, and statistical analysis data (the area of each mitochondrion in the section) on the middle (mean ± s.e.m.; $n = 57$ (vehicle of male mice), 56 (LCA of male mice), or 103 (female mice) mitochondria for each condition, and P value by two-sided Student's t-test)), the protein levels of muscular OXPHOS complexes by immunoblotting (upper panel of **f**), the mtDNA:nDNA ratios by RT-PCR (lower panel of **f**; as mean ± s.e.m., normalized to the vehicle group; $n = 4$ (male) or 6 (female) mice for each condition, and P value by two-sided Student's t-test), and the mRNA levels of OXPHOS (**g**; results are mean ± s.e.m., normalized to the vehicle group; $n = 4$ mice for each treatment, and P value by two-sided Student's t-test) and TCA cycle genes (**h**; results are mean ± s.e.m., normalized to the vehicle group; $n = 6$ mice for each treatment, and P value by two-sided Student's t-test) by RT-PCR. **i**, LCA increases respiratory function in muscles of aged mice. Aged ad libitum-fed mice were treated as in **a**, followed by determination of OCR in muscles by the Seahorse Mito Stress Test. Results are mean ± s.e.m.; $n = 10$ mice for each condition, and P value by two-sided Student's t-test. Experiments in this figure were performed three times.

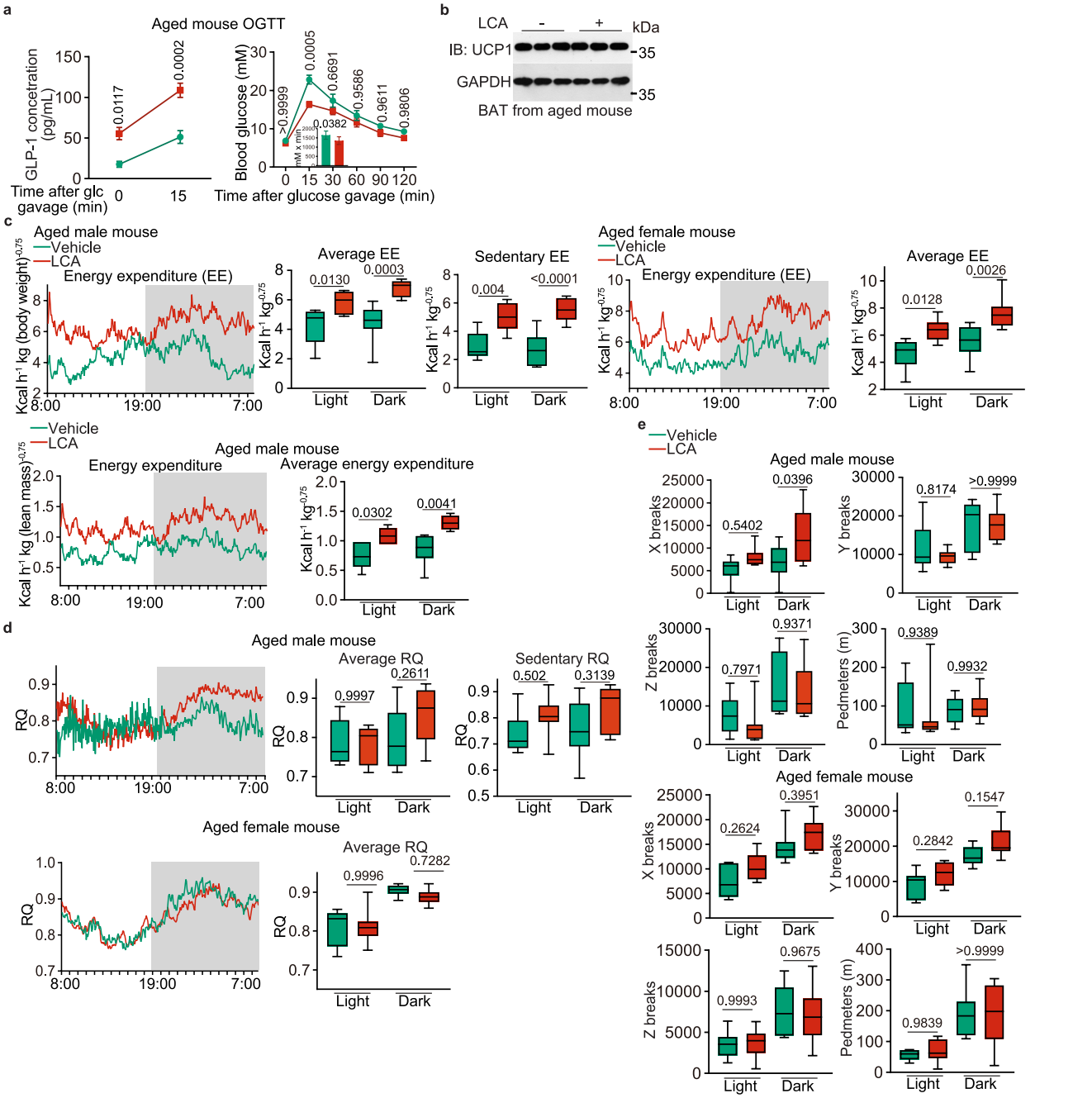

Extended Data Fig. 4 | LCA elevates respiratory activity in aged mice. a, LCA increases plasma GLP-1 levels in mice. Ad libitum-fed, aged male mice were fed with (2-hydroxypropyl)-β-cyclodextrin-coated LCA at 1 g/l in drinking water for 1 month, followed by oGTT (right panel, results of blood glucose and area under the curve (AUC) are shown as mean ± s.e.m.; $n = 6$ mice for each condition, and P value by two-way repeated-measures (RM) ANOVA followed by Tukey's test (blood glucose), or by two-sided Student's t-test (AUC)). Plasma GLP-1 levels before and after 15 min of glucose gavaging were determined and are shown on the left panel, results are mean ± s.e.m.; $n = 5$ mice and P value by two-way RM ANOVA followed by Tukey's test. **b**, LCA does not promote expression of UCP1 in the mouse BAT. Ad libitum-fed mice were fed with LCA as in **a**, followed by determination of the protein levels of UCP1 in the BAT by immunoblotting. **c**, LCA elevates energy expenditure (EE) in aged mice. Ad libitum-fed mice, both male and female, were treated with LCA as in **a**, followed by determination of EE. Data are shown as mean (left panel of each gender; at 5-min intervals during a 24-h course after normalization to the body weight ($kg^{0.75}$)), or as box-and-whisker plots (other panels of each gender, in which the lower and upper bounds of the box represent the first and the third quartile scores, the centre line represents the median, and the lower and upper limits denote minimum and maximum scores, respectively; and the same hereafter for all box-and-whisker plots; P value by two-way ANOVA, followed by Tukey), $n = 6$ (vehicle group of male mice, light cycle of sedentary EE), 7 (LCA group of male mice, dark cycle of sedentary EE), or 8 (others) mice for each condition. See also EE data of male mice after normalising to lean mass ($kg^{0.75}$) on the lower left panel. **d**, **e**, LCA elevates respiratory quotient (RQ) in aged mice. Mice were treated as in **a**, followed by determination of RQ (**d**) and ambulatory activity (**e**). Data are shown as mean (left panel of **d**, which is shown at 5-min intervals during a 24-h course), or as box-and-whisker plots (others); $n = 6$ (vehicle of male mice, light cycle of sedentary RQ), 7 (LCA of male mice, dark cycle of sedentary RQ), or 8 (others) mice for each treatment, and P value by two-way ANOVA followed by Tukey's test. Experiments in this figure were performed three times.

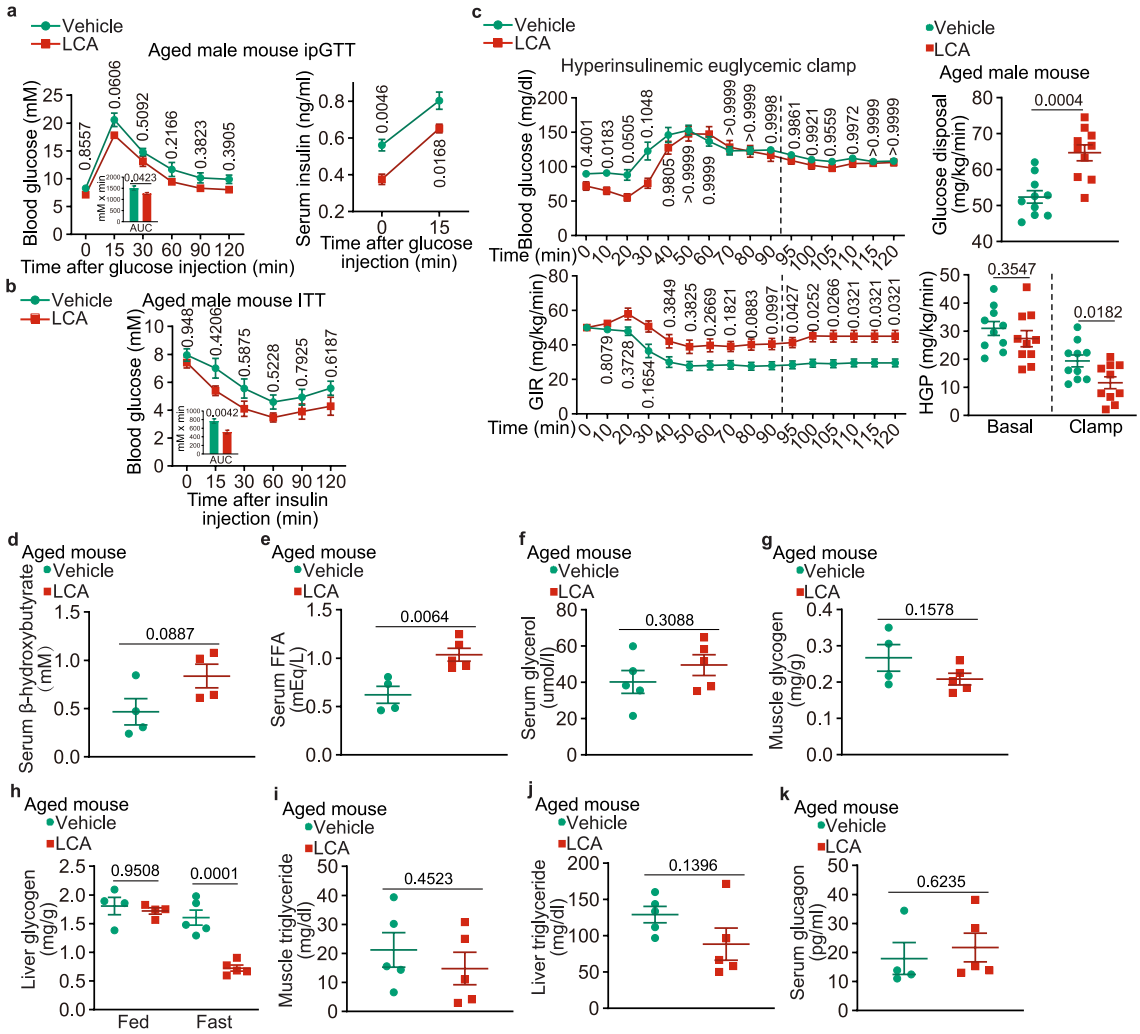

Extended Data Fig. 5 | LCA ameliorates age-related insulin resistance without decreasing glucose production. a-c, LCA ameliorates age-associated insulin resistance in mice. Ad libitum-fed, aged male mice were fed with (2-hydroxypropyl)-β-cyclodextrin-coated LCA at 1 g/l in drinking water for 1 month, followed by ipGTT (**a**, results of blood glucose and area under the curve (AUC) are shown as mean ± s.e.m. on the left panel; $n = 5$ (vehicle) or 6 (LCA) mice for each condition, and P value by two-way repeated-measures (RM) ANOVA followed by Sidak's test (blood glucose), or by two-sided Student's t-test (AUC); and the serum insulin levels during ipGTT are shown on the right panel, results are mean ± s.e.m.; $n = 4$ mice and P value by two-way RM ANOVA followed by Sidak's test), ITT (**b**, results of blood glucose and AUC are shown as mean ± s.e.m.; $n = 5$ (vehicle) or 6 (LCA) mice for each condition, and P value by two-way RM ANOVA followed by Sidak's test (blood glucose), or two-sided Student's t-test (AUC)), and the hyperinsulinaemia euglycaemic clamp (**c**, the blood glucose levels and the GIR values during the clamp are shown on the left panel as mean ± s.e.m.; $n = 10$ mice; P value by two-way RM ANOVA followed by Sidak's test; and the glucose disposal rates and the HGP rates, calculated according to the average values of GIR during the steady-state (90–120 min, indicated by a dashed line), on the right panel as mean ± s.e.m.; P value by two-sided Student's t-test). **d-k**, LCA ameliorates insulin resistance in aged mice without decreasing glucose production. Mice were treated as in **a**, followed by an 8 h-fasting period (except for liver glycogen, in which both fed and fasting mice were used). The carbon sources responsible for glucose production, including serum β-hydroxybutyrate (**d**), serum free fatty acids (**e**), serum glycerol (**f**), muscle glycogen (**g**), liver glycogen (**h**), muscle (**i**) and liver triglyceride (**j**), along with serum glucagon (**k**), were determined. Results are mean ± s.e.m.; $n = 4$ (**d**, vehicle groups of **e** and **g**, feeding group of **h**, and vehicle group of **k**) or 5 (others) mice for each treatment, and P value by two-way ANOVA followed by Tukey's test (**h**), or by two-sided Student's t-test (others). Experiments in this figure were performed three times.

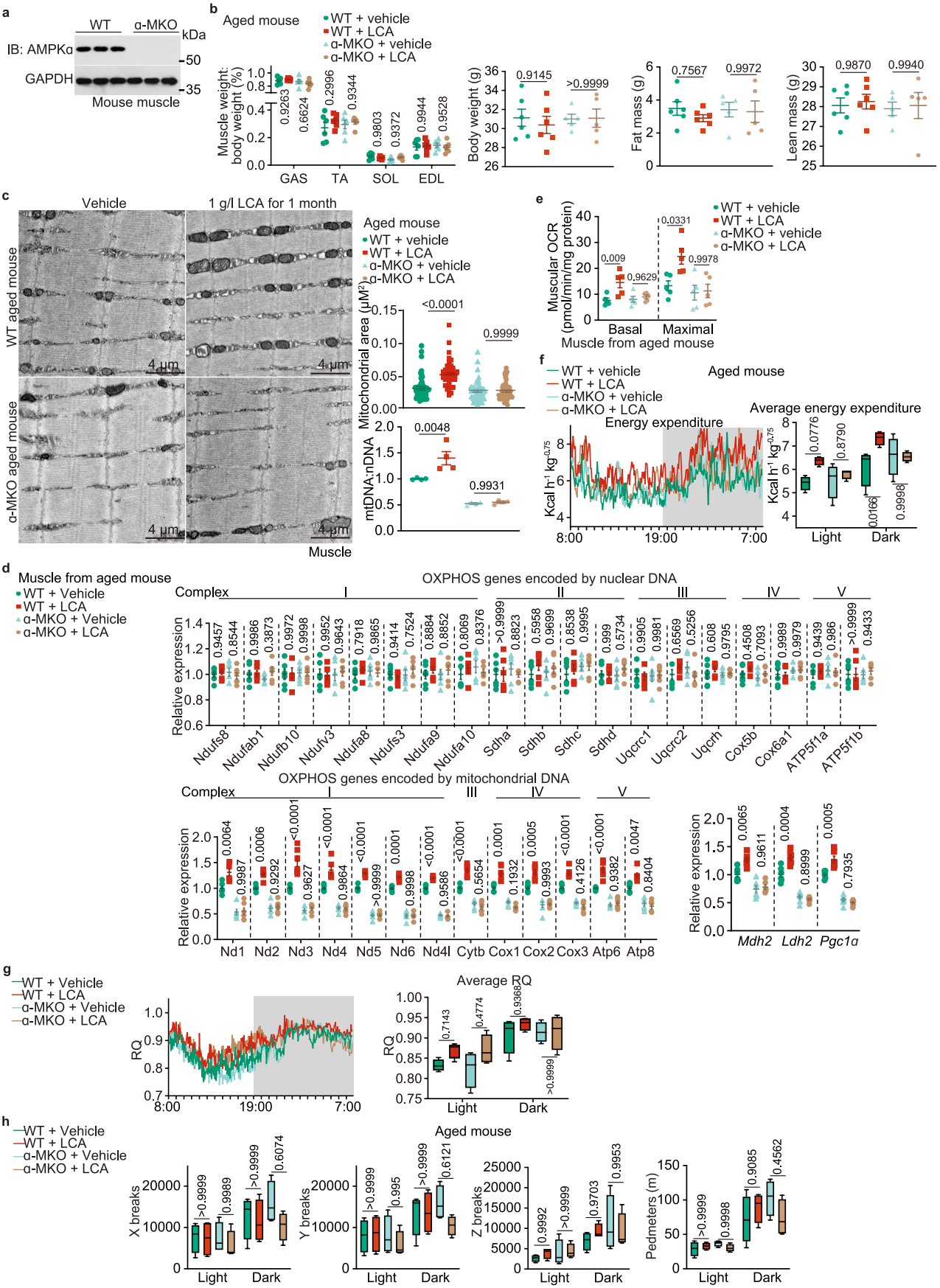

Extended Data Fig. 6 | See next page for caption.

Extended Data Fig. 6 | LCA exerts the rejuvenating activity through activating AMPK. a, Validation data for the muscle-specific knockout of AMPK (AMPKα-MKO) in mice. Muscle tissues from AMPKα-MKO (α-MKO) mice and wildtype (WT) littermates were lysed, followed by determination of the levels of AMPKα by immunoblotting. **b**, Muscle-specific AMPK knockout does not affect muscle mass. The aged, ad libitum-fed α-MKO mice and WT littermates were fed with (2-hydroxypropyl)-β-cyclodextrin-coated LCA at 1 g/l in drinking water for 1 month, followed by determination of muscle mass (also the body composition. Results are mean ± s.e.m.; $n = 5$ (body composition of α-MKO) or 6 (others) mice for each genotype/treatment, and P value by two-way ANOVA followed by Tukey's test). **c**, **e**, LCA improves mitochondrial respiratory function in aged mouse muscles in an AMPK-dependent manner. Mice were treated as in **b**, followed by determination of the mitochondrial area on the section (**c**; representative images are shown on the left panel, and statistical analysis data on the right (mean ± s.e.m.; $n = 53$ (WT, vehicle), 62 (WT, LCA), 58 (α-MKO, vehicle) or 57 (α-MKO, LCA) mitochondria for each genotype/treatment, and P value by two-way ANOVA followed by Tukey's test)), the mtDNA:nDNA ratios (right panel of **c**; results are shown on the right panel as mean ± s.e.m., normalized to the WT vehicle group; $n = 4$ mice for each genotype/treatment, and P value by two-way ANOVA followed by Tukey's test), and the muscular OCR (**e**; results are mean ± s.e.m.; $n = 5$ mice for each genotype/treatment, and P value by two-way ANOVA followed by Tukey's test). **d**, LCA elevates mitochondrial gene expression in an AMPK-dependent manner in aged mice. Mice were treated as in **b**, followed by determination of the mRNA levels of OXPHOS and TCA cycle genes in the muscle. Results are mean ± s.e.m.; $n = 6$, and P value by two-way ANOVA followed by Tukey's test. **f**, LCA elevates EE in aged mice depending on AMPK. Mice were treated as in **b**, followed by determination of EE. Data are shown as mean (left panel; at 5-min intervals during a 24-h course after normalization to the body weight ($kg^{0.75}$); mean), or as box-and-whisker plots (right panel; P value by two-way ANOVA followed by Tukey's test), $n = 4$ mice for each genotype/treatment. **g**, **h**, LCA elevates RQ in an AMPK-dependent manner in aged mice. Mice were treated as in **b**, followed by determination of RQ (**g**) and ambulatory activity (**h**). Data are shown as mean (left panel of **g**; at 5-min intervals during a 24-h course), or as box-and-whisker plots (other panels); $n = 4$ mice for each treatment, and P value by two-way ANOVA followed by Tukey's test. Experiments in this figure were performed three times.

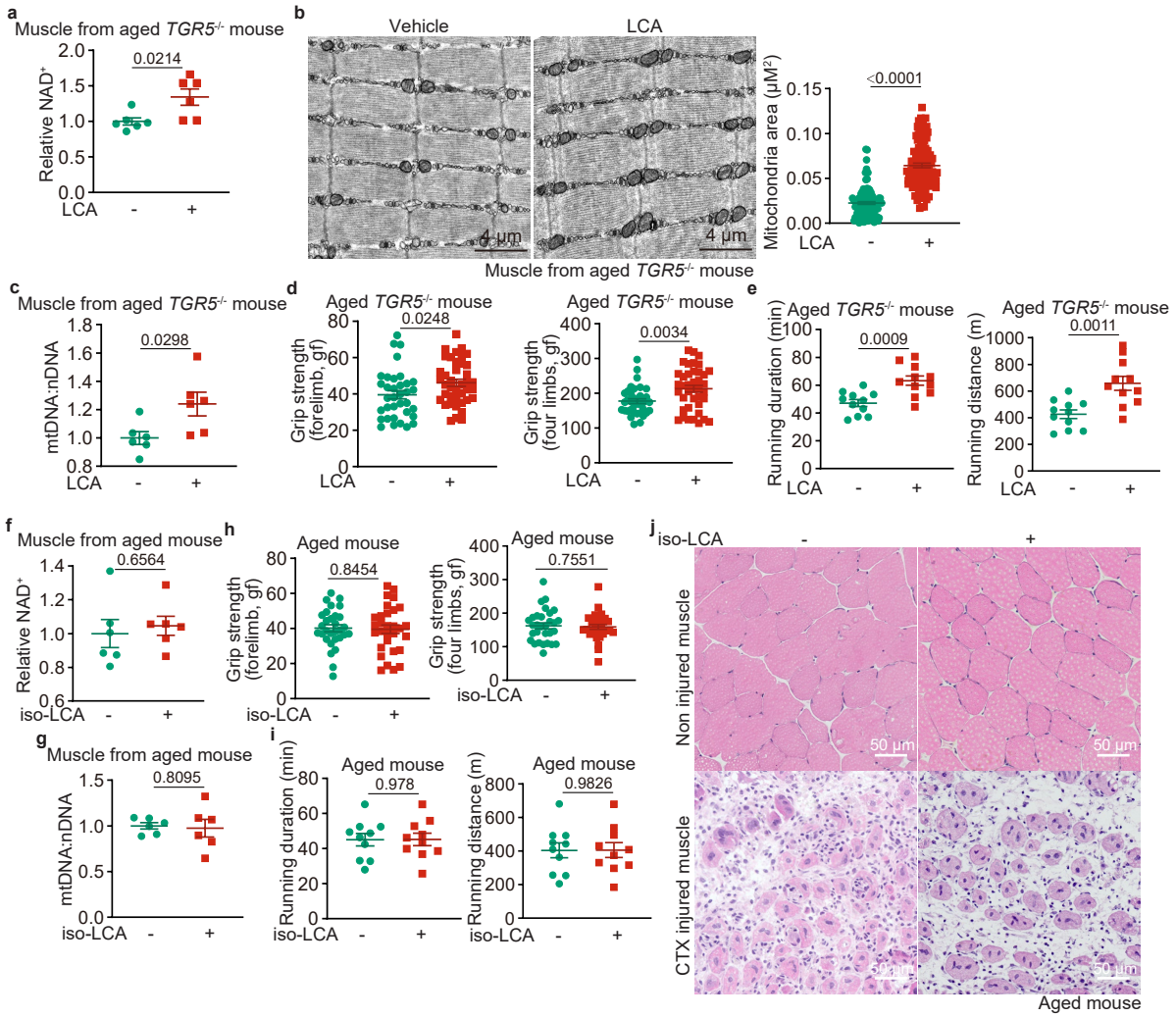

Extended Data Fig. 7 | LCA exerts rejuvenating activity in an TGR5-independent manner. a-e, LCA can effectively enhance muscle functions in aged *TGR5*$^{-/-}$ mice. The aged, ad libitum-fed *TGR5*$^{-/-}$ mice were fed with (2-hydroxypropyl)-β-cyclodextrin-coated LCA at 1 g/l in drinking water for 1 month. The muscular NAD^+ levels (**a**), mitochondrial areas (**b**), and mtDNA:nDNA ratios (**c**), grip strength (**d**), and running capacity (**e**), were then determined. Data are shown as mean ± s.e.m.; $n = 6$ (**a**, **c**), 106 (**b**), 35 (**d**, control), 40 (**d**, LCA), 11 (**e**) biological replicates for each genotype/treatment, and *P* value by two-sided Student's *t*-test. **f-j**, iso-LCA does not enhance muscle functions in aged mice. Ad libitum-fed mice were fed with (2-hydroxypropyl)-β-cyclodextrin-coated iso-LCA at 1 g/l in drinking water for 1 month (**f-i**), followed by intramuscular injection of cardiotoxin to induce muscle damage (**j**). The muscular NAD^+ levels (**f**), muscular mtDNA:nDNA ratios (**g**), muscle grip strength (**h**) and running distance (**i**), and muscle regeneration (**j**) were then determined. Results are mean ± s.e.m.; $n = 6$ (**f**, **g**), 30 (**h**) or 10 (**i**) biological replicates for each condition, and *P* value by two-sided Student's *t*-test. Experiments in this figure were performed three times.

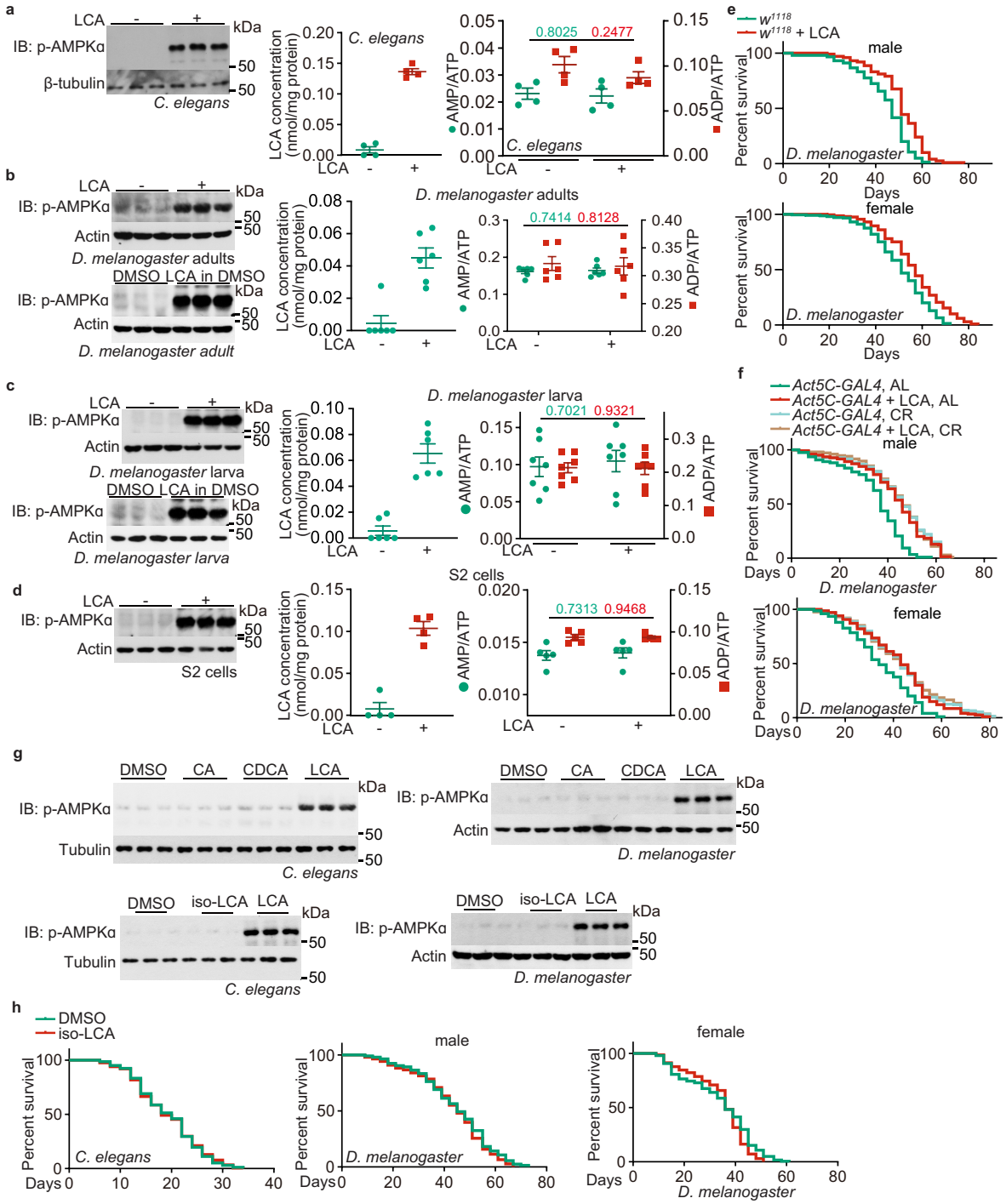

Extended Data Fig. 8 | LCA activates AMPK in nematodes and flies in a similar way to that in mice. a-**d**, LCA, accumulated in nematodes and flies to the same concentrations as seen in the muscles of CR mice, activates AMPK without elevating AMP levels. Nematodes at L4 stage (**a**), adult flies (**b**, mixed gender), third instar larvae of flies (**c**) and the S2 cells (**d**) were cultured in agar medium containing 100 μM LCA (**a**-**c**), either dissolved in DMSO (lower left panel of **b** and **c**) or coated by (2-hydroxypropyl)-β-cyclodextrin (others), for 1 day (**a**) or 7 days (**b**, **c**), or in Schneider's *Drosophila* Medium containing 100 μM LCA for 2 h (**d**), followed by determination of AMPK activities by immunoblotting (left panels of **a**-**d**), concentrations of LCA by HPLC-MS (middle panels of **a**-**d**) and the AMP:ATP and ADP:ATP ratios (right panels of **a**-**d**). Results are mean ± s.e.m.; $n = 4$ (**a**, and middle panel of **d**), 5 (right panel of **d**), 7 (right panel of **c**), or 6 (others) samples for each treatment, and P value by two-sided Student's t-test. **e**, **f**, LCA extends the lifespan of flies similarly to that by CR. The wildtype w^{1118} flies (**e**), or the control flies for the *AMPKα*-knockdown flies (**f**; *Act5C-GAL4*), were cultured in medium containing LCA at 100 μM (**e**, **f**), or subjected to CR (**f**). Lifespan data are shown as Kaplan-Meier curves. **g**, LCA, but not the derivative iso-LCA or precursors CA and CDCA, activates AMPK in nematodes and flies. Nematodes at L4 stage (left) or adult flies (right, mixed gender) were cultured in agar medium containing 100 μM CA, CDCA, iso-LCA or LCA as a control, followed by determination of AMPK activities by immunoblotting. **h**, iso-LCA cannot extend lifespan in nematodes or flies. Wildtype nematodes (left) and flies (middle and right) were cultured in medium containing iso-LCA at 100 μM. Lifespan data are shown as Kaplan-Meier curves. Experiments in this figure were performed three times.

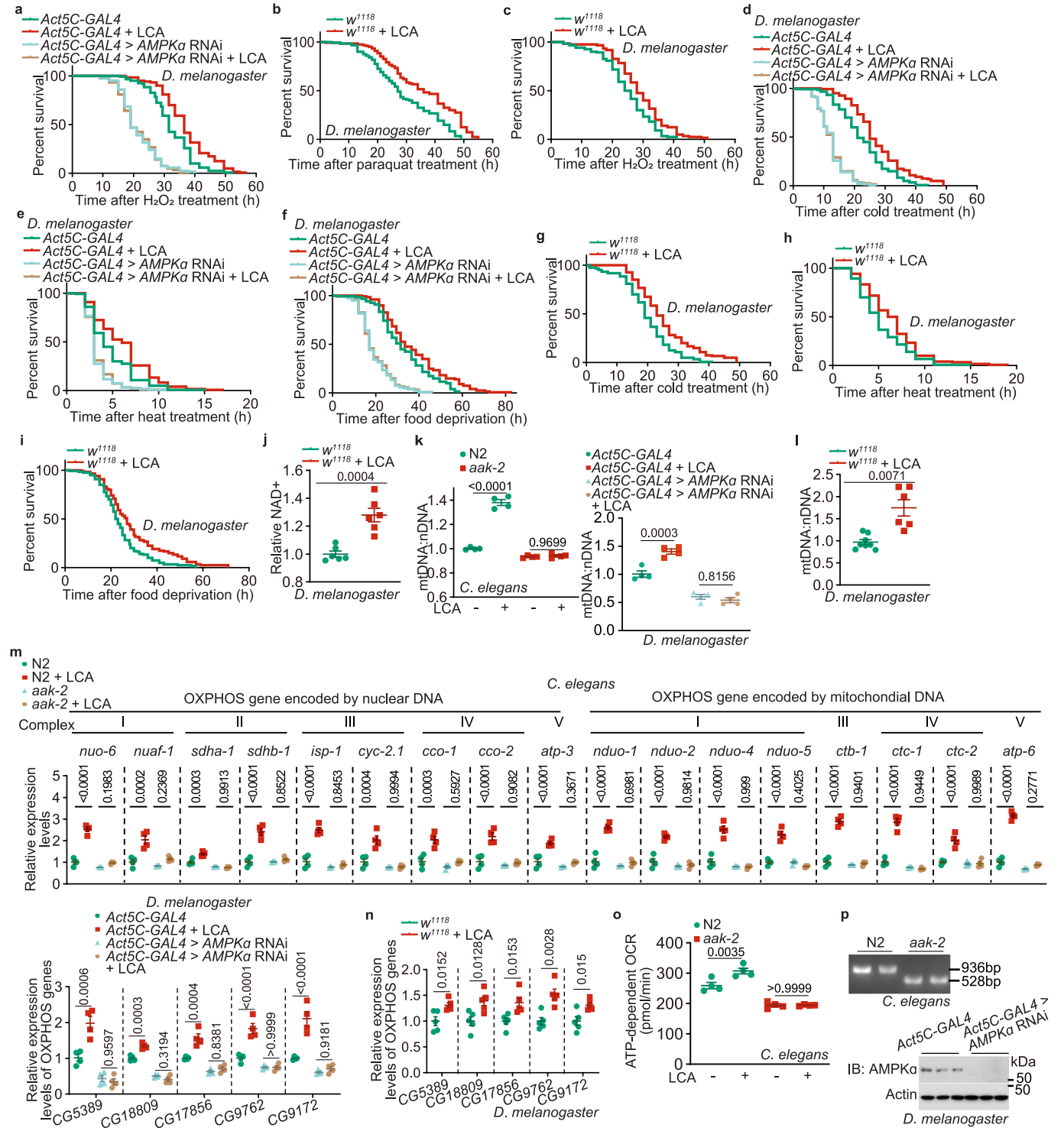

Extended Data Fig. 9 | See next page for caption.

Extended Data Fig. 9 | LCA extends healthspan in nematodes and flies. a, LCA promotes oxidative stress resistance in flies via AMPK. The control and the *AMPKα* knockdown flies were cultured in medium containing LCA at 100 μM for 30 days, followed by transferring to medium containing 5% H_2O_2 to elicit oxidative stress. Lifespan data are shown as Kaplan-Meier curves. **d**-**f**, LCA improved cold, heat and starvation resistance in flies through AMPK. the control and the *AMPKα* knockdown flies were treated with 100 μM LCA for 30 days, followed by transferring to cold (4 °C; **d**), heat (37 °C; **e**) or food deprivation (**f**) conditions. Lifespan data are shown as Kaplan-Meier curves. **k**, **m**, **o**, LCA elevates mitochondrial contents and improves mitochondrial functions in nematodes and flies depending on AMPK. Wildtype or *AMPKα* knockout nematodes (left panels of **k**, and **o**, and upper panel of **m**), and the control or the *AMPKα* knockdown flies (right panel of **k**, and lower panel of **m**), were cultured in medium containing LCA at 100 μM for 2 days (left panels of **k**, and **o**, and upper panel of **m**) or 30 days (right panel of **k**, and lower panel of **m**), followed by determination of the ratios of mtDNA:nDNA (**k**), the mRNA levels of mitochondrial OXPHOS complexes (**m**), and OCR (**o**). Results are mean ± s.e.m., normalized to the WT/control vehicle group (**k**, **m**) or not (others); $n = 4$ samples for each genotype/treatment, and P value by two-way ANOVA followed by Tukey's test. **b**, **c**, **g**-**j**, **l**, **n**, LCA improves the healthspan of w^{1118} flies. The wildtype w^{1118} flies were cultured in medium containing LCA at 100 μM, followed by determination of oxidative resistance (**b**, **c**), cold resistance (**g**), heat resistance (**h**), food deprivation resistance (**i**), NAD^+ levels (**j**), mtDNA:nDNA levels (**l**), and OXPHOS mRNA levels (**n**). Results of **j**, **l** and **n** are shown as mean ± s.e.m.; $n = 5$ (**n**), 8 (vehicle group of **l**) or 6 (others) samples for each treatment, and P value by two-sided Student's t-test. **p**, Validation for the knockout and knockdown efficiency of AMPK in *aak-2* nematodes, by PCR, and AMPK-knockdown flies, by immunoblotting. Experiments in this figure were performed three times.

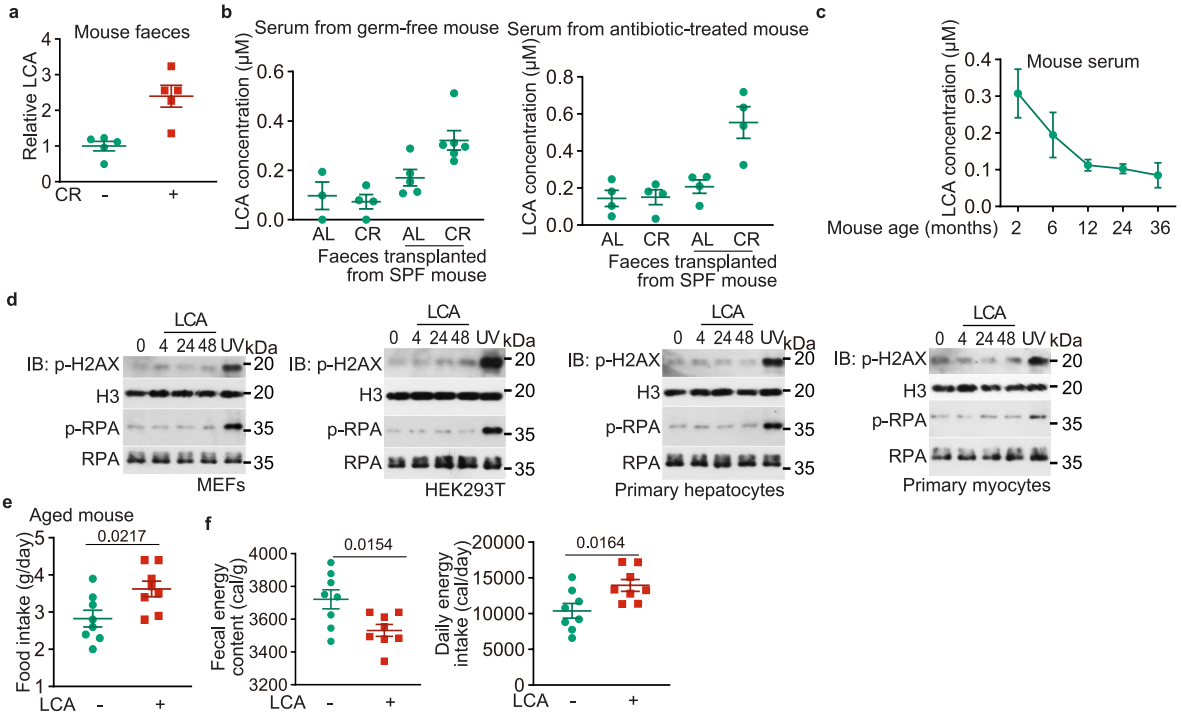

Extended Data Fig. 10 | CR induces changes of gut microbiome. a, CR elevates faecal concentrations of LCA. Mice were subjected to CR for 4 months, followed by determination of LCA in the intestine. Results are mean ± s.e.m., normalized to the AL group; $n = 5$ mice for each treatment. **b**, CR increases LCA by altering gut microbiome. Germ-free (left) or antibiotic-treated mice (right) were subjected to CR for 3.5 months, or transplanted with faeces from SPF mice that underwent 4 months of CR or fed ad libitum, for a duration of 1 month, followed by determination of the levels of LCA in the serum. Results are mean ± s.e.m., $n = 3$ (left panel, AL), 4 (left panel, CR; and right panel), 5 (left panel, AL-transplanted), or 6 (left panel, CR-transplanted) mice for each treatment. **c**, LCA decreases with age in mice. Mice at different ages were sacrificed, followed by determination of LCA in the serum. Results are mean ± s.e.m., $n = 4$ mice for each age. **d**, LCA does not cause DNA damage at the concentrations similar to that in serum or muscle tissues of CR mice. MEFs, HEK293T cells, primary hepatocytes and primary myocytes were treated with 1 μM LCA for indicated time durations, or exposed to 75 J/m^2 UV followed with incubation in fresh DMEM for another 2 h as a control; the levels of H2AX and RPA32 phosphorylation were determined by immunoblotting. **e**, **f**, LCA increases energy intake of mice. Ad libitum-fed mice were fed with (2-hydroxypropyl)-β-cyclodextrin-coated LCA at 1 g/l in drinking water for 1 month, followed by determination of daily food intake (**e**), energy content in the food consumed in a day (**f**, right panel), and energy content of faeces excreted in a day (**f**, left panel). Results are mean ± s.e.m., $n = 8$ mice for each treatment, and P value by two-sided Student's t-test.

nature portfolio

Corresponding author(s): Chen-Song Zhang and Sheng-Cai Lin

Last updated by author(s): 2024/9/17

Reporting Summary

Nature Portfolio wishes to improve the reproducibility of the work that we publish. This form provides structure for consistency and transparency in reporting. For further information on Nature Portfolio policies, see our Editorial Policies and the Editorial Policy Checklist.

Statistics

For all statistical analyses, confirm that the following items are present in the figure legend, table legend, main text, or Methods section.

n/a	Confirmed
☐	☒ The exact sample size (*n*) for each experimental group/condition, given as a discrete number and unit of measurement
☐	☒ A statement on whether measurements were taken from distinct samples or whether the same sample was measured repeatedly
☐	☒ The statistical test(s) used AND whether they are one- or two-sided *Only common tests should be described solely by name; describe more complex techniques in the Methods section.*
☐	☒ A description of all covariates tested
☐	☒ A description of any assumptions or corrections, such as tests of normality and adjustment for multiple comparisons
☐	☒ A full description of the statistical parameters including central tendency (e.g. means) or other basic estimates (e.g. regression coefficient) AND variation (e.g. standard deviation) or associated estimates of uncertainty (e.g. confidence intervals)
☐	☒ For null hypothesis testing, the test statistic (e.g. *F*, *t*, *r*) with confidence intervals, effect sizes, degrees of freedom and *P* value noted *Give P values as exact values whenever suitable.*
☒	☐ For Bayesian analysis, information on the choice of priors and Markov chain Monte Carlo settings
☒	☐ For hierarchical and complex designs, identification of the appropriate level for tests and full reporting of outcomes
☒	☐ Estimates of effect sizes (e.g. Cohen's *d*, Pearson's *r*), indicating how they were calculated

Our web collection on statistics for biologists contains articles on many of the points above.

Software and code

Policy information about availability of computer code

Data collection	Epson Scan software (v.3.9.3.4) was used to scan blots from X-ray films. AxioScan 7 scanner (Zeiss), Zen 3.4 (Zeiss) and LAS X (version 3.0.2.16120, Leica) were used to collect microscopic images, as described in related method sections. OCR results were collected by Wave 2.6.1 (for nematodes) or Wave 2.6.3 (for muscle). Analyst 1.6.3 software (SCIEX) was used to collect data from quantitative lipidomics. Analyst software (v.1.7.1, SCIEX) was used to collect data from preparative HPLC-MS. MassHunter GC/MS Acquisition software (v.B.07.04.2260, Agilent) was used to collect data from GC-MS. Data from CE/MS were collected using MassHunter LC/MS acquisition 10.1.48 (Agilent). TEM system control software (Ver. 01.20, Hitachi) was used to collect TEM images. Pharyngeal pumping rates of nematodes were recorded using the Capture software (v.2021.1.13, Capture Visualisation). Data acquisition and instrument control of mouse energy expenditure were performed using MetaScreen software (v.2.3.15.12, Sable Systems) RT-PCR results were analysed using LightCycler software (v.96 1.1, Roche) Images (determining the localisation of TFEB) were taken by LAS X Software (version 3.0.2.1620, Leica), and formatted using Photoshop 2023 software (Adobe).
Data analysis	Blots were generated by Prism 9, measured by ImageJ software (v.1.8.0, National Institutes of Health Freeware) and were formatted by Illustrator 2022. Statistical analysis was performed by Prism 9 (GraphPad Software) and SPSS 27.0 (IBM). Microscopic images were analysed and processed by Zen 3.4 and LAS X (version 3.0.2.16120), as described in related Methods section, and were formatted on Photoshop 2023 software (Adobe). Results of metabolites measured on GC-MS were analysed using GC-MS MassHunter Workstation Qualitative Analysis software (v.10.1.733.0, Agilent Technologies). Results of metabolites measured on HPLC-MS were analysed using MultiQuant software (v.3.0.3, SCIEX).

Results of metabolites measured on CE-MS were processed using Qualitative Analysis B.06.00 (Agilent).
Measurements of TEM images were acquired using the ImageJ (v.1.8.0, National Institutes of Health Freeware).
Pharyngeal pumping rates of nematodes were calculated using the Aimersoft Video Editor software (v.3.6.2.0, Aimersoft).
Data of mouse energy expenditure processed using Macro Interpreter (v.2.32, Sable Systems)

For manuscripts utilizing custom algorithms or software that are central to the research but not yet described in published literature, software must be made available to editors and reviewers. We strongly encourage code deposition in a community repository (e.g. GitHub). See the Nature Portfolio guidelines for submitting code & software for further information.

Data

Policy information about availability of data

All manuscripts must include a data availability statement. This statement should provide the following information, where applicable:

- Accession codes, unique identifiers, or web links for publicly available datasets
- A description of any restrictions on data availability
- For clinical datasets or third party data, please ensure that the statement adheres to our policy

All plasmids and experimental data that support the findings of this study are available from the corresponding author upon request. Full immunoblots are provided as Supplementary Information. Source data are provided with this paper.
The analysis was performed using standard protocols with previously described analysis tools. No custom code was used in this study.

Field-specific reporting

Please select the one below that is the best fit for your research. If you are not sure, read the appropriate sections before making your selection.

☒ Life sciences ☐ Behavioural & social sciences ☐ Ecological, evolutionary & environmental sciences

For a reference copy of the document with all sections, see nature.com/documents/nr-reporting-summary-flat.pdf

Life sciences study design

All studies must disclose on these points even when the disclosure is negative.

Sample size	The chosen sample sizes were similar to those used in this field: n = 4-12 samples were used to evaluate the levels of metabolites in serum (ref. 81,82), cells (ref. 76,83), tissues (ref. 76,83-85), nematodes (ref. 86-88) and flies (ref. 89-91); n = 4-10 samples to determine OCR in tissues (ref. 76,92) and nematodes (ref. 93-95); n = 3-4 samples to determine the mRNA levels of a specific gene (ref. 96,97); n = 2-6 samples to determine the expression levels and phosphorylation levels of a specific protein (ref. 96); n = 200 worms to determine lifespan (ref. 98-100); n = 60 worms to determine healthspan (ref. 101-103), except n = 10 worms for pharyngeal pumping rates (ref. 76,104); n = 200 flies, male or female, to determine lifespan (ref. 105-107); n = 60 flies, male or female, to determine healthspan (ref. 108-110); n = 4-8 mice for EE and RQ (ref. 76); n = 10 mice for hyperinsulinemic-euglycemic clamping (ref. 76,111); n = 5-6 mice for GTT and ITT (ref. 76); n = 6 mice for body composition (ref.76); n = 6 mice for muscle fibre type (ref. 44,112,113); n = 3 mice for muscle regeneration (ref. 103,114,115); n = 53-62 mitochondria from 3 mice for muscular mitochondrial content (ref. 116,117); n = 9-23 mice for running duration (ref68,76); and n = 36-75 mice for grasp strength (ref. 76). No statistical methods were used to predetermine sample size.
Data exclusions	No data was excluded.
Replication	All experimental findings were repeated at least three times as stated in figure legends.
Randomization	Randomisation was applied wherever possible. For example, during MS analyses (metabolites, proteins and pharmacokinetics), samples were processed and subjected to the mass spectrometer in random orders. For animal experiments, sex-matched (only for rodents), age-matched litter-mate animals in each genotype were randomly assigned to pharmacological treatments. In cell experiments, cells of each genotype were parallel seeded and randomly assigned to different treatments. Otherwise, randomisation was not performed. For example, when performing immunoblotting, samples needed to be loaded in a specific order to generate the final figures.
Blinding	Blinding was applied wherever possible. For example, samples, cages or agar plates during sample collection and processing were labelled as code names that were later revealed by the individual who picked and treated animals or cells, but did not participate in sample collection and processing, until assessing outcome. Similarly, during microscopy data collection and statistical analyses, the fields of view were chosen on a random basis, and are often performed by different operators, preventing potentially biased selection for desired phenotypes. Otherwise, blinding was not performed, such as the measurement of aldolase activity in vitro, as different reagents were added for particular reactions.

Reporting for specific materials, systems and methods

We require information from authors about some types of materials, experimental systems and methods used in many studies. Here, indicate whether each material, system or method listed is relevant to your study. If you are not sure if a list item applies to your research, read the appropriate section before selecting a response.

Materials & experimental systems

n/a	Involved in the study
☐	☒ Antibodies
☐	☒ Eukaryotic cell lines
☒	☐ Palaeontology and archaeology
☐	☒ Animals and other organisms
☒	☐ Human research participants
☒	☐ Clinical data
☒	☐ Dual use research of concern

Methods

n/a	Involved in the study
☒	☐ ChIP-seq
☒	☐ Flow cytometry
☒	☐ MRI-based neuroimaging

Antibodies

Antibodies used

Rabbit anti-phospho-AMPKα-Thr172 (cat. #2535, RRID: AB_331250; 1:1,000 for IB), anti-AMPKα (cat. #2532, RRID: AB_330331; 1:1,000 for IB), anti-phospho-ACC-Ser79 (cat. #3661, RRID: AB_330337; 1:1,000 for IB), anti-ACC (cat. #3662, RRID: AB_2219400; 1:1,000 for IB), anti-GAPDH (cat. #5174 RRID: AB_10622025; 1:1,000 for IB) and anti-AXIN1 (cat. #2074, RRID: AB_2062419; 1:1,000 for IB) antibodies were purchased from Cell Signaling Technology. Rabbit anti-tubulin (cat. #10068-1-AP; RRID: AB_2303998; 1:1,000 for IB) was purchased from Proteintech. Mouse anti-total OXPHOS (cat. ab110413, RRID: AB_2629281; 1:5,000 for IB), and rabbit anti-Laminin (cat. ab11575, RRID: AB_298179; 1:200 for IF) antibodies were purchased from Abcam. Mouse anti-eMHC (cat. BF-G6, RRID: AB_10571455; 1:100 for IHC), anti-Pax7 (cat. Pax-7, RRID: AB_2299243; 1:100 for IHC), anti-MHCIIa (cat. SC71, RRID: AB_2147165; 1:100 for IHC), anti-MHCIIb (cat. BF-F3, RRID: AB_2266724; 1:100 for IHC), and anti-MHCI (cat. C6B12, RRID: AB_528351; 1:100 for IHC) antibodies were purchased from Developmental Studies Hybridoma Bank. Mouse anti β-ACTIN (cat. A5316, RRID: AB_476743; 1:1,000 for IB) was purchased from Sigma. Goat anti-Mouse IgM (Heavy chain) Cross-Adsorbed Secondary Antibody, Alexa Fluor 488 (cat. A-21042, RRID: AB_2535711; 1:200 for IHC), Goat anti-Mouse IgG2b Cross-Adsorbed Secondary Antibody, Alexa Fluor 594 (cat. A-21145, RRID: AB_2535781; 1:200 for IHC), Goat anti-Mouse IgG1 Cross-Adsorbed Secondary Antibody, Alexa Fluor 647 (cat. A-21240, RRID: AB_2535809; 1:200 for IHC), Goat anti-Mouse IgG1 Cross-Adsorbed Secondary Antibody, Alexa Fluor 488 (cat. A-21121, RRID: AB_2535764; 1:200 for IHC), and Goat anti-Rabbit IgG (H+L) Cross-Adsorbed Secondary Antibody, Alexa Fluor 594 (cat. A-11012, RRID: AB_2534079; 1:200 for IHC) were purchased from Thermo. The horseradish peroxidase (HRP)-conjugated goat anti-mouse IgG (cat. 115-035-003, RRID: AB_10015289; 1:5,000 dilution for IB) and goat anti-rabbit IgG (cat. 111-035-003, RRID: AB_2313567; 1:5,000 dilution for IB) antibodies were purchased from Jackson ImmunoResearch.

Validation

The following commercially available antibodies were validated by the company, as well as other researchers (as the information collected by the RRID database):
Rabbit anti-phospho-AMPKα-Thr172 (cat. #2535, RRID: AB_331250; 1:1,000 for IB), anti-AMPKα (cat. #2532, RRID: AB_330331; 1:1,000 for IB), anti-phospho-ACC-Ser79 (cat. #3661, RRID: AB_330337; 1:1,000 for IB), anti-ACC (cat. #3662, RRID: AB_2219400; 1:1,000 for IB), anti-GAPDH (cat. #5174 RRID: AB_10622025; 1:1,000 for IB) and anti-AXIN1 (cat. #2074, RRID: AB_2062419; 1:1,000 for IB) antibodies were purchased from Cell Signaling Technology. Rabbit anti-tubulin (cat. #10068-1-AP; RRID: AB_2303998; 1:1,000 for IB) was purchased from Proteintech. Mouse anti-total OXPHOS (cat. ab110413, RRID: AB_2629281; 1:5,000 for IB), and rabbit anti-Laminin (cat. ab11575, RRID: AB_298179; 1:200 for IF) antibodies were purchased from Abcam. Mouse anti-eMHC (cat. BF-G6, RRID: AB_10571455; 1:100 for IHC), anti-Pax7 (cat. Pax-7, RRID: AB_2299243; 1:100 for IHC), anti-MHCIIa (cat. SC71, RRID: AB_2147165; 1:100 for IHC), anti-MHCIIb (cat. BF-F3, RRID: AB_2266724; 1:100 for IHC), and anti-MHCI (cat. C6B12, RRID: AB_528351; 1:100 for IHC) antibodies were purchased from Developmental Studies Hybridoma Bank. Mouse anti β-ACTIN (cat. A5316, RRID: AB_476743; 1:1,000 for IB) was purchased from Sigma. Goat anti-Mouse IgM (Heavy chain) Cross-Adsorbed Secondary Antibody, Alexa Fluor 488 (cat. A-21042, RRID: AB_2535711; 1:200 for IHC), Goat anti-Mouse IgG2b Cross-Adsorbed Secondary Antibody, Alexa Fluor 594 (cat. A-21145, RRID: AB_2535781; 1:200 for IHC), Goat anti-Mouse IgG1 Cross-Adsorbed Secondary Antibody, Alexa Fluor 647 (cat. A-21240, RRID: AB_2535809; 1:200 for IHC), Goat anti-Mouse IgG1 Cross-Adsorbed Secondary Antibody, Alexa Fluor 488 (cat. A-21121, RRID: AB_2535764; 1:200 for IHC), and Goat anti-Rabbit IgG (H+L) Cross-Adsorbed Secondary Antibody, Alexa Fluor 594 (cat. A-11012, RRID: AB_2534079; 1:200 for IHC) were purchased from Thermo. The horseradish peroxidase (HRP)-conjugated goat anti-mouse IgG (cat. 115-035-003, RRID: AB_10015289; 1:5,000 dilution for IB) and goat anti-rabbit IgG (cat. 111-035-003, RRID: AB_2313567; 1:5,000 dilution for IB) antibodies were purchased from Jackson ImmunoResearch.

Eukaryotic cell lines

Policy information about cell lines

Cell line source(s)

HEK293T cells and Drosophila Schneider 2 (S2) cells were purchased from ATCC. MEFs were obtained from the indicated mouse strains.

Authentication

HEK293T cells and MEFs were authenticated by STR sequencing, and Drosophila Schneider 2 (S2) cells by species identification using DNA-barcode assay, performed by Immocell Biotechnology Corporation (Xiamen, China).

Mycoplasma contamination

The cell lines were routinely tested negative for mycoplasma contamination in our lab.

Commonly misidentified lines
(See ICLAC register)

No commonly misidentified lines were used.

Animals and other organisms

Policy information about studies involving animals; ARRIVE guidelines recommended for reporting animal research

Laboratory animals	Animal maintenance: Unless stated otherwise, mice were housed with free access to water and standard diet (65% carbohydrate, 11% fat, 24% protein) under specific pathogen-free conditions. The light was on from 8:00 to 20:00, with the temperature kept at 21-24°C and humidity at 40-70%. Only male mice were used in the study, and male littermate controls were used throughout the study. Mice were individually caged for 1 week before each treatment. For starvation, the diet was withdrawn from the cage at 5 p.m., and mice were sacrificed at desired time points by cervical dislocation. For CR, each mouse was fed with 2.5 g of standard diet (70% of ad libitum food intake for a mouse at 4 months old and above) at 5 p.m. at each day. For analysing AMPK activation, wild-type and AMPKα-MKO mice of 5 weeks old were used for the administration of LCA (treated with LCA for 1 week starting from 4 weeks old), and wild-type 8 months old for CR (CR for 4 months starting from 4 months old); for determining rejuvenating effects of LCA or iso-LCA: wild-type, AMPKα-MKO, and TGR5-/- mice, aged 18 months (treated with LCA or iso-LCA for 1 month starting from 17 months old); for determining rejuvenating effects of CR: wild-type, aged 20.5 months (subjected to CR for 3.5 month starting from 17 months old); for analysing the pharmacokinetics of LCA: wild-type mice aged 18 months (aged mice; treated with LCA or for 1 month starting from 17 months old); for determining the changes of LCA concentrations in serum and tissue: wild-type or Cyp2c-null mice aged 8 months old (subjected to CR for 4 months starting from 4 months old), germ-free mice aged 5 months (gavaged with faeces for 1 week starting from 4 months old, and were ad libitum fed for another 3 weeks), and antibiotic-treated mice 7.5 months old (subjected for CR for 3.5 months starting from 4 months old), except that in Fig. 2c, in which mice were subjected to CR for indicated time durations starting from 4 months old; for determination of serum metabolome in CR mice: wild-type mice aged 8 months old (subjected to CR for 4 months starting from 4 months old); and for isolating primary hepatocytes and myocytes: wild-type mice aged 1 month. Unless stated otherwise, all flies were cultured at 25 °C and 60% humidity with a 12-hour light and dark cycle. The light was on from 8:00 to 20:00. Adult flies were cultured in Bloomington Drosophila Stock Center (BDSC) Standard Cornmeal Medium (for regular culture), 2% (for CR), or 3% (the control, ad libitum fed group for CR) CSY agar diet. Larvae and the crossed fly strains were reared on Semi-Defined, Rich Medium, which is prepared as described previously, with minor modifications. Briefly, 10 g of agar, 80 g of dry yeast, 20 g of yeast extract, 20 g of peptone, 30 g of sucrose, 60 g of glucose, 0.5 g of $MgSO_4 \cdot 6H_2O$ and 0.5g of $CaCl_2 \cdot 6H_2O$ were dissolved in 1,000 ml of di-distilled water, and then boiled, followed by cooling to 60 °C. Some 6 ml of propionic acid was then added to the medium, and the medium was dispensed into culture vials, 6 ml each. The media vials were covered with gauze and blown with the breeze as in BDSC and CSY diets, and were kept at 20 °C (for no more than 3 days) before experiment. In this study, the following ages of flies were used: a) for analysing AMPK activation and the pharmacokinetics of LCA, third instar larvae or newly eclosed adults were used; b) for determining lifespan, adults at day 2 after eclosion were used (for LCA or CR treatment); c) for determining healthspan, mtDNA:nDNA, NAD+ levels and mitochondrial genes expression, adults at day 30 after eclosion (treated with LCA for 28 days starting from 2 days after eclosion) were used. Unless stated otherwise, nematodes (hermaphrodites) were maintained on nematode growth medium (NGM) plates (1.7% (w/v) agar, 0.3% (w/v) NaCl, 0.25% (w/v) bacteriological peptone, 1mM $CaCl_2$, 1mM $MgSO_4$, 25mM KH_2PO_4-K_2HPO_4, pH6.0, 0.02% (w/v) streptomycin and 5μg/ml cholesterol) spread with Escherichia coli OP50 as standard food. All worms were cultured at 20 °C. The administration of LCA or DMSO was initiated at the L4 stage. Animal source: Wildtype C57BL/6J mice (#000664) were obtained from The Jackson Laboratory. AXINF/F and LAMTOR1F/F mice were generated and validated as described previously116. AMPKα1F/F (#014141) and AMPKα2F/F mice (#014142) were obtained from Jackson Laboratory, provided by Dr. Sean Morrison. AMPKα-MKO mice were generated by crossing AMPKα1/2F/F mice with Mck-Cre mice, as described and validated previously101. Cyp2c cluster-KO mice (Cat. NM-KO-18019) were purchased from Shanghai Model Organisms Center, Inc. The wildtype fly strain (w1118; #3605) and the GAL4-expressing strain (y1 w*; P{Act5C-GAL4-w}E1/CyO; #25374) were obtained from the BDSC. The GAL4-induced, AMPKα RNAi-carrying strain (w1118; P{GD736}v1827; #1827) was obtained from the Vienna Drosophila Resource Center (VDRC). The w1118; Sp/CyO strain was obtained from the Core Facility of Drosophila Resource and Technology, Chinese Academy of Sciences. To obtain the flies with AMPKα knocked down on the w1118 background, a GAL4-expressing strain on the w1118 background (w1118; P{Act5C-GAL4-w}E1/CyO) was first generated by crossing the y1 w*; P{Act5C-GAL4-w}E1/CyO males with w1118; Sp/CyO females, followed by crossing the F1 males with red eyes and straight wings (w1118; P{Act5C-GAL4-w}E1/Sp) with w1118; Sp/CyO females. The GAL4-expressing flies (w1118 background) were then crossed with the AMPKα RNAi-carrying flies, and the F1 offspring with red eyes and straight wings were the AMPKα-KD flies (w1118; P{Act5C-GAL4-w}E1/P{GD736}v1827; +/+). The F1 offspring of wildtype flies crossed with the GAL4-expressing flies (w1118 background), i.e., the w1118; P{Act5C-GAL4-w}E1/+; +/+ flies, were used as the control files. Wildtype (N2 Bristol) and aak-2 (ok524) strains were obtained from Caenorhabditis Genetics Center. All mutant strains were outcrossed 6 times to N2 before the experiments.
Wild animals	The study did not involve wild animals
Field-collected samples	The study did not involve samples collected from the field.
Ethics oversight	Protocols for all rodent experiments were approved by the Institutional Animal Care and the Animal Committee of Xiamen University (XMULAC20180028 and XMULAC20220050).

Note that full information on the approval of the study protocol must also be provided in the manuscript.